



HAL
open science

Geological and hydrological histories of the Argyre province, Mars

J.M. Dohm, T.M. Hare, S.J. Robbins, J.-P. Williams, R.J. Soare, M.R. El-Maarry, S.J. Conway, D.L. Buczkowski, J.S. Kargel, M.E. Banks, et al.

► **To cite this version:**

J.M. Dohm, T.M. Hare, S.J. Robbins, J.-P. Williams, R.J. Soare, et al.. Geological and hydrological histories of the Argyre province, Mars. *Icarus*, 2015, 253, pp.66-98. 10.1016/j.icarus.2015.02.017 . insu-02274347

HAL Id: insu-02274347

<https://insu.hal.science/insu-02274347>

Submitted on 8 Jan 2021

HAL is a multi-disciplinary open access archive for the deposit and dissemination of scientific research documents, whether they are published or not. The documents may come from teaching and research institutions in France or abroad, or from public or private research centers.

L'archive ouverte pluridisciplinaire **HAL**, est destinée au dépôt et à la diffusion de documents scientifiques de niveau recherche, publiés ou non, émanant des établissements d'enseignement et de recherche français ou étrangers, des laboratoires publics ou privés.

Geological and Hydrological Histories of the Argyre Province, Mars

J. M. Dohm^a, T. M. Hare^b, S. J. Robbins^c, Jean-Pierre Williams^d, R. J. Soare^e, M. R. El Maarry^f,
S. J. Conway^g, Debra L. Buczkowski^h, Jeffrey S. Kargelⁱ, M. E. Banks^{j,k}, Alberto G. Fairén^l, D.
Schulze-Makuch^m, G. Komatsuⁿ, Hirdy Miyamoto^a, R.C. Anderson^o, A.F. Davila^p, W.C.
Mahaney^q, W. Fink^r, H. J. Cleaves^{s,t}, J. Yan^u, B. Hynek^v, S. Maruyama^s

^aThe University Museum, The University of Tokyo, Hongo 7-3-1, Bunkyo-ku, Tokyo 113-0033,
Japan

^bU.S. Geological Survey, Flagstaff, AZ 86001, USA

^cSouthwest Research Institute, Boulder CO 80302, USA

^dDepartment of Earth and Space Sciences, University of California, Los Angeles, CA
90095, USA

^eDepartment of Geography, Dawson College, 3040 Sherbrooke St. W., Montreal, Canada, H3Z
1A4

^fPhysikalisches Institut, Bern Universität, Berne, Switzerland 3012

^gDepartment of Physical Sciences, Open University, Milton Keynes, UK, MK7 6AA

^hApplied Physics Laboratory, Johns Hopkins University, Laurel, MD, 20723, USA

ⁱDepartment of Hydrology and Water Resources, University of Arizona, Tucson, AZ 85721, USA

^jSmithsonian Institution, National Air and Space Museum, Center for Earth and Planetary Studies,
Washington, DC 20013, USA

^kPlanetary Science Institute, Tucson, AZ 85719, USA

^lDepartment of Planetology and Habitability, Centro de Astrobiología, Madrid 28850, Spain

^mCenter of Astronomy and Astrophysics, Technical University Berlin, 10623 Berlin, Germany

ⁿInternational Research School of Planetary Sciences, Università d'Annunzio, 65421 Pescara, Italy

^oJet Propulsion Laboratory, California Inst. Of Technology, Pasadena, CA 91109

^pSETI Institute, Mountain View, California 94043, USA

^qQuaternary Surveys, 26 Thornhill Ave., Thornhill, ON L4J 1J4, Canada

^rCollege of Engineering, Department of Electrical and Computer Engineering, University of Arizona,
Tucson, AZ 85721, USA

^sEarth-Life Science Institute, Tokyo Institute of Technology, Meguro, Tokyo, Japan, 152-8551

^tThe Institute for Advanced Study, Princeton, NJ 08540 USA

^uRISE Project Office, National Astronomical Observatory of Japan, Oshu 0230861, Japan

^vLaboratory for Atmospheric and Space Physics and Geological Sciences, University of Colorado, 80309,
USA

E-mail: jmd@um.u-tokyo.ac.jp

Manuscript pages (double space including references): **

Figures: 20

Tables: 4

Proposed running title: Argyre basin, Mars.

Editorial correspondence to:

Dr. James M. Dohm

Project Associate Professor

Branch of Space Exploration Education & Discovery (SEED) UMUT (University Museum,
University of Tokyo)

Tokyo, Japan

E-mail: jmd@um.u-tokyo.ac.jp

1 **ABSTRACT.**

2 The geologic history of the multi-ringed Argyre impact basin and surroundings has been
3 reconstructed on the basis of geologic mapping and relative-age dating of rock materials and
4 structures. The impact formed a primary basin, rim materials, and a complex basement structural
5 fabric including faults and valleys that are radial and concentric about the primary basin, as well
6 as structurally-controlled local basins. Since its formation, the basin has been a regional
7 catchment for volatiles and sedimentary materials as well as a dominant influence on the flow of
8 surface ice, debris flows, and groundwater through and over its basement structures. The basin is
9 interpreted to have been occupied by lakes, including a possible Mediterranean-sized sea that
10 formed in the aftermath of the Argyre impact event. The hypothesized lakes froze and
11 diminished through time, though liquid water may have remained beneath the ice cover and
12 sedimentation may have continued for some time. At its deepest, the main Argyre lake may have
13 taken more than a hundred thousand years to freeze to the bottom even absent any heat source
14 besides the sun, but with impact-induced hydrothermal heat, geothermal heat flow due to long-
15 lived radioactivities in early Martian history, and concentration of solutes in sub-ice brine, liquid
16 water may have persisted beneath thick ice for many millions of years. Existence of an ice-
17 covered sea perhaps was long enough for life to originate and evolve with gradually colder and
18 more hypersaline conditions. The Argyre rock materials, diverse in origin and emplacement
19 mechanisms, have been modified by impact, magmatic, eolian, fluvial, lacustrine, glacial,
20 periglacial, alluvial, colluvial, and tectonic processes.

21 Post-impact adjustment of part of the impact-generated basement structural fabric such as
22 concentric faults is apparent. Distinct basin-stratigraphic units are interpreted to be linked to
23 large-scale geologic activity far from the basin, including growth of the Tharsis magmatic-

24 tectonic complex and the growth into southern middle latitudes of south polar ice sheets. Along
25 with the migration of surface and sub-surface volatiles towards the central part of the primary
26 basin, the substantial difference in elevation with respect to the surrounding highlands and
27 Tharsis and the Thaumasia highlands result in the trapping of atmospheric volatiles within the
28 basin in the form of fog and regional or local precipitation, even today. In addition, the impact
29 event caused long-term (millions of years) hydrothermal activity, as well as deep-seated
30 basement structures that have tapped the internal heat of Mars, as conduits, for far greater time,
31 possibly even today. This possibility is raised by the observation of putative open-system pingos
32 and nearby gullies that occur in linear depressions with accompanying systems of faults and
33 fractures. Long-term water and heat energy enrichment, complemented by the interaction of the
34 nutrient-enriched primordial crustal and mantle materials favorable to life excavated to the
35 surface and near-surface environs through the Argyre impact event, has not only resulted in
36 distinct geomorphology, but also makes the Argyre basin a potential site of exceptional
37 astrobiological significance.

38

39 **KEYWORDS:** Mars, Argyre, impact basin; water; early Mars; sedimentary; geology,
40 stratigraphy, geomorphology, sedimentology, lakes, tectonics, glaciation, astrobiology, mapping.

41

42

43

1 **1. Introduction**

2 A detailed reconstruction of the geologic history of the Argyre impact basin and
3 surroundings (30°S to 65°S, 290°E to 340.0°E; **Figs. 1-2**), referred to hereafter as the Argyre
4 province, is presented through a preliminary United States Geological Survey (USGS) map
5 based on stratigraphic, structural, and geomorphic mapping using Viking Orbiter, Mars Global
6 Surveyor (MGS), Mars Odyssey (ODY), and Mars Reconnaissance Orbiter (MRO) data (**Fig. 3**).
7 The Argyre province includes the primary impact basin, basin floor and rim materials, the
8 transition zone (region between the Thaumasia highlands mountain range and the Argyre basin
9 and rim materials), and the southeastern margin of the Thaumasia plateau (**Figs. 1-2**). The large
10 impact event resulted in the construction of the primary Argyre basin and the uplift of a
11 mountainous rim. It also produced deep-seated and shallow basement structures such as radial
12 structurally-controlled valleys and concentric ring scarps, as well as local (i.e., secondary) basins
13 occurring among the rim materials and away from the primary basin and rim materials; impact-
14 related deformation occurred as much as 2,000 kilometers away from the impact site (Dohm et
15 al., 2001a) (**Fig. 2**).

16 Since the formation of the impact basin, erosional and depositional processes have
17 substantially modified the Argyre basin and rim materials, including the emplacement of five
18 major and distinct basin-stratigraphic units (units NAb1, NAb2, NAb3, ANb4b, HAb4a, which
19 are detailed in Section 3.1 and in **Fig. 3 and Tables 1-3**). As shown below, the Argyre impact
20 event has been a significant influence on the geologic and hydrologic history of the region from
21 when the basin formed until now. Unraveling the history of the Argyre province is important to
22 understanding the overall influence of the Argyre impact event on the regional and local geology

23 and hydrology. Being one of the largest impact basins on Mars, it also offers a unique
24 opportunity to peer deep into the crust and upper mantle and to discern hydrological processes
25 and depositional surface environments across a span of billions of years.

26 Previous geologic mapping investigations of all or parts of the Argyre province, which
27 involved data from the Mariner and Viking missions, resulted in: (1) maps of Coprates
28 (McCauley, 1978), Margaritifer Sinus (Saunders, 1979), Argyre (Hodges, 1980), Thaumasia
29 (McGill, 1978), and Mare Australe (Condit, 1978) quadrangles at 1:5,000,000-scale based
30 mainly on Mariner 9 images; (2) the global map of Mars at 1:25,000,000 scale (Scott and Carr,
31 1978) compiled largely from the 1:5,000,000-scale geologic maps; (3) maps of the western
32 equatorial and south polar regions of Mars at 1:15,000,000-scale based on Viking images (Scott
33 et al., 1986-1987); and (4) the Viking-based map of the Thaumasia region at 1:5,000,000 scale,
34 which covers the extreme northwestern part of the Argyre basin (Dohm et al., 2001a).

35 Study of the hydrogeologic evolution of the Argyre province through Viking Orbiter data
36 (images at resolutions ranging from ~50-150 m/pixel) indicated that post-impact basin
37 development has been heavily influenced by lacustrine, fluvial, and glacial processes (Parker,
38 1985, 1989, 1994; Parker and Gorsline, 1991, 1992, 1993; Kargel and Strom, 1992; Parker et al.,
39 2000; Dohm et al. 2001a; Kargel, 2004). These investigations revealed evidence of a broad
40 integration of hydrogeologic activity within the basin extending to headwaters in the highlands
41 south and east of the basin. In particular, the multiple Parker et al. (Parker, 1985, 1989, 1994;
42 Parker and Gorsline, 1991, 1992, 1993; Parker et al., 2000) found evidence for deep water
43 ponding in the basin and water drainage northward both into Argyre from the south and from
44 Argyre through Uzboi Vallis into the northern plains; this included basin filling to a spillpoint
45 (refer to **Figs. 1-3** for locations of highlighted features of interest). In addition, Kargel and Strom

46 (1992) detailed a role of wet-based alpine and continental scale glaciation in southern Argyre and
47 adjoining highlands, with the glacial system extending as far as the south polar region and
48 eastward halfway to Hellas. Baker et al. (1991) suggested a latitude limit of south polar
49 glaciation having been roughly halfway through the Argyre basin, making the southern part
50 glaciated and the northern part unglaciated.

51 Subsequent to these Mariner- and Viking-era mapping investigations, using image data at
52 what is now considered low resolutions, there has not been a new, detailed geologic map
53 produced of the Argyre province using more recently available higher resolution data (e.g.
54 images acquired by the High Resolution Imaging Science Experiment (HiRISE), on MRO, with
55 a scale as small as 0.25 m/pixel). Post-Viking-era topographic, geomorphologic, and
56 spectroscopic investigations (e.g., Hiesinger and Head, 2002; Kargel, 2004; Buczkowski et al.,
57 2008a,b, 2010; Banks et al., 2008, 2009; Jones et al., 2011) have provided helpful information
58 for this investigation.

59 Here, we discuss the results of our systematic geologic mapping of the Argyre province
60 (**Figs. 1-3**). This work will be portrayed in a USGS geologic map product at 1:5,000,000 scale in
61 both digital and print formats (Dohm et al., USGS map, in preparation). Although earlier
62 geologic maps include all or parts of the Argyre province, none focuses on understanding the
63 geologic and hydrologic histories of the province using post-Viking-era data. Additionally,
64 detailed studies that did make use of post-Viking-era data did not make use of a systematic map-
65 based approach and did not encompass the breadth of landscapes mapped in this geologic
66 mapping investigation. We present the stratigraphic, hydrologic, and tectonic histories of the
67 Argyre province as reconstructed from our geologic mapping, with particular focus on: (1)
68 whether the Argyre basin contained lakes; (2) the extent of flooding and glaciation; (3) the origin

69 of the narrow ridges located in the southeastern part of the basin floor and how the ridges fit into
70 the context of the geologic mapping results; (4) the extent of Argyre-related tectonism and its
71 influence on the surrounding regions and conversely the role of tectonics in adjoining regions in
72 affecting the Argyre basin and its deposits; and (5) possible very Late Amazonian modifications
73 by periglacial (cold-climate and non-glacial) processes.

74

75 **2. Geologic setting**

76 The Argyre province (**Figs. 1-3**) is located in the southern cratered highlands, which occur
77 across nearly half of Mars; the highlands comprise the majority of exposed ancient Noachian
78 rocks (Scott et al., 1986-87; Tanaka, 1986; Tanaka et al., 2014). The Martian highlands also
79 contain the Hellas basin and surroundings. Unlike the Argyre province, the latter has received
80 significant attention and is mapped in great detail (e.g., Crown et al., 1992; Mest and Crown,
81 2001; Leonard and Tanaka, 2001; Moore and Wilhelms, 2007; Glamoclija et al., 2011).

82 The southern highlands display geologic terrains that involved high rates of geologic and
83 hydrologic activity during the Noachian Period (e.g., Scott et al., 1986-87; Tanaka, 1986; Tanaka
84 et al., 1988, 2014; Dohm et al., 2001a, 2013; Hartmann and Neukum, 2001; Hynek et al., 2010).
85 Dynamic activity, including mountain building, formation of structurally-controlled basins, and
86 possible plate tectonism (Sleep, 1984; Maruyama et al., 2001a; Dohm et al., 2001c, 2002a,
87 2005a, 2013; Anguita et al., 2001; Fairén et al., 2002; Baker et al., 2002, 2007; Fairén and
88 Dohm, 2004; Connerney et al., 2005; Yin, 2012a,b), is pronounced prior to the incipient
89 development of the Tharsis rise, a long-lived (nearly 4.0 Ga) magmatic complex (Dohm et al.,
90 2001b; Anderson et al., 2001), interpreted here to be a superplume (Maruyama et al., 2001b,
91 2008; Dohm et al., 2001d, 2007a; Baker et al., 2002, 2007). This pre-Tharsis activity is also

92 prominent before the Argyre, Hellas, and Isidis impact events (Dohm et al., 2002a,b, 2005a,
93 2013; Baker et al., 2002). This dynamic activity was followed by sporadic magmatic, tectonic,
94 climatic, and hydrologic activity driven mainly by endogenic activity from the growth of Tharsis
95 superplume until present-day (Dohm et al., 2007a; Baker et al., 2007) (**Fig. 4**), but also by the
96 giant impact events such as Argyre, and to the development of the Elysium superplume (Baker et
97 al., 2007). Other influences including changes in the spin axis magnitude and precession and
98 orbital eccentricity of Mars (Touma and Wisdom 1993, Laskar et al. 2004), steadily brightening
99 solar luminosity (Kasting et al. 1993), and volatile releases from other large impacts (Segura et
100 al., 2002) also have contributed to climate change and the geomorphology and surficial deposits
101 of Mars (Head et al. 2003, Kargel 2004).

102 Dominant in the geologic, hydrologic, and climatic histories of Mars since its incipient
103 development, Tharsis superplume locates to the northwest of and adjacent to the Argyre basin.
104 Based on topographic, stratigraphic, paleoerosional, and paleotectonic information, Tharsis is
105 interpreted to have recorded five major stages of magmatic-driven activity (**Fig. 4**) (for details on
106 the major stages of development of Tharsis, please refer to Dohm et al. (2001b, 2007a, 2009a)
107 and Anderson et al. (2001), and for general stratigraphic information and time-chronologic
108 information of Tharsis and the rest of Mars, the new global map of Mars by Tanaka et al.
109 (2014)). The five major stages of development and a representative features of each stage (from
110 oldest to youngest with some overlap largely due to uncertainty in the crater statistics) include:
111 Stage 1 (Early to Middle Noachian)—Tharsis basin with subsequent uplift of the Thaumasia
112 Plateau and incipient development of Syria Planum; Stage 2 (Late Noachian to Early
113 Hesperian)—opening of Valles Marines cutting the northern part of the Thaumasia Plateau, as
114 well as major development of Syria Planum; Stage 3 (Early Hesperian)—early development of

115 the prominent volcanoes of Tharsis Montes and Alba Mons; Stage 4 (Late Hesperian to Early
116 Amazonian)—major magmatic outgassing of Tharsis, including related major growth of the Alba
117 Mons, Olympus Mons, the Tharsis Montes, and associated major incisement of the circum-
118 Chryse outflow channel system that began to form as early as and associated with major Stage 2
119 Tharsis activity; and Stage 5—(Amazonian) all of the components of Tharsis forged by this time
120 with concentrated magmatic-driven tectonic activity in parts into the Late Amazonian.

121 These five major thermal pulses of Tharsis activity, which includes magmatism and
122 associated release of volatiles, major outflows, inundations of the northern plains to form oceans,
123 and hydrological cycles, have manifested themselves at regional and possibly global scales at
124 least since the Middle Noachian epoch (**Fig. 4**). This includes the influence of the topography
125 and stratigraphy of the northern plains (Tanaka et al., 2005), which correlate with the timing of
126 the major pulses (Fairén et al., 2003). In the new global geologic map of Mars by Tanaka et al.
127 (2014), the Hesperian and Noachian transition unit (unit HNt) links to Stages 1 and 2 (i.e., larger
128 and older ocean; Fairén et al., 2003), the Early Hesperian transition unit (unit eHt) to Stages 2
129 and 3 (i.e., either the waning of the larger and older ocean, or possibly another ocean-inundation
130 phase of the northern plains; Fairén et al., 2003), and the regional Late Hesperian lowland unit
131 (unit lHl) and Late Hesperian transition unit (unit lHt) to Stages 4 and 5 (i.e., the smaller ocean
132 inset within the larger older ocean; Fairén et al., 2003). Tharsis-driven activity has also been a
133 major influence on the adjacent Argyre impact basin and surroundings as revealed in this
134 geologic investigation.

135 The primary Argyre impact basin is more than 1,200 kilometers in diameter and more than 4
136 kilometers in depth (**Fig. 2**). The basin formed during the Noachian Period, or an absolute age
137 estimated to be ~3.93 Ga (Robbins and Hynek, 2012; Robbins et al., 2013); the upper terminus

138 of the Noachian Period (see Tanaka et al. (2014) for details and references therein) is estimated
139 to have started at about 3.85 Ga (Hartmann, 2005) or 3.83 Ga (Ivanov, 2001; Hartmann and
140 Neukum, 2001). Argyre is the best preserved of the large multi-ringed impact basins on Mars,
141 comparable to the ~ 327 km-diameter Orientale basin of the Moon when viewed at resolutions
142 less than one kilometer per pixel. The profound differences of the Argyre and Orientale basins
143 due to pervasive post-impact modification of the former by geologic, hydrologic, and aeolian
144 processes, are evident at higher resolutions. Unlike the Moon, there is no absolute radiometric
145 chronology of Mars. However, a wide range of circumstantial evidence, including
146 comprehensive impact crater statistics, points towards the formation of Argyre, and similar large
147 Martian basins (including Hellas and Isidis), at about the same time as large and distinct multi-
148 ring impact basins on the Moon such as Oriental (*i.e.*, somewhere between about 3.8-4.0 billion
149 years ago) (based on Wilhelms (1987) for the Moon and Robbins and Hynes (2012) and Robbins
150 et al. (2013) for Mars).

151 Compared to the Hellas basin, which is estimated to have formed at about 4.0 Ga, the
152 Argyre basin, occurring nearly 70 million years later than the Hellas impact event (both
153 estimated ages based on Robbins et al. (2013)), is much more pristine than Hellas, including the
154 impact-induced radial and concentric structures that can be more readily mapped and
155 characterized (Dohm et al., 2002a). This difference in degradational state is interpreted to mark
156 major changing planetary conditions at a time when the internal dynamo of Mars had shut down
157 due to planetary cooling, putative plate tectonism was nearing its end, and the atmosphere was
158 thinning (Baker et al., 2007).

159 Other basin examples, though much older than Hellas, include putative Utopia (e.g., McGill,
160 1989) and Arabia Terra (Dohm et al., 2007b) impact basins, largely subdued to the untrained

161 eye. The putative Arabia Terra basin, for example, is not visible in present-day topography, but
162 its hypothesized existence is supported by distinct characteristics such as stratigraphy,
163 physiography, paleotectonism, and geomorphology, as well as notable structural, albedo, thermal
164 inertia, gravity, magnetic, and elemental signatures (Dohm et al., 2007b). Similarly, ancient
165 basins on Earth, particularly those tectonically-derived, that have been all but destroyed, are
166 revealed through geologic investigation. Another example of an ancient, heavily eroded basin is
167 the Chryse impact basin infilled by sediments derived from adjoining chaotic terrains and
168 outflow channels (Rotto and Tanaka 1997; Rodriguez et al. 2011). There are also relatively large
169 features referred to as quasi-circular depressions interpreted to be impact in origin (Frey et al.,
170 2002). Similar to Hellas, the younger Argyre impact event appears to have taken place after the
171 shutdown of the planetary dynamo; the remanent magnetic anomalies (Acuña et al., 1999, 2001;
172 Connerney et al., 1999, 2001; Arkani-Hamed, 2003, 2004; Roberts et al., 2009; Roberts and
173 Arkani-Hamed, 2012), distinct in the extremely ancient geologic provinces of Mars (e.g., Terra
174 Cimmeria, Terra Sirenum, Arabia Terra, Xanthe Terra, and the Thaumasia highlands and
175 Coprates rise mountain ranges), are not observed in and nearby the giant impact structure (Dohm
176 et al., 2005, 2013). “Extremely ancient” refers to pre-Hellas Mars, or estimated to be > 4.0 Ga
177 (Robbins et al., 2013), equivalent to the Hadean of Earth, of which the rock record has been all
178 but destroyed aside from traces, such as zircon grains in meta-sandstones (Harrison, 2009). There
179 are other post-dynamo-shutdown geologic provinces such as Tharsis, Syrtis, Malea Planum, and
180 Tyrrhena/Hadriaca volcanic provinces and the northern plains, which includes the
181 Tharsis/Elysium corridor region (Dohm et al., 2008, 2013). The termination of the global
182 magnetic field may have occurred between the formation of Ladon and Hellas impact basins
183 (Lillis et al., 2008) and the formation of Ladon and Prometheus basins (**Fig. 1**), the latter of

184 which is dated to be older than Hellas through comprehensive global crater statistics (Robbins et
185 al., 2013).

186 The multi-ringed Argyre impact structure appears to have influenced the geophysical and
187 geological development of a large part of Mars. This includes modification of the southeastern
188 part of the Thaumasia plateau and control of the Uzboi drainage system and other systems of
189 surface and subsurface movement of liquid water and water-ice (Parker and Gorsline 1991, 1993;
190 Kargel and Strom, 1990, 1992; Dohm et al., 2001a, 2011a; Kargel, 2004;). The influence of the
191 Argyre impact has even been proposed to have fixed the location of the Tharsis superplume
192 through impact-induced subduction and slab rollback during an incipient plate tectonic period
193 (Yin, 2012a). Though the onset and origin of Tharsis still remains in question according to
194 various working hypotheses, such as focused subduction of hydrated crustal slab materials
195 (Baker et al., 2007), the Argyre impact event and the development of the Tharsis superplume had
196 an influence on one another. While the Argyre impact influenced the development of the
197 southeast margin of the Thaumasia plateau, Tharsis-superplume-driven outgassing, flooding, and
198 associated climate and environmental change significantly contributed to the modification of the
199 Argyre basin (**Figs. 2 and 4**).

200 Impact-induced features such as rim-forming mountains (e.g., the Charitum and Nereidum
201 Montes), local basins among the mountains, radial and concentric structures (including valleys),
202 and the primary basin floor have all been altered by diverse processes since their formation both
203 within and outside of the Argyre province. These include magmatic, impact cratering, tectonic
204 (e.g., reactivated basement structures), eolian, fluvial, alluvial, colluvial, periglacial, glacial, and
205 lacustrine (e.g., Parker, 1985, 1989, 1994; Scott et al., 1986,87; Tanaka, 1986; Parker and
206 Gorsline, 1991, 1992, 1993; Kargel and Strom, 1992; Dohm and Tanaka, 1999; Parker et al.,

207 2000; Hiesinger and Head, 2002; Siebert and Kargel, 2001; Banks et al., 2008, 2009; Jones et al.,
208 2011; Soare et al., 2012a, 2014a, 2014b; El Maarry and Dohm, 2013; El Maarry et al., 2013).
209 Geologically recent activity is highlighted by high-resolution data sets such as the Context
210 Camera (CTX) at ~6 m/pixel and the High Resolution Imaging Science Experiment (HiRISE). It
211 has involved liquid water, water-ice, and wind that suggest distinct and significant changes in
212 regional environmental conditions (including both surface and near-surface modifications in
213 temperature, moisture, hydrology, and surface morphology) generally in geologically recent
214 time, including the very Late Amazonian (within the last roughly thousands of years) (e.g., El
215 Maarry et al., 2013; Soare et al., 2014a,b).

216 Henceforth, “geologically recent activity” refers to Middle Amazonian and younger activity.
217 This is in part based on the superposed crater counts (i.e., those impact craters which are
218 superposed and pristine with distinct rims and ejecta blankets that are not visibly resurfaced) of
219 many of the units in the Argyre province shown in Table 3, which give crater-retention ages of
220 Late Hesperian and Early Amazonian epochs. This retention age is coeval with major Tharsis-
221 driven activity during the Late Hesperian and Early Amazonian epochs (i.e., Stages 4 and 5; **Fig.**
222 **4**). In a marked shift from most Viking Orbiter-era geochronologies of Mars, in recent years it
223 has been increasingly evident that intensive or widespread episodes of Martian hydrogeologic
224 activity took place at intervals throughout the Amazonian, even into the very Late Amazonian
225 (Kargel et al., 1995; Head et al., 2003; Madeleine et al., 2009; Skinner et al., 2012; Rodriguez et
226 al., 2014). Thus, “geologically recent” should be considered here as activity correlative in time
227 with the latter part of Stage 5 Tharsis activity (schematically depicted in Fig. 4 through a
228 narrowing of the solid area representative of decreased Stage-5 activity). Other processes
229 documented during recent years include seasonal deposition and sublimation of a thin CO₂ ice

230 cover and locally intense and frequent dust devils which distinctly leave their marks (Kargel,
231 2004). The rich and diverse history of the Argyre province, and its far-reaching record in terms
232 of both time and space at local to regional and even global scales, is detailed below.

233

234 **3. Mapping investigation**

235 ***3.1 Mapping overview and data***

236 Geologic units and tectonic and erosional structures primarily were identified and mapped
237 using Odyssey Thermal Emission Imaging System (THEMIS) data (100 m/pixel near-infrared
238 (IR) daytime and nighttime images and 18 m/pixel visible multi-band images) (Christensen et al.,
239 2004), images from the HiRISE camera (McEwen et al., 2007) and CTX on MRO (Malin et al.,
240 2007), and Viking Mars Digital Image Mosaic 2.1 information (generally 100 m-200 m/pixel)
241 (e.g., Archinal et al., 2002, 2003).

242 The MGS Mars Orbiter Laser Altimeter (MOLA) has provided an unprecedented
243 topographic information in the form of a digital-elevation model at 1/128° resolution (~460
244 m/pixel) (e.g., Smith et al., 1999). The MOLA data have helped: (1) define stratigraphic units;
245 (2) determine the stratigraphic relations among the map units; (3) evaluate whether an impact
246 crater or deposit was superposed or embayed or partly buried; and (4) assess spatial and temporal
247 relations among map units, structures, terraces, valleys incised into existing valleys at distinct
248 elevation ranges around parts of the basin, and possible equipotential surfaces.

249 Geologic information was assembled into a Geographic Information System (GIS) database,
250 which enables the attribution of individual geologic features according to type and size,
251 comparative analysis of the spatial and temporal relations among the rock outcrops and

252 topography (**Fig. 5**), and area calculations of the map units for compiling crater statistics (**Tables**
253 **1 and 3**).

254 The materials of the Argyre province are divided into 20 distinct geologic units, as discussed
255 in Section 4.2, shown in **Fig. 3**, and detailed in **Tables 1-3**. The map units are categorized into
256 Argyre basin stratigraphic units (units HAb4a, NAb4b, NAb3, NAb2, and NAb1, in which H
257 refers to the Hesperian Period, N—Noachian Period, Ab—Argyre basin materials divided into
258 members 4a, 4b, 3, 2, and 1), Argyre rim materials (units NAr, NArb, NAbr, and NArsp, in
259 which N refers to the Noachian Period, A—Argyre, r—rim, b—basin, and sp—smooth plains),
260 highlands materials (units AHtp, HNTh, HNh4, HNh3, Nhb, Nh2, and Nh1, in which A refers to
261 the Amazonian Period, H—Hesperian Period, N—Noachian Period, tp—Thaumasia plateau,
262 Th—Thaumasia highlands, and h—highlands divided into members 4-1), and impact crater
263 materials post-dating the Argyre impact event (units C1, C2, Cfs, and Cfr, in which C stands for
264 crater, C1—older crater materials, C2—younger crater materials, Cfs—smooth crater floor
265 materials, and Cfr—rough crater floor materials) (**Fig. 3, Tables 1-3**). The map units are
266 delineated based on stratigraphic relations, topography, and morphologic characteristics.
267 Morphologic characteristics include albedo and bedform types such as valleys, terraces,
268 knobs/massifs/plateaus, ridges, scarps, flow features, and pristine and highly degraded impact
269 craters and other topographic lows such as Argyre-induced topographic basins.

270 By merging daytime THEMIS data and MOLA topography, distinct topographic levels with
271 spatially associated bedforms were observed, aiding in the identification, characterization, and
272 mapping of the basin units. The geologic contacts of the basin units are generally gradational due
273 to major resurfacing through time, and have been delineated approximately on the geologic map.
274 For example, there are distinct topographic levels evident where valleys incise into older valley

275 segments often at terraces and erosional scarps. These topographic levels are particularly distinct
276 along the floors of the three valleys that debouch into the southern and southeast parts of the
277 Argyre basin; from west to east, they are: Surlus Vallis, Dzigai Vallis, and Nia Valles,
278 respectively (**Figs. 3 and 6**). These levels are interpreted to indicate changing hydraulic head
279 (depth to the water table) and associated major changes in basin conditions.

280 The relative ages of rock materials were derived from stratigraphic and structural relations
281 and crater densities. The formal stratigraphic systems (Noachian, Hesperian, and Amazonian)
282 devised by Scott and Carr (1978) and the series (upper, middle, and lower divisions of systems)
283 defined by Tanaka (1986) are used in this work.

284 The stratigraphic, hydrologic, and tectonic histories in the Argyre province, as discussed in
285 Section 4, are based on stratigraphic and crosscutting relations among rock materials and
286 structures (*i.e.*, that are tectonic, erosional, and depositional in origin), and relative ages are
287 further constrained through detailed impact crater investigations detailed in the following Section
288 3.2. We mapped the stratigraphy and structure including: channels, troughs, scarps, broad ridges,
289 wrinkle ridges, crater rims, lineaments that may have a tectonic origin, graben, and faults.
290 Mapped tectonic features with lengths ranging from hundreds of kilometers to more than a
291 thousand kilometers are referred to as macrostructures and are interpreted to be major deep-
292 seated (lower crust and possibly upper mantle) dislocations (faults) produced by the giant Argyre
293 impact event and other dynamic geologic activity mostly prior to the development of Tharsis.

294

295 **3.2 Impact crater dating**

296 To evaluate the formation and modification ages of the Argyre rock units, crater statistics
297 were compiled for 16 of the 20 units; this accounted for approximately 90% of the map region

298 (Tables 1 and 3, and corresponding Fig. 3). Impact craters with diameters generally > 50 km
299 and their associated ejecta blankets were mapped, but crater statistics not tallied. This included
300 units C1 (older crater materials), C2 (young crater materials), Cfr (rough crater floor materials),
301 and smooth crater floor materials (Cfs). This age information was derived by counting all craters
302 having rim diameters larger than or equal to 3 km and by calculating unit areas from our digital
303 geologic map (Fig. 3). The crater populations were compiled using the global data base of
304 Robbins and Hynek (2012). At the time of the compiling, the global data base was complete for
305 impact craters with diameters down to 3 km. Thus, our counts included those craters with
306 diameters ≥ 3 km.

307 Though crater statistics used in geologic investigations often include impact craters with ≥ 2
308 km (e.g., Scott et al., 1986-87), we believe that ≥ 3 km-diameter craters are better for assessing
309 the minimum relative ages of the rock materials. We have greater confidence using larger
310 diameter craters for determining the minimum relative ages of the rock materials due to the
311 major resurfacing reported here for the Argyre province; i.e., part of the crater populations have
312 been destroyed by magmatic-, tectonic-, water-, wind-, gravity- (e.g., colluvial deposition),
313 and/or subsequent impact-driven resurfacing especially at smaller diameters. Results of Irwin et
314 al. (2013) point to major resurfacing and destruction of crater populations on Mars during the
315 Noachian Period, highlighted through stratigraphy and impact crater statistics; this geologic
316 investigation of the Argyre province shows that the Argyre impact event among other activity
317 would have contributed to the resurfacing of extremely ancient terrains, which includes
318 destruction of part of the global crater population. Barlow (1990, 2004, 2005) reported greater
319 confidence using larger impact craters (> 5 km) for relative-age dating, also because of the
320 recognized major resurfacing. Here, we have compiled cumulative crater densities for 3-km-

321 diameter, 5-km-diameter, and 16-km-diameter impact craters (**Table 3**). Kargel et al. (1995)
322 considered the crater population in southern Argyre Planitia larger than 4 km diameter to be
323 indicative of the basement rock materials or early massive basin deposits, whereas the crater
324 population between 1.0 and 1.41 (square-root of 2) km to be indicative of modification (e.g., by
325 glacial and lacustrine processes). Similar to those findings, 2 km-diameter and smaller diameter
326 impact craters have been shown to be useful in analyzing resurfacing ages (Platz and Michael,
327 2011; Platz et al., 2013). In a study related to this geologic investigation, detailed analysis using
328 HiRISE and CTX images of parts of the basin included counts down to 50-meter-diameter
329 craters (El Maarry et al., 2013).

330 The crater statistics consist of total crater populations (including partly buried, degraded,
331 and pristine impact craters), which may indicate minimum emplacement ages (since part of the
332 population is destroyed due to resurfacing through time). The crater statistics also include
333 pristine craters only (*i.e.*, craters and their associated ejecta blankets that have not been visibly
334 resurfaced at resolution, which includes dissection, tectonic deformation, or partial burial by lava
335 flows and fluvial, alluvial, and colluvial deposits), which indicate ages of Hesperian and
336 Amazonian resurfacing depending on the particular map unit and estimated absolute chronology
337 systems (**Table 3**). A similar approach proved to be useful in unraveling the geologic evolution
338 of the Thaumasia region (Dohm et al., 2001a). In addition, our approach of defining primary
339 depositional and modification ages based on total crater populations and pristine-only crater
340 counts is somewhat similar to that employed by Kargel et al. (1995). Though, here we have
341 much more robust results afforded through the combined comprehensive mapping, GIS-based
342 area calculations of the map units for compiling crater statistics, and usage of THEMIS, CTX,
343 and MOLA data, in addition to Viking data.

344 Cumulative size-frequency diagrams (SFDs) were created (Crater Analysis Techniques
345 Working Group, 1979) and isochrons were fitted from both the Hartmann (2005) and Neukum et
346 al. (2001) production functions (**Table 3**). Estimated absolute ages are based on the Hartmann
347 (2005) and Neukum et al. (2001) chronology systems. These ages were assigned a range of
348 chronostratigraphic epochs based on the boundaries defined in Neukum et al. (2001), Hartmann
349 (2005), and Werner and Tanaka (2011), and compared with that shown in Tanaka et al. (2014)
350 (**Table 3**). This range of assignments is an attempt to encompass the uncertainty and error
351 inherent in the varied models, conservatively. As with all crater counts, these should be treated as
352 an approximate guide, and the relative differences between each unit are more certain than the
353 actual model ages (for more discussion, see section 4.2 of Robbins et al. (2013)). Also, a part of
354 the crater populations of the ancient terrains (particularly Early Amazonian or older) have been
355 destroyed, and thus the range of chronostratigraphic epochs for a specific unit includes the rock
356 materials with estimated minimum age of emplacement and subsequent modification.

357 Using THEMIS, CTX, and MOLA data, a total of 82 impact craters (**Table 4**) were either
358 deleted from the total count of a specific geologic unit (if embayed or buried by the geologic-unit
359 materials) or added to older adjacent polygons (if they formed part of the basement of an
360 adjacent unit). For example, an impact crater that forms part of the floor of a glaciated valley but
361 is embayed and partly buried by valley-fill materials was not included in the valley-fill materials;
362 instead, it was compiled with the valley-forming materials. The valley infill deposits would
363 otherwise be errantly given older ages. Such a revision to crater populations of specific unit
364 polygons is unique from existing geologic mapping investigations, as the total number of impact
365 craters are normally tallied for determining the relative age of the rock materials without scrutiny
366 of whether they are associated with underlying materials.

367 The geologic information was critical for estimating ages of several of the units. For
368 example, unit HAb4a includes major emplacement of materials within the primary Argyre basin
369 from Late Hesperian activity, with underlying basin materials extending at depth to the basin
370 floor emplaced by earlier post-Argyre-impact activity, including Argyre-impact-related lake
371 formation and subsequent climate/environmental conditions detailed below; i.e., part of the
372 impact population includes exposed parts of the underlying craters and their rims. Coupled with
373 the stratigraphic and cross-cutting relations, identification of the superposed (i.e., pristine and not
374 visibly resurfaced; **Table 3**) >3-km-diameter impact craters using CTX data clearly indicates that
375 a late stage of major resurfacing occurred during the Late Hesperian and Early Amazonian
376 epochs, corresponding to Stages 4-5 (Late Hesperian-Early Amazonian) Tharsis development
377 (**Fig. 4**).

378

379 **4. Discussion**

380 Here we give a brief overview of pre-Argyre and Argyre impact activity in the Argyre
381 province. We then discuss: (1) the stratigraphic record of the Argyre province; (2) the basin
382 conditions through time since the Argyre impact event, such as ancient surface modification
383 including the timing and origin of the putative eskers located in the southeast part of the basin
384 floor, new evidence for a paleolake within the Argyre basin that sourced Uzboi Vallis, and
385 geologically-recent surface modification; and (3) the extent of Argyre-related tectonism and its
386 influence on the surrounding regions, which includes a geophysical perspective.

387

388 ***4.1. Overview of pre-Argyre and Argyre impact activity***

389 The giant Argyre impact event led to major resurfacing of the extremely ancient cratered
390 highlands in the Argyre province, which includes destruction of the remanent magnetic
391 signatures (Acuña et al., 1999, 2001; Connerney et al., 1999, 2001; Arkani-Hamed, 2003, 2004;
392 Roberts et al., 2009; Roberts and Arkani-Hamed, 2012). Pre-Argyre deformation and uplift of
393 the extremely ancient crustal materials included the formation of extremely ancient mountain
394 ranges (*e.g.*, the Thaumasia highlands and Coprates rise; **Figs. 1-2**), marking a dynamic ancient
395 phase (*i.e.*, during an active dynamo (Baker et al., 2007; Dohm et al., 2013; Ruiz, 2014)) of
396 Mars. This includes major crustal contraction and shortening exemplified by thrust faults
397 (Schultz and Tanaka, 1994; Dohm et al., 2001a, 2002a; Nahm and Schultz, 2011) and other
398 prominent features (Dohm and Maruyama, 2014a; Dohm et al., 2014a,b).

399 The Argyre impact resulted in the formation of the primary Argyre basin, rim materials,
400 deep-seated basement structures including faults, and structurally-controlled valleys and basins
401 which have routed subsurface and surface water and rock materials. In addition, the impact event
402 appears to have deformed the Thaumasia highlands mountain range and the southeast part of the
403 Thaumasia plateau, as their southeast margins parallel the shape of the basin and outer ring
404 structures (Dohm et al., 2001a) (**Figs. 1-2**). The Thaumasia highlands comprise distinct remanent
405 magnetic signatures, large tectonic structures, and a relatively high density of impact craters
406 distinct from the younger Tharsis lavas to the north-northwest and Argyre impact basins and
407 mesas to the south-southeast.

408

409 ***4.2. Overview of the stratigraphic record***

410 The oldest units of Early-Middle Noachian age consist of ancient, heavily cratered rock
411 materials that form plateaus, hills, rugged mountains such as of the Thaumasia highlands

412 mountain range which extend west to east for nearly 2,400 km, approximately the length of the
413 Himalayas, prominent ridges, and highly degraded crater rims (unit Nh1; see **Tables 1-3** and **Fig.**
414 **3** for this and other units) away from the Argyre basin and rim. A relatively small part of the
415 Thaumasia highlands, located in the northwest part of the map region, is composed of mountain-
416 range-forming materials, which have been highly modified by water-, wind-, gravity- magmatic-,
417 and tectonic-driven activity and impact cratering. These materials have been mapped as unit
418 HNTh, and interpreted as highly resurfaced basement complex, among other materials associated
419 with the formation of an orogenic complex (**Table 2**).

420 This varied landscape was likely blanketed by ejecta from the Argyre impact event, at least
421 within the Argyre province. Complex modification of these ancient rock materials due to
422 cratering, tectonic deformation, erosional processes, and volcanic and sedimentary burial has
423 degraded or destroyed many of the older morphologic features. This includes a substantial
424 proportion of the superposing crater populations, which makes it difficult to constrain the onset
425 of unit formation (see Section 3.2). Thus, in many cases, morphologic features and rocky mantles
426 postdating the rock-unit materials characterize the surfaces of these ancient units.

427 The giant Argyre impact event created distinct rim materials, mapped as units NAr, NArb,
428 NAbr, and NArsp, likely excavated from deep within the mantle, and/or including primordial
429 lower crustal materials transferred at and near the Martian surface by the impact event and
430 associated overturn and inversion of stratigraphy. Subsequently they were sculpted by liquid
431 water, water-ice, wind, and mass wasting. The impact also formed a primary basin, which served
432 as a catchment of rock materials and water since the event. Source regions of the materials and
433 water include the nearby rim materials to at least as far away as Tharsis to the northwest and the
434 South Pole to the south.

435 There are several indications of a high-standing lake that fed the Uzboi system, supportive
436 of the original hypothesis presented through the multiple Parker et al. (Parker, 1985, 1989, 1994;
437 Parker and Gorsline, 1991, 1992, 1993; Parker et al., 2000). Distinct from this original
438 hypothesis, which includes the system having formed at a time when there reportedly was
439 change from a warm/wet climate to a drier climate that allowed surface water (channels and
440 lakes) during the Late Noachian (see Parker, 1996), this geologic investigation points to the
441 Argyre lake-Uzboi system having formed much earlier due to the giant Argyre impact event and
442 the associated regional melting of ice (water inundation in the Argyre province maps out at least
443 within the dark blue regions shown in **Fig. 1**). The indications include impact-crater retention
444 ages of the high-standing materials in the primary basin identified, mapped, and interpreted to be
445 the oldest basin-filling materials emplaced through major hydrological and environmental
446 change directly associated with the giant impact event, which includes lake formation (i.e.,
447 member 1 of the Argyre basin infill materials designated as unit NAb1; **Fig. 3 and Tables 1-3**).
448 Also, there are spatial associations (including stratigraphic and elevation) among the source
449 region of Uzboi Vallis, terraces, benches, a possible spillway of a local basin shown in **Figs. 7**
450 **and 8**, and the mean elevation of unit NAb1 (**Fig. 5**), all of which near an elevation of 0 km (as a
451 potential equipotential surface (compare **Figs. 5-9**)). The close timing of the Argyre impact event
452 and lake formation is corroborated by similar crater retention ages amongst the Argyre-rim
453 materials (*e.g.*, units NAb1 and NAb2) and the older, higher-standing unit Nab1 materials. An
454 older retention age of the latter (see **Table 3**) could be explained by the rim-forming materials
455 having undergone greater erosion due to their greater relief. An extensive impact-associated lake
456 could have existed well above 0 km, nearing an elevation of 1.5 km. This is particularly evident
457 when using GIS to visualize the potential water extent beyond the primary Argyre basin, which

458 includes mapped elongated basins with valley networks along their margins and dendritic valleys
459 (**Fig. 9**), further detailed in Section 4.3.2.

460 In addition to the primary basin resulting from the Argyre impact event, local structurally-
461 controlled basins also formed among rim materials and adjacent to the primary basin and its rim,
462 as well as served as catchments for liquid water, water-ice, and sediments. For example,
463 drainages, which include valley networks, mark the margins of and debouch into many of the
464 local basins indicating that many contain sedimentary, lacustrine, and evaporite deposits, mapped
465 as units NHb and NArsp (*e.g.*, **Figs. 3, 7-8**; See also Section 4.3). Hydrothermal deposits related
466 to the Argyre impact event, eolian deposits sourcing from nearby (rim materials) and distant
467 provenances (*e.g.*, Tharsis), and lower crustal materials and/or upper mantle materials also likely
468 contribute to the rim materials and basin infill deposits of the basins structurally controlled by
469 the Argyre impact. Consistent with this is the CRISM-based identification of olivine, prehnite,
470 chlorite, low-calcium pyroxene, high-calcium pyroxene, and phyllosilicates such as iron-
471 magnesium smectite among some of the local basins and rim materials, as well as parts of the
472 primary basin margin (**Figs. 10-11**; also see Poulet et al., 2007; Buczkowski et al., 2008a,b,
473 2010; Lane and Goodrich, 2010; Ody et al., 2012). In addition, phyllosilicates are relatively
474 common in the cratered highlands as observed by both Omega instrument onboard the Mars
475 Express spacecraft (*e.g.*, Bibring et al., 2004, 2005; Poulet et al., 2005, 2007) and CRISM
476 instrument onboard the Mars Reconnaissance Orbiter (Murchie et al., 2007, 2009a,b; Mustard et
477 al., 2008), and in particular, exemplified in structurally-controlled basins such as in Terra
478 Sirenum (*e.g.*, Davila et al., 2011) and those Argyre-impact-induced in the Argyre province (*e.g.*,
479 Buczkowski et al., 2008b).

480 Following the Argyre impact event, climatic perturbations away from the prevailing cold
481 and dry conditions (Fairén et al., 2003; Baker et al., 2007; Hynes et al., 2010; Rossi et al., 2011),
482 related to the major stages of growth of the Tharsis superplume such as exemplified by the
483 opening of Valles Marineris, major activity at Syria Planum, and the uplift of Thaumasia plateau
484 and associated circum-Chryse and putative northwestern slope valleys development (Stages 1-3
485 of Tharsis evolution as shown in **Fig. 4**), resulted in transient hydrological cycling and related
486 dynamic landscape modification of the Argyre province. This included major etching of the rim
487 materials, units NAr, NArb, NAb, NArsp, as well as resurfacing of the cratered highlands away
488 from the Argyre rim materials, such as the rock materials of unit Nh1 which includes extremely
489 ancient crustal materials which were blanketed by extensive Argyre impact ejecta in the Argyre
490 province. Resurfacing of the ancient cratered highland materials included erosion and the
491 emplacement of deposits on the Argyre-impact-controlled landscape well into the Hesperian
492 Period, contributing to units Nh1-Nh3, HNh4, Nhb, HNTh, AHTp. Both endogenic and exogenic
493 activity contributed to the resurfacing of the terrains within and marginal to the Argyre basin and
494 rim materials, including precipitation and the growth of glaciers and the formation of gullies
495 within impact craters, even into the very Late Amazonian epoch (El Maarry et al., 2013; Soare et
496 al., 2014a,b).

497 Associated with the major resurfacing described above are Argyre basin infill deposits (units
498 NAb2, NAb3, NAb4b, and HAb4a) which overly unit NAb1 materials, as the Argyre basin has
499 served as a large repository of the eroded Argyre rim materials and cratered highland materials
500 away from the rim materials following the Argyre impact event. The spiked hydrologic activity
501 related to Tharsis activity resulted in the migration of groundwater and surface water and the
502 eventual formation of ice-covered lakes which would wane in volume and transition into frozen

503 ice bodies, as well as the growth of glaciers, but to a lesser extent than the former impact-
504 induced lake. Pronounced growth of Argyre's neighboring prominent Martian feature, Tharsis
505 superplume, during the Middle Noachian to Early Hesperian, had accompanying flooding, ocean
506 formation, hydrological cycling, and dissection of the Martian landscape which included the
507 rugged rim materials. This Tharsis-driven resurfacing shed materials into the basin distinctly
508 recorded in units Nab2, Nab3, and Nab4b (see **Table 2** for details, including descriptions and
509 interpretations).

510 Near the upper left corner of the geologic map shown in **Fig. 3**, at an apparent break
511 between the Thaumasia highlands and the Coprates rise mountain ranges near the southeastern
512 margin of the Thaumasia plateau, networking troughs source from a rift system. The troughs
513 appear to dissect friable materials interpreted to be ignimbrites (unit HNplt of Dohm et al.,
514 2001a—see Fig. 9a), mapped and identified here as unit AHtp of the Thaumasia plateau. Such
515 geologic and hydrologic activity (including fluvial, alluvial, colluvial, and glacial), which
516 includes the formation of the troughs, resulted in a transferal of water and rock materials from
517 the Thaumasia highlands and Coprates rise mountain ranges and the Thaumasia plateau to the
518 transition zone at lower elevations (**Figs. 1-2**). The emplacement of the materials along the break
519 in slope is evident by partial burial of wrinkle ridges, with only ridge crest exposed in places.

520 Major Tharsis activity during the Late Hesperian (Stage 4) included major outgassing
521 associated with the development of the Tharsis Montes shield volcanoes, Olympus Mons, and
522 Alba Mons, as well as rapid emplacement of circum-Chryse floodwaters and sediments to form
523 an ocean inset within the extent of the previous larger ocean and associated hydrological cycling
524 (Baker et al., 1991; Fairén et al., 2003). This would have driven environmental change in the
525 giant catchment basin, resulting in the emplacement of fluvial, lacustrine, and glacial deposits on

526 the basin floor, mapped and defined as unit HAb4a. Unit HAb4a records the final major
527 sedimentary sequence in the Argyre basin, with the deeper floor deposits underlying this unit
528 likely to be related to the initial Argyre-impact-related lake (unit Nab1) and Stages 1-3
529 (Noachian-Early Hesperian) of Tharsis development (**Fig. 4**), correlating in age with units Nab2,
530 NAb3, and NAb4b (unit NAb4b occurs along a part of the northern and northeastern margins of
531 the central basin floor materials, being distinctly embayed by unit HAb4a). This final sequence
532 included flooding and emplacement of sediments and burial of volatiles and eventual release to
533 form vent structures. For example, related to this geologic investigation, Argyre Mons is a newly
534 identified feature interpreted to have formed from subterranean gas releases (*e.g.*, mud
535 volcanoes), magmatic-driven activity, or an impact event, with gas release being the favored
536 hypothesis (**Fig. 12**; Williams et al., 2014). Numerous and widespread vent structures in the
537 northern plains, interpreted to be mud volcanoes, are likely the result of rapid emplacement of
538 circum-Chryse floodwaters and sediments and associated ocean formation (Skinner and Tanaka,
539 2007; Skinner and Mazzini, 2009; Oehler and Allen, 2010; Komatsu et al., 2011, 2012), related
540 to Stage-4 Tharsis-driven activity.

541 The emplacement of unit HAb4a is coincident with the development of equatorial glacial
542 landscapes in the Aeolis Mensae region (Davila et al., 2013) and possibly along parts of Mount
543 Sharp (Fairén et al., 2014), all of which could be tied to Stage-4, Tharsis-driven environmental
544 change (**Fig. 4**). Magmatism and associated flooding sourcing from the Tharsis superplume, with
545 floodwaters more acidic and briny at the source of the superplume-driving heat engine, included
546 ponding of sediment-laden floodwaters in the northern plains (Dohm et al., 2009b). We
547 hypothesize here that the Tharsis-induced transient hydrological cycling included precipitation
548 over the promontories of Tharsis and away from Tharsis such as at the south pole and Argyre

549 with the concentration of more neutral water; i.e., the initial water outbursts were more acidic
550 due to its magmatic source resulting in magma-water-related deposits such as sulfates vs. latter
551 phases of the magmatic-induced transient hydrological cycle such as snowfall and related ice
552 sheet, glacial, and ground ice accumulations. Such relatively cold hydrological cycling beyond
553 the Tharsis Superplume may have contributed to the growth of glaciers in Gale Crater and
554 elsewhere (Davila et al., 2013; Fairén et al., 2014)

555 In addition to late-stage Tharsis superplume activity, but to a lesser extent, the growth of
556 Elysium superplume (e.g., Baker et al., 2007) and changes in obliquity and eccentricity (e.g.,
557 Touma and Wisdom, 1993; Laskar et al., 2004), may have also contributed to the youngest
558 mapped basin unit (member HAb4a), as well as resurfacing of most of the surfaces within and
559 outside of the Argyre basin. This includes the partial infill of topographic lows of the modified
560 highlands terrain largely through sedimentary processes, as well as rock materials being shed
561 from the Thaumasia highlands into the transition zone (**Figs. 1-2**). Corroborating this, the
562 superposed-only crater statistics point to final major resurfacing during the Late Hesperian/Early
563 Amazonian for most of the geologic units (i.e., that which could destroy crater populations
564 exceeding 3 km; **Table 3**).

565 Basin-forming events are not limited to the Early-Middle Noachian, as there were impact
566 events such as the formation of Lowell Crater (Late Hesperian and possibly much more recent)
567 that post-dated the Argyre basin-forming one; this would have resulted in local to regional
568 deformation and flooding (Lias et al., 1997). Another example includes Galle Crater. Not only
569 does it deform the southeast part of the Argyre basin, but also appears to have contributed to the
570 formation of valleys that debouch into the southeast part of the basin (south of the impact crater;

571 see the features mapped as troughs in **Fig. 3** located along the southern margin of the central part
572 of the ejecta blanket of Galle) and disrupted floor deposits.

573 The volatile enrichment of the Argyre basin and its associated structures and rock materials,
574 resulting from the climatic perturbations and environmental changes discussed above, largely
575 shielded from atmospheric conditions by dry mantles similar to ancient glacial ice in Antarctica,
576 would play a significant role in shaping a dynamic landscape in geologically recent time, and
577 possibly presently. Relatively recent atmospheric precipitation is likely to have played a role in
578 the modification of the regional landscape, including the flow of materials from high reaches
579 towards the basin floor pronounced in the basin materials (El Maarry et al., 2013). Such
580 evidence, possibly indicative of glacial, colluvial, and/or alluvial activities, corroborates earlier
581 investigations that indicated widespread glacial activity in Martian history, some of it
582 comparatively recent, perhaps as late as the Middle or even Late Amazonian (Kargel et al., 1995;
583 Head et al., 2003; Kargel, 2004; Madelaine et al., 2009).

584 Periglacial activity, climate-controlled and influenced by such long-term (i.e., since the
585 Argyre impact event), water-enrichment in the basin and surroundings, has been and continues to
586 be a major resurfacing agent (El Maarry et al., 2013; Soare et al., 2014a,b). The primary basin,
587 local basins, and structurally-controlled valleys may contain Antarctic-like paleosols that record
588 far-reaching environmental information dating back billions of years (Mahaney et al., 2001,
589 2009, 2011). In addition, internal heat and volatiles migrating along basement structures may
590 contribute to geologically recent and even possibly present-day modification of parts of the
591 basin, expressed in the form of fault and fracture systems, gullies, and open-system-pingo-like
592 structures (Soare et al., 2014b). Characteristics of multiple Argyre gullies are consistent with an
593 origin involving liquid water (Conway and Soare, 2013), which could involve brines, a

594 hypothesis consistent with features elsewhere on Mars interpreted to involve brines such as dark
595 slope streaks (Ferris et al., 2002; Miyamoto et al., 2004) and slope linea (McEwen et al., 2013).
596 The impact-influenced dynamic landscape during ancient and geologically recent times is further
597 discussed in Section 4.3.

598

599 ***4.3. Basin conditions from impact to today***

600 Ancient (Argyre impact and post-impact) and geologically recent activity induced by
601 magmatic-, orbital-, impact-, weathering-, and climatic-driven phenomena (some of which are
602 often interlinked) are recorded in the fluvial-, lacustrine-, glacial-, and periglacial-sculpted
603 terrains of the Argyre province. For example, there is a wide array of landforms suggestive of a
604 dynamic landscape modified by wind, liquid water,– water ice, and gravity-driven processes.
605 This includes dune deposits in topographic lows, valleys that dissect the Argyre basin rim
606 materials and the margins of local basins, alluvial fans, valley-filling deposits with flow features,
607 crevasse-like fractures, tarns, cirques, megafaults, drumlins, eskers, gullies, and terraces, and
608 small-scale polygonal-patterned ground comprising high and low-centered polygons (e.g.,
609 Hiesinger and Head 2002; Kargel, 2004; Banks et al., 2008, 2009; Soare et al., 2014a,b). The
610 polygons mark relatively young and possibly ice-rich mantled terrain that is extant in wide-
611 ranging and pristine in some instances and truncated and/or dissected in others (see discussion in
612 Section 4.3.3).

613 During ancient times (Noachian-Early Amazonian: \sim 1.23 Ga based on the model of
614 Hartmann and Neukum (2001)), hydrological cycling due to major geologic activity outside of
615 the Argyre province, following the Argyre-basin-filling lake (Argyre-impact induced, as further
616 discussed below), exchanged water from both the atmosphere and groundwater. This is

617 exemplified by sharp, transient climatic changes triggered by igneous activity of the Tharsis
618 superplume (Baker et al. 1991, 2000, 2002; Dohm et al., 2000, 2007a, 2009b; Fairén et al., 2003;
619 Kargel 2004) (**Fig. 4**). This water cycling in the Argyre basin could have included south-to-north
620 hydraulic gradients in the groundwater system built up over time by south polar glacial activity
621 (e.g., Head and Pratt, 2001).

622 Other geologic activities outside of the Argyre province, such as the growth of Elysium and
623 impacts events such as Lowell and Galle would have also influenced hydrological and
624 environmental conditions in the deep Argyre impact basin. Lowell crater, a relatively pristine,
625 double-ring impact crater, located to the west of the Argyre basin, is interpreted to have formed
626 during the Late Hesperian-Early Amazonian. This crater in particular may have contributed to
627 environmental change in and surrounding Argyre basin following its formation. The diameters of
628 the outer and inner rings are about 195 km and 85 km, respectively, comparable to the 180-km-
629 diameter Chicxulub crater, which is associated with profound global-scale environmental
630 changes that most likely contributed to the demise of the dinosaurs at the boundary of the
631 Cretaceous and Tertiary Periods (Alvarez et al., 1980). The Lowell impact triggered a series of
632 events: (1) formation of secondary craters on surrounding rock outcrops in the Lowell and
633 Thaumasia regions as much as 800 km from the rim of the impact crater, (2) production of
634 meltwater and associated channel dissection of rock outcrops to the northeast and southwest,
635 indicating ice-enriched target materials, and (3) a massive debris flow, which embayed and
636 partly buried structures to the southeast (Lias et al., 1997).

637 Depending on climatic conditions and the nature of the cycling processes, whether
638 endogenic or exogenic, the cycling may have involved groundwater discharges into an ice-
639 covered lake, spring-fed activity, catastrophic outburst floods, ponding to form lakes in the

640 primary basins that would eventually freeze, gelifluction of rock materials, debris flow and
641 alluvial fan development, and glacier accumulation and inflow into the basin. The water
642 reservoirs would eventually ablate and be mantled and shielded from atmospheric conditions.

643 During geologically recent times, the atmospheric cycling of water through late-stage
644 volcanism, such as from the Tharsis/Elysium corridor region (Dohm et al., 2008 and the
645 references therein), may have contributed to environmental changes in the Argyre basin and
646 surrounding regions as well, especially when considering the physiographic setting of the deep
647 Argyre basin and the adjacent Tharsis. In addition, variations in orbital and spin parameters
648 within the last tens of millions of years, and associated hydrological cycling, may be responsible
649 for the development of glacial deposits down to the mid latitudes (Head et al., 2003), and
650 potentially would have had a bearing on changing environmental conditions of the Argyre basin
651 and surrounding regions.

652 Orbital and spin parameters have been invoked by numerous authors to explain various sets
653 of features on the surface of Mars. These include the presence of debris aprons and potential
654 dust-covered glaciers at the mid-latitudes, latitude-dependent mantling, and aureole deposits
655 associated with Olympus Mons and other volcanoes in the Tharsis region, as well as very recent
656 (i.e., within thousands of years) landscape changes putatively ascribed to periglacial processes
657 and freeze-thaw cycling (*e.g.*, Costard et al., 2002; Banks et al., 2008, 2009; Fastook et al., 2008;
658 Raack et al., 2012). The first comprehensive solutions for the variation in obliquity and
659 eccentricity for Mars were presented by Laskar et al. (2004) and remain the most accurate
660 solutions for the last ~20 million years.

661 Periods of high obliquity (> 30 degrees) are usually invoked in order to trigger the
662 sublimation of ice deposits at the poles into the atmosphere and their deposition at the mid-

663 latitudes (e.g., Laskar et al., 2004). Such periods of high obliquity would have affected
664 environmental conditions in the Argyre basin including possibly allowing the melting of ice-rich
665 materials (*i.e.*, interstitial ice in the pore space of sediments, lenses of ground ice, and mantled
666 covered glaciers and ice) (Kargel, 2004). Contributions in geologically recent times from
667 precipitation, and possibly present-day fog (Neumann et al., 2003) and snow, all may have
668 contributed to surface modification, including periglacial activity, as well as life if existing. The
669 above conditions make the Argyre province a prime astrobiologic target on Mars, but due to its
670 vastness, new mission designs will likely be required to optimize the search for life (Fink et al.,
671 2005, 2007a,b, 2008; Schulze-Makuch et al., 2012).

672

673 *4.3.1. Ancient surface modification*

674 On Earth, large and often structurally-controlled basins act as catchments for volatiles and
675 sediments. They record geologic and hydrologic activity including environmental changes and
676 perturbations in climate at local and global scales. Basement structures, including faults,
677 fractures, and joints, often serve as conduits for the movement of volatiles in both the subsurface
678 and surface environments. Even in arid deserts on Earth water can be routed along basement
679 structures at depth, as occurs in the Atacama Desert; here, water runoff from the Andes is
680 channeled to the Pacific Ocean along deep-seated basement structures in which microbial life
681 may thrive (Dohm et al., 2011b).

682 In the case of the Argyre impact event that resulted in a complex of basement faults,
683 fractures, and joints, including deep-seated and shallow faults concentric and radial about the
684 basin, the structural control of volatile migration likely played a significant role in the
685 hydrogeologic history of the Argyre province. This includes the formation of the hypothesized

686 Argyre impact-induced lake and linked Uzboi Vallis, as well as subsequent hydrogeologic
687 activity such as related to major pulses of Tharsis-driven activity (**Fig. 4**). Groundwater models
688 by Harrison and Grimm (2009) corroborate structurally-controlled migration of groundwater into
689 the Argyre basin highlighted by this geologic investigation.

690 If the basin filled during a glacial climate period, ice accumulation and glacial inflow into an
691 ice-covered lake or sea may have taken place (Kargel and Strom 1992, Kargel 2004). The ice
692 cover may have acted to dam the Uzboi outlet, but periodic disruptions of the dam may have
693 generated megafloods, which helped to carve Uzboi Vallis and could have contributed to
694 environmental and marine depositional changes in the northern plains (Parker and Gorsline,
695 1991; Dohm et al., 2011a).

696 The influence of the Argyre impact extends well beyond the basin, rim, and adjoining
697 cratered plateau regions. For example, impact-influenced terrain and regional drainage is
698 observed along the southeastern margin of the Thaumasia plateau and the transitional zone that
699 separates the Thaumasia plateau from the Argyre basin and rim regions (Dohm et al., 2001a).
700 Also, major drainages originate on plateaus 1600 km to the south (to Dorsa Argentea's system of
701 sinuous ridges; Kargel and Strom (1990, 1992)), over 700 km to the southeast, and 900 km east
702 of Argyre; these ancient valley systems incise the Charitum Montes and terminated near the
703 margin of the primary basin near sinuous ridges in the southern Argyre Planitia.

704 Deposits, which partly infill the impact-derived structurally-controlled primary and
705 secondary basins and modified valleys, record surface modification in the Argyre province
706 resulting from major changes in environmental and hydrological conditions detailed above.
707 These include the initial Argyre impact event and associated lake formation followed by
708 endogenic activity largely related to major stages of growth of the Tharsis superplume (**Fig. 4**),

709 with lesser activity such as related to other volcanic provinces such as Elysium, the
710 Tharsis/Elysium corridor, impact events such as Lowell and Galle, and changes in obliquity and
711 eccentricity. Possible lake formation in the immediate aftermath of the Argyre impact event may
712 have been followed by progressive deep freezing of the lake as hydrothermal activity decreased
713 over time, as radiogenic heat flow then also declined, and sublimation of ice gradually thinned
714 the frozen lake until the cold climate froze it completely to its base. Climatic oscillations may
715 have caused debris-covered glaciers to wax and wane episodically and gradually erode the rim
716 mountains and transfer sediment deeper into the basin.

717 Detailed topographic analysis of the sinuous ridges located in the southern Argyre basin was
718 completed for three of the main ridges of the southeast part of the Argyre basin (**Fig. 3**): Cleia
719 Dorsum, Pasithea Dorsum, and Charis Dorsum (Banks et al. 2009). Results of this analysis
720 indicated that the Argyre sinuous ridges cross topography and that the ridges tend to have
721 sharper crested shapes and increasing ridge heights on descending slopes, and low, broad, and
722 more rounded shapes and decreasing ridge heights on ascending slopes (see Fig. 5 of Banks et al.
723 (2009) for location within basin and profiles). These results indicated that the Argyre sinuous
724 ridges may have been formed by a pressurized flow as opposed to an open air, gravity-driven
725 flow such as in an open river channel (Banks et al., 2009). The characteristics of the southern
726 Argyre sinuous ridges are therefore consistent with those of terrestrial eskers and are related to
727 flow processes associated with meltwater flowing in tunnels beneath or within a large ice deposit
728 (Shreve, 1985). Terrestrial eskers commonly climb and cross topographic divides because water
729 flowing within or beneath a large ice mass is under hydraulic pressure. In descending ice tunnels,
730 viscous heat produced by flow of meltwater causes melting of the tunnel walls increasing the
731 height of the tunnel and the resulting, sharper esker ridge. Meltwater flowing in ascending

732 tunnels has less viscous energy resulting in freezing of water onto the walls and particularly the
733 top of the tunnel and, consequently, the formation of shorter, broader, and more rounded ridge
734 heights (Shreve, 1985). Conversely, the ascending and descending undulations of the sinuous
735 ridges appear to be inconsistent with the shoreline origins hypothesized by Parker (1994) and
736 Parker and Gorsline (1992). However, some local ponding of water may have contributed to the
737 layering observed in terrain surrounding many of these ridges (Kargel and Strom 1992; Kargel,
738 2004; Banks et al. 2009). Altogether, these observations support the hypothesis that the Argyre
739 sinuous ridges are eskers that formed from meltwater flowing at times in tunnels beneath a large
740 ice deposit and at times in open channels within the ice deposit in the southern Argyre basin
741 (Kargel and Strom, 1992; Hiesinger and Head 2002; Kargel, 2004; Banks et al. 2009).

742 Mapping efforts of this geologic investigation indicate that the esker-like narrow ridges
743 would have been associated with the late-stage emplacement of basin sediments mapped as unit
744 HAb4a, which is interpreted to be related to Stage-4 Tharsis (Late Hesperian-Early Amazonian)
745 development (**Fig. 4**), or the last major stratigraphic sequence of the basin infill deposits (NAb1,
746 Nab2, Nab3, NAb4b, HAb4a) discussed above.

747

748 *4.3.2. New evidence for a lake within the Argyre basin that sourced Uzboi Vallis*

749 Did a large Argyre lake source the Uzboi Vallis drainage system during the Noachian
750 Period, as hypothesized during a Viking-era investigation (Parker and Gorsline, 1991)? This very
751 important question, being a main focus of this geologic investigation, is addressed through
752 comparative analysis among the stratigraphic, geomorphologic, structural, and MOLA
753 topographic information. For example, spatial and temporal relations amidst the possible
754 equipotential surface of the Uzboi spillway (**Fig. 8**) can be readily compared to features around

755 the basin. These features include high-standing unit NAb1 materials, which are mapped as the
756 oldest valley- and basin-filling materials (member 1 of the Argyre basin sequence; **Tables 1-3,**
757 **Figs. 3, 5, and 6**), terraces and benches (**Fig. 7-8**), and valleys incised into existing valleys at
758 certain elevations (**Figs. 3 and 6**). There is a direct correlation between these feature types,
759 indicating that the base level of a water body played a significant role in resurfacing the basin.
760 The base level hovers around the zero-elevation level (**Fig. 5**) due to a likely change in a
761 fluctuating hydraulic head following the formation of the Argyre lake, as well as extensive
762 resurfacing (i.e., both erosional and depositional processes) since the lake formed directly
763 following the impact event (~ 3.93 Ga), and isostatic adjustment since the impact event
764 interpreted based on stratigraphy and impact crater statistics.

765 A possible key piece of evidence that the base level of the putative Argyre lake may have
766 reached the height of the spillway of Uzboi Vallis (including the surface of the lake and
767 associated groundwater system) is a recently identified lake basin located on the western margin
768 of the Argyre impact basin (**Figs. 1, 7-8**); this is referred to as the Argyre western-margin-
769 paleolake basin (AWMP; Dohm et al., 2011a). A paleolake is inferred by the series of distinct
770 drainage systems that debouch into the basin (**Fig. 7**). Drainage systems terminate near a possible
771 bench that occurs at a topographic interval ranging from 1 to 1.5 km, an elevation range which
772 corresponds with a possible spillway that separates the paleolake basin from the Argyre basin
773 (**Fig. 8**). The spillway divide occurs at an elevation of ~ 1.5 km. It must be noted that
774 paleotopography may vary significantly from the present-day topography due to factors such as
775 post-impact isostatic adjustment, which includes tectonic uplift or subsidence, and erosion.

776 The paleolake, alternatively, may be independent of the Argyre lake, having formed later in
777 time and with no link to an Argyre-lake-related hydrologic system. But if the water was as high

778 as 1 km as shown in **Fig. 9**, or more, or ranging between 0 km and 1 km, then a linkage is
779 possible. In addition to the high-standing unit Nab1 materials and terraces and benches in part
780 formed by valleys that dissect these oldest basin infill deposits within existing valleys (**Figs. 3**
781 **and 6**), by considering a water column of the lake that would reach the 0 km contour interval
782 (**Figs. 5, 7-9**) - a conservative value (nearly the base of AWMP) based on geomorphic and
783 topographic analysis of different parts of the Argyre basin - the extent of the lake would link to
784 distinct dendritic valley systems, broad valley systems, and local basins that occur among the
785 basin rim materials, as well as the Uzboi drainage system (**Fig. 9**—left). If the hypothesized
786 Argyre lake reached an elevation of 1.0 km, then it would have an estimated volume of 3.1
787 million km³. For comparison, this closely approximates the volume of the Mediterranean Sea,
788 estimated to be 3.75 million km³ (**Fig. 9**—right; also compare with the dark blue region of **Fig.**
789 **1**). Such a relatively high-standing water body makes sense when compared to other topographic
790 basins outside of the Argyre basin, including the basin in the bottom-left part of **Fig. 9** (compare
791 left and right scenes with the latter highlighting a lake, marked as SWB, that would infill the
792 basin), which displays drainages along its margin. But where did water come from to form such
793 a large water body? One plausible explanation is that an impact event generated hydrogeologic
794 conditions that would have resulted in the formation of the relatively large water body, such as
795 the melting of surface and subsurface ice, migration of surface and subsurface water from great
796 distances, and impact-induced precipitation.

797 A figure of merit regarding the impact-melting hypothesis can be obtained by considering
798 some basic energy considerations. The estimated volume of water— 3.05×10^6 km³, would
799 require about 1.0×10^{24} J of thermal energy to produce the water by melting ice, or a bit more if
800 the ice was initially much colder than the freezing point. For an Argyre impact energy of around

801 6×10^{25} J (Williams and Greeley, 1994), only about 1.7% of the Argyre impactor's kinetic
802 energy is needed to melt ice to make a sea the size of Argyre's. For comparison, Braslau (2012)
803 found that 26% of a 6 km/s bolide impact's kinetic energy was transferred into heating of a
804 granular target. The energy partitioning varies depending on details of the impact and target.
805 Most partitioning relations require $< 10\%$ of the Argyre impact's heat energy going into melting
806 ice in order to generate the Mediterranean Sea-size quantity of liquid water. Thus, from an
807 energy perspective melting the needed amount of melted ice is entirely plausible. Of course it
808 would require the target to be extremely ice-rich, for example, an ice sheet or polar layered
809 deposit or ice-rich permafrost extending kilometers deep. This calculation raises a possibility
810 that Argyre's glacial and lacustrine history may have started immediately upon impact into an icy
811 region. The geomorphology and crater counts further require that renewed glacial and lake
812 processes then continued afterward in much more recent times.

813 This geologic mapping investigation and geomorphic analysis of the Argyre province,
814 therefore, ties the lake that formed shortly following the Argyre impact event with Uzboi Vallis
815 and the northern plains, which includes a possible northern plains ocean, and thus pointing to an
816 extensive hydrological system. The putative existence of a giant lake indicates that Mars was a
817 highly water-enriched planet at the time of the ~ 3.93 Ga Argyre impact event, supported by the
818 stratigraphy and accompanying crater statistics such as the relatively high-standing oldest basin
819 unit (unit Nab1) (**Table 3 and Figs. 3 and 6**). Thus, we provide strong support for and add new
820 details to the hypothesis of Parker and Gorsline (1991).

821 The source of water of the initial highest-standing lake is hypothesized to be from the
822 Argyre impact event, an event which would have induced major environmental change in the
823 Argyre province and surroundings, including the melting of ice, as well as the formation of a

824 complex of basement faults, fractures, and joints, including deep-seated and shallow faults
825 concentric and radial about the basin. These structures controlled the migration of water in the
826 subsurface as conduits and surface as structurally-controlled valleys, focusing water migration to
827 the basin from great distances (thousands of kilometers) from the impact site.

828

829 4.3.3. *Geologically-recent surface modification*

830 At HiRISE resolution (~25-50cm/pixel), the terrain in parts of the Argyre province often
831 appears mantled by material that exhibits a high albedo, is relatively smooth (although meter-
832 sized boulders often overlie it), and varies in ground coverage from continuous to dissected to
833 discontinuous. This type of terrain is ubiquitous at the middle to high latitudes in both
834 hemispheres and commonly is referred to as the latitude-dependent mantle (*LDM*) (*i.e.*, Mustard
835 et al. 2001; Milliken et al. 2003; Morgenstern et al. 2007; Lefort et al. 2009, 2010; Madeleine et
836 al., 2009; Zanetti et al., 2010; Mangold, 2011; Raack et al., 2012; Wilmes et al., 2012). The *LDM*
837 is hypothesized to be water-ice rich and either comprised uniquely of ice-dust accumulated by
838 air-fall deposition (*i.e.*, Morgenstern et al., 2007; Levy et al., 2009, 2011; Lefort et al. 2009,
839 2010; Madeleine et al., 2009; Zanetti et al., 2010; Wilmes et al., 2012) or of ice-dust and loess
840 that is transformed epigenetically into ground ice (Mustard et al., 2001; Soare et al., 2012b;
841 Skinner et al., 2012). Based on age estimates derived from crater-retention rates, the *LDM* could
842 have been emplaced during the very Late Amazonian Epoch, in response to changes of obliquity
843 and eccentricity (*i.e.*, Mustard et al. 2001; Milliken et al. 2003; Madeleine et al. 2009; Mangold,
844 2011; Wilmes et al., 2012).

845 Recent water-related modifications (**Fig. 13-14**) of the landscape putatively comprise three
846 assemblage types: (1) glacial; (2) periglacial; and, (3) crater-wall “wet-debris” flows. The glacial

847 assemblages comprise landforms whose shape, size, and geological traits, i.e. terminal and
848 recessional lobes, lateral and medial ridges, slope-side location, and esker-like lineations, would
849 be indicative of glaciation were they collectively observed on Earth (i.e. Kargel and Strom, 1990,
850 1992; Baker, 2001; Kargel, 2004; Banks et al., 2008; El Maarry et al., 2013). See Kargel et al.
851 (2014) for a thorough review of glaciation on Earth as viewed from space, with field validations.

852 Possible periglacial landforms include: multi-metre and non-sorted polygons with high
853 and low-centres, formed by thermal-contraction cracking and possibly underlain at the margins
854 by water ice; multi-metre and sorted polygons that are the work of freeze-thaw cycling and
855 cryoturbation; and, decametre-scale mounds whose shape, height, occasional summit-
856 depressions and slope-side location coincide with the traits of open-system pingos on Earth, i.e.
857 perennial (water) ice-cored mounds formed by hydrostatic pressure (Seibert and Kargel, 2001;
858 Kargel, 2004; Soare et al., 2014a-b, 2015; Banks et al., 2008; Raack et al., 2012). Lineaments,
859 which we interpret to be faults and fractures, also are commonly observed at OSP locations (**Fig.**
860 **15**). Based on field investigation of pingos on Earth, Soare et al. (2014b) propose that the
861 candidates could be the result of a glacially-driven hydraulic gradient (*e.g.*, Liestöl, 1975), a
862 topographically-driven hydraulic gradient (*e.g.*, Müller, 1959), and a tectonic hydraulic gradient
863 (i.e., regional faults and structural-discontinuities which channel and concentrate groundwater,
864 possibly deeply-seated water, to form a pingo (*e.g.*, Müller, 1959)). The third possibility could
865 indicate flow along deep-seated basement structures associated with the ancient giant impact
866 basin and possibly internal heat flow of Mars vented through the structural conduits.

867 Throughout the region gully-like landforms observed on crater-walls exhibit significant
868 channel sinuosity, braiding and benches or levees. The depositional fans show multiple
869 superpositions (**Fig. 14**) and often are incised by channels or channel segments (Soare et al.,

870 2014a-b, 2015; Conway et al., 2015). On Earth, these traits would be markers of “wet-debris”
871 flows.

872

873 ***4.4. Impact-induced tectonism and geophysical assessment***

874 The Argyre impact event excavated a broad, deep basin and produced small and large
875 extensional and compressional structures; these include structurally controlled fault scarps, broad
876 ridges, valleys, and mountain ranges within several hundred kilometers of the basin margin
877 which are generally oriented radially and concentric to the basin. Farther away, toward the
878 Thaumasia plateau, more subtle basins and broad rises may in part have resulted from Argyre-
879 related deformation (also compare with Craddock et al. (1990)). Some 2,000 km away from the
880 basin, the outline of the southeast margin of the Thaumasia plateau is roughly concentric with the
881 Argyre basin, suggesting that the margin could be controlled by the impact-related crustal
882 structure (**Figs. 1-2**) (*e.g.*, Dohm et al., 2001a; Yin, 2012a).

883 Structurally-controlled local basins among the rim material and outside of the primary
884 Argyre basin also resulted from the large impact event. These small exterior basins served as
885 local catchments for water and sediments. Isostatic adjustments following the formation of the
886 Argyre basin (Thomas and Masson, 1984; Wichman and Schultz, 1989; Dohm et al., 2001a)
887 include normal faulting possibly related to the reactivation of some of the impact-induced older
888 basement structures. An example is the deformation of a structurally-controlled basin and its
889 sedimentary deposits (**Fig. 16**).

890 Argyre-induced basement structures have not only controlled major watersheds, but also
891 have influenced the geometric patterns of some subsequent impact craters, *i.e.* the observed
892 polygonal impact craters (Öhman et al., 2008). The simple polygonality of craters is formed

893 early in the cratering process and is somewhat similar to the structure-controlled square planview
894 shape of Meteor Crater, Arizona (Shoemaker, 1963; Quaide et al., 1965), whereas the complex
895 craters' polygonal planview forms later in the cratering process (Öhman et al. 2008, and
896 references therein). The Argyre impact-resulting structures are distinct in the MOLA map (**Fig.**
897 **17a**) and topographic profile (**Fig. 18a**), and their general signatures can be observed in the
898 gravity map data as gravity highs and lows (**Fig. 17b**).

899 The interior of the Argyre basin, for example, is characterized by a positive free-air gravity
900 anomaly (mascon) with a magnitude ~ 140 mGal surrounded by an annulus of low gravity at the
901 basin's inner periphery (**Figs. 17b and 18b**). This is observed for the Isidis basin and commonly
902 observed for lunar impact basins (Muller and Sjogren, 1968; Konopliv et al., 2001; Matsumoto et
903 al., 2010). Such mascons have been attributed to the super-isostatic uplift of the Moho beneath
904 the basin (Neumann et al., 1996; Wieczorek and Phillips, 1999) and/or the infilling and partial
905 burial of the basins by material, such as flood basalts and sediments, that are at least partially
906 flexurally supported (Solomon and Head, 1980).

907 The floor deposits of the Argyre basin are comprised of sedimentary rocks that, depending
908 on their thickness, porosity, and state of compensation, may contribute to the gravity anomaly if
909 accumulation occurred without complete isostatic compensation. Based on the observed relation
910 between crater depth to diameter for large crater basins (Howenstine and Kiefer, 2005), the inner
911 basin diameter of Argyre, ~ 915 km, implies an unfilled basin depth of ~ 6 km. The actual basin
912 depth of ~ 4 km suggests ~ 2 km of burial if flexure of the basin floor is minimal. Several quasi-
913 circular features are apparent on the interior floor of Argyre basin and are likely buried impact
914 craters. The largest of these features has a diameter of ~ 60 km (**Fig. 19**). The crater depth to
915 diameter power law fit to craters between 7 and 110 km in diameter (Garvin et al., 2002) yields a

916 depth of ~2 km indicating at least 2 km of material filling this crater to its rim. Taking $h = 2$ km
917 as the thickness of deposits in the basin, the magnitude of the resulting gravity anomaly is
918 estimated assuming a simple slab model (Schubert and Turcotte, 2002):

919

$$920 \Delta g = 2\pi G \rho h [1 - C(r_p / (r_p + t_c))^2],$$

921

922 where G is the gravitational constant, ρ is the fill density, h is the thickness of deposits in the
923 basin, r_p is the radius of Mars, t_c is the crust thickness assumed to be 50 km, and C is the degree
924 of compensation which is zero for a completely rigid lithosphere and approaches unity for Airy
925 isostasy. The resulting gravity anomaly is shown in **Fig. 20**. The ~140 mGal mascon within the
926 basin can be explained by post-impact deposition alone if the compensation of the load is no
927 greater than ~45%. A fill density < 1670 kg m⁻³ results in a gravity anomaly < 140 mGal for any
928 compensation state suggesting this is an approximate lower bound on the fill density.

929

930 **5. Conclusions.**

931 Detailed geologic investigation using Viking and post-Viking data has revealed the
932 evolutionary history of the Argyre province. This includes distinct basin units most likely marking
933 a lake that formed as a result of the Argyre impact event, as well as subsequent perturbations in
934 environmental conditions (climate, surface, and subsurface) associated with major stages of
935 Tharsis superplume development among other lesser endogenic-driven activity such as Elysium
936 rise. It has also revealed newly identified lake-containing basins, mapped the extent of Argyre-
937 related tectonism and the influence of the giant impact on the surrounding regions, corroborated
938 the esker hypothesis, with details on the timing of formation being the Late Hesperian, and

939 highlighted ancient, geologically-recent, and possibly present-day surface modification.
940 Examples of geologically-recent landforms and possible present-day activity include polygonal-
941 patterned ground, gullies, open-system pingos, and flow-like features of the valley-fill materials,
942 including glacier-like landforms. Possible contributors to the water enrichment and
943 remobilization of water and sediment in Argyre in geologic recent time could include local
944 precipitation related to atmospheric cycling of water vapor such as from the south pole into the
945 deep basin and an intrabasinal water cycle including fog.

946 A hypothesized generalized summary of the geologic evolution of the Argyre province
947 based on this geologic investigation includes: (1) the Argyre impact event and related formation
948 of the Argyre basin, rim materials, ejecta blanket, basement structures (faults and structurally-
949 controlled valleys, basins, and mesas) radial and concentric about the basin, and lake and
950 associated sedimentation (marked by unit Nab1) with connecting Uzboi Vallis, (2) waning and
951 eventually frozen Argyre lake with associated glaciers extending away from the lake, (3)
952 mantling of basin and rim materials including the ice bodies due primarily to wind- and gravity-
953 driven processes, (4) Stages 1-3 Tharsis-driven activity and associated transient hydrological
954 cycling and major environmental change and landscape modification in and surrounding the
955 Argyre basin, including melt and associated flooding and spring activity, gelifluction, and
956 alluvial, colluvial, lacustrine, glacial, and periglacial activity (recorded by units Nab2, Nab3,
957 Nab4b), (5) Stage 4 Tharsis-driven activity and related hydrological cycling and major
958 environmental change and landscape modification, including lake formation and associated
959 sedimentation (marked by unit HAb4a), though much less in extent when compared to the
960 Argyre-impact-related lake that sourced Uzboi Vallis, and subsequent freezing and esker
961 development distinct in the southeast part of the Argyre basin, as well as the development of

962 glaciers such as those that were directed through Surlus Vallis, Dzigai Vallis, and Nia Vallis and
963 that linked to the basin environment, (6) impact events such as Lowell, Galle, and Hale
964 contributed to environment change and surface modification, and (7) ice enrichment of the rock
965 materials of the Argyre province, environmental changes related to changes in orbital parameters
966 (spin axis and orbital eccentricity) and endogenic activity such as in the Tharsis/Elysium corridor
967 region, relatively steep slopes, and Argyre-impact-induced structures as conduits for the
968 transfer of heat and volatiles also has contributed to surface modification in geologic recent
969 times. This history points to Argyre as a prime target for the search for life on Mars.

970

971 **Acknowledgements**

972 J.M. Dohm was supported by the National Aeronautics and Space Administration (NASA)
973 Planetary Geology & Geophysics Program. Professors Dohm and Miyamoto express their
974 gratitude to the Tokyo Dome Corporation for their support of the TeNQ exhibit and the branch of
975 Space Exploration Education & Discovery, the University Museum, the University of Tokyo.
976 We are grateful for the thoughtful reviews by T. Öhman and an anonymous reviewer which
977 ultimately resulted in an improved manuscript.

978

979

980 **References**

- 981 Abramov, O., Kring, D.A., 2005. Impact-induced hydrothermal activity on early Mars. *J.*
982 *Geophys. Res.* 110, E12S09, doi:10.1029/2005JE002453.
- 983 Acuña, M.H., Connerney, J.E.P., Ness, N.F., Lin R.P., Mitchell, D., Carlson, C.W., Mcfadden,
984 J., Anderson, K.A., Reme, H., Mazelle, C., Vignes, D., Wasilewski, P., Cloutier, P., 1999.
985 Global distribution of crustal magnetization discovered by the Mars Global Surveyor
986 MAG/ER experiment. *Science* 284, 790-793.
- 987 Acuña, M.H., Connerney, J.E.P., Wasilewski, P., Lin, R.P., Mitchell, D., Anderson, K.A.,
988 Carlson, C.W., McFadden, J., Réme, H., Mazelle, C., Vignes, D., Bauer, S.J., Cloutier, P.,
989 Ness, N.F., 2001. Magnetic field of Mars: Summary of results from the aero-braking and
990 mapping orbits. *J. Geophys. Res.* 106, 23,403-23,417.
- 991 Alvarez, L.W., Alvarez, W., Asaro, F., Michel, H., 1980. Extraterrestrial cause for the
992 Cretaceous-Tertiary extinction. *Science* 208, 1095-1108.
- 993 Anderson, R.C., Dohm, J.M., Golombek, M.P., Haldemann, A., Franklin, B.J., Tanaka, K., Lias,
994 J., Peer, B., 2001. Significant centers of tectonic activity through time for the western
995 hemisphere of Mars, *J. Geophys. Res.* 106, 20,563-20,585.
- 996 Anguita, F., Farello, A.-F., López, V., Mas, C., Muñoz-Espadas, M.-J., Márquez, Á., Ruiz, J.,
997 2001. Tharsis dome, Mars: new evidence for Noachian-Hesperian thick-skin and Amzonian
998 thin-skin tectonics. *J. Geophys. Res.* 106, 7577-7589.
- 999 Archinal, B.A., Colvin, T.R., Davies, M.E., Kirk, R.L., Duxbury, T.C., Lee, E.M., Cook, D.,
1000 Gitlin, A. R., 2002. A MOLA-controlled RAND-USGS control network for Mars (abs.).
1001 *Lunar Planet. Sci. XXXIII*, Abstract #1632 (CD-ROM). (PDF: 110k).
- 1002 Archinal, B.A., Kirk, R.L., Duxbury, T.C., Lee, E.M., Sucharski, R., Cook, D., 2003. Mars
1003 Digital Image Model (MDIM) 2.1 control network. ISPRS Working Group IV/9 Workshop
1004 "Advances in Planetary Mapping 2003", Houston, March 2003. (PDF: 285k).
- 1005 Arkani-Hamed, J., 2003. Thermoremanent magnetization of the Martian lithosphere. *J. Geophys.*
1006 *Res.* 108, 10.1029/2003JE002049.
- 1007 Arkani-Hamed, J., 2004. Timing of the Martian core dynamo. *J. Geophys. Res.* 109,
1008 doi:10.1029/2003JE002195.
- 1009 Aubrey, A. et al., 2006. Sulfate minerals and organic compounds on Mars. *Geology* 34, 357-360,
1010 doi:10.1130/g22316.1.
- 1011 Baker, V.R., 2001. Water and the Martian land-scape. *Nature*, 412, 228-236.

- 1012 Baker, V.R., Strom, R.G., Gulick, V.C., Kargel, J.S., Komatsu, G., Kale, V.S., 1991. Ancient
1013 oceans, ice sheets and the hydrological cycle on Mars. *Nature* 352, 589-594.
- 1014 Baker, V.R., Strom, R.G., Dohm, J.M., et al., 2000. Mars' Oceanus Borealis, ancient glaciers,
1015 and the MEGAOUTFLO hypothesis. *Lunar Planet. Sci. Conf. [CD-ROM], XXXI*, abstract
1016 1863.
- 1017 Baker, V.R., Maruyama, S., Dohm, J.M., 2001b. Tharsis superplume (3): Implications on the
1018 role of water, environmental change and life. *Geol. Soc. America Abstracts with Programs*,
1019 33(7), A432.
- 1020 Baker, V.R., Maruyama, S., Dohm, J.M. 2002. A theory of plate tectonics and subsequent long-
1021 term superplume activity on Mars. in *International Workshop: Role of superplumes in the*
1022 *Earth System, Electronic Geosciences*, 312-316.
- 1023 Baker, V.R., Maruyama, S., Dohm, J.M., 2007. Tharsis superplume and the geological evolution
1024 of early Mars. In *Superplumes: beyond plate tectonics*. D.A Yuen, S. Maruyama, S-I Karato,
1025 and B.F. Windley (eds.). Springer, pgs. 507-523.
- 1026 Banks, M.E., McEwen, A.S., Kargel, J.S., Baker, V.R., Strom, R.G., Mellon, M.T., Pelletier,
1027 J.D., Gulick, V.C., Keszthelyi, L., Herkenhoff, K.E., Jaeger, W L., the HiRISE Team, 2008.
1028 High Resolution Imaging Science Experiment (HiRISE) observations of glacial and
1029 periglacial morphologies in the circum-Argyre Planitia highlands. *J. Geophys. Res.* 113,
1030 E12015, doi:10.1029/2007JE002994.
- 1031 Banks, M. E., Lang, N. P., McEwen, A. S., Kargel, J. S., Baker, V. R., Strom, R. G., Grant, J. A.,
1032 Pelletier, J. D., and the HiRISE Team, 2009. An Analysis of the Sinuous Ridges in the
1033 Southern Argyre Planitia, Mars using HiRISE and CTX Images and MOLA Data. *J.*
1034 *Geophys. Res.* 114, E09003, doi:10.1029/2008JE003244.
- 1035 Barlow, N.G., 1990. Constraints on early events in Martian history as derived from the cratering
1036 record. *J. Geophys. Res.* 95, 14,191-14,201.
- 1037 Barlow, N.G., 2004. Martian subsurface volatile concentrations as a function of time: Clues from
1038 layered ejecta craters. *Geophys. Res. Lett.* 31.
- 1039 Barlow, N.G., 2005. A review of Martian impact crater ejecta structures and their implications
1040 for target properties. In: Kenkmann, T., Hörz, F., Deutsch, A. (Eds.), *Large Meteorite*
1041 *Impacts III*. Geological Society of America Special Paper 384, 433–442.
- 1042 Bibring, J.-P., Soufflot, A., Berthé, M., Langevin, Y., Gondet, B., Drossart, P., Bouyé, M.,
1043 Combes, M., Puget, P., Semery, A., Bellucci, G., Formisano, V., Moroz, V., Kottsov, V.,
1044 Bonello, G., Erard, S., Forni, O., Gendrin, A., Manuad, N., Poulet, F., Poulleau, G.,
1045 Encrenaz, T., Fouchet, T., Melchiori, R., Altieri, F., Ignatiev, N., Titov, D., Zasova, L.,

- 1046 Coradini, A., Capacionni, F., Cerroni, P.F., Mangold, N., Penit, P., Schmitt, B., Sotin, C.,
1047 Hauber, E., Hoffmann, H., Jaumann, R., Keller, U., Arvidson, R., Mustard, J.F., and Forget,
1048 F., 2004. OMEGA: Observatoire pour la Minéralogie, l'Eau, les Glaces et l'Activité, in Mars
1049 Express: the scientific payload. Edited by A. Wilson, pp. 37-49, ESA, Noordwijk,
1050 Netherlands.
- 1051 Bibring J.-P., Langevin, Y., Gendrin, A., Gondet, B., Poulet, F., Berthé, M., Soufflot, A.,
1052 Arvidson, R.E., Mangold, N., Mustard, J.F., Drossart, P., the OMEGA team, 2005. Mars
1053 surface diversity as revealed by the OMEGA/Mars Express observations. *Science* 307(5715),
1054 1576-81.
- 1055 Braslau, D., 2012, Partitioning of energy in hypervelocity impact against loose sand targets, *Jour.*
1056 *Geophys. Res. Atmospheres*, 75(2): 3987-3999.
1057
- 1058 Buczkowski, D.L., Murchie, S., Seelos, F., Malaret, E., Hash C., the CRISM science team,
1059 2008a. CRISM analyses of Argyre basin. LPSC XXXIX, abs. 1030, (CD-ROM), Lunar
1060 Planet. Inst., Houston, TX.
- 1061 Buczkowski D.L., Murchie, S., Clark, R., Seelos F., the CRISM Science Team, 2008b.
1062 Mineralogic and morphologic signatures of Noachian water in the Argyre impact basin. *EOS*
1063 *Trans.*, AGU Fall Mtg., San Francisco, CA.
- 1064 Buczkowski, D.L., Murchie, S., Clark, R., Seelos, K., Seelos, F., Malaret, E., Hash, C., 2010.
1065 Investigation of an Argyre basin ring structure using Mars Reconnaissance Orbiter/Compact
1066 Reconnaissance Imaging Spectrometer for Mars. *J. Geophys. Res.* 115, E12011,
1067 doi:10.1029/2009JE003508.
- 1068 Christensen, P.R., Jakosky, B.M., Kieffer, H.H., et al., 2004. The Thermal Emission Imaging
1069 System (THEMIS) for the Mars 2001 Odyssey mission. *Space Science Reviews* 110, 85–
1070 130.
- 1071 Condit, C.D., 1978. Geologic map of the Mare Australe area of Mars. US Geol. Survey Map
1072 Misc. Invest. Ser. Map I-1076, scale 1:5,000,000.
- 1073 Connerney, J.E.P., Acuña, M.H., Wasilewski, P.J., Kletetschka, G., Ness, N.F., Rème, H., Lin,
1074 R.P., and Mitchell, D.L., 1999. The global magnetic field of Mars and implications for
1075 crustal evolution. *Science* 284, 790-793.
- 1076 Connerney, J.E.P., Acuña, M.H., Wasilewski, P.J., Kletetschka, G., Ness, N.F., Rème, H., Lin,
1077 R.P., Mitchell, D.L., 2001. The global magnetic field of Mars and implications for crustal
1078 evolution. *Geophys. Res. Lett.* 28, 4015-4018.
- 1079 Connerney, J.E.P., et al., 2005. Tectonic implications of Mars crustal magnetism. *Science* 102,
1080 14970–14975.

- 1081 Conway, S.J., Soare, R.J., 2013. Gully morphometrics as indicators of degradation intensity
1082 around the Argyre basin. LPSC 44th, abstract #2488.
- 1083 Conway, S.J., Balme, M.R., Soare, R.J., 2015. Using gullies to estimate the thickness of the
1084 latitude-dependent mantle. Lunar Planet. Sci. Conf. XXXXVI, Houston, Texas. Abstract #
1085 2964
- 1086 Costard, F., Forget, F., Mangold, N., Peulvast, J.P., 2002. Formation of recent Martian debris
1087 flows by melting of near-surface ground ice at high obliquity. *Science* 295, 5552, 110-113.
1088 doi:10.1126/science.1066698.
- 1089 Craddock, R.A., Greeley, R., Christensen, P.R., 1990. Evidence of an ancient impact basin in
1090 Daedalia Planum, Mars. *J. Geophys. Res.* 95, 10,729-10,740.
- 1091 Crater Analysis Techniques Working Group, 1979. Standard techniques for presentation and
1092 analysis of crater size-frequency data. *Icarus* 37, 467-474.
- 1093 Crown, D.A., Price, K.H., Greeley, R., 1992. Geologic evolution of the east rim of the Hellas
1094 basin, Mars. *Icarus* 100, 1-25.
- 1095 Davila, A.F., Gross, C., Marzo, G.A., et al., 2011. A large sedimentary basin in the Terra
1096 Sirenum region of the southern highlands of Mars. *Icarus* 212, 579-589.
- 1097 Davila, A.F., Fairén, A.G., Stokes, C.R., Platz, T., Rodriguez, A.P., Lacelle, D., Dohm, J.,
1098 Pollard, W., 2013. Evidence for Hesperian glaciation along the Martian dichotomy boundary.
1099 *Geology* 41, 755-758, doi:10.1130/G34201.1.
- 1100 Dohm, J.M., Tanaka, K.L., 1999. Geology of the Thaumasia region, Mars: plateau development,
1101 valley origins, and magmatic evolution. *Planet. & Space Sci.* 47, 411-431.
- 1102 Dohm, J.M., Maruyama, S., 2014a. New evidence for plate tectonism on Mars: accreted terrains.
1103 Japan Geoscience Union meeting, April 28-May 2, 2014, PPS02-02, #418.
1104
- 1105 Dohm, J.M., Maruyama, S., 2014b. Habitable Trinity. *Journal of Geoscience Frontiers*, DOI:
1106 10.1016/j.gsf.2014.01.005.
1107
- 1108 Dohm, J.M., Anderson, R.C., Baker, V.R., et al., 2000. Pulses of magmatic activity through time:
1109 potential triggers for climatic variations on Mars. Lunar Planet. Sci. Conf. XXXI, abstract #
1110 1632 (CD-ROM).
- 1111 Dohm, J. M., Tanaka, K. L., Hare, T. M., 2001a. Geologic map of the Thaumasia region of Mars.
1112 US Geol. Survey Map I-2650.
- 1113 Dohm, J.M., Ferris, J.C., Baker, V.R., Anderson, R.C., Hare, T.M., Strom, R.G., Barlow, N.G.,
1114 Tanaka, K.L., Klemaszewski, J.E., Scott, D.H., 2001b. Ancient drainage basin of the Tharsis

- 1115 region, Mars: Potential source for outflow channel systems and putative oceans or
1116 paleolakes. *J. Geophys. Res.* 106, 32,943-32,958.
- 1117 Dohm J.M., Maruyama, S., Baker, V.R., 2001c. Mars plate tectonics: surface geology and
1118 analyses of topographic and geophysical data. *AGU*, 82(47), F713.
- 1119 Dohm, J.M., Maruyama, S., Baker, V.R., et al., 2001d. Earth-like evolution of the Tharsis
1120 Magmatic Complex: Traits of a Terrestrial Superplume (2). *Geol. Soc. America Abstracts*
1121 *with Programs*, 33(7), A309.
- 1122 Dohm, J.M., Maruyama, S., Baker, V.R., Anderson, R.C., Ferris, J.C., Hare, T.M., 2002a. Plate
1123 tectonism on early Mars: Diverse geological and geophysical evidence. *Lunar Planet. Sci.*
1124 *Conf.*, XXXIII, Abstract #1639 (CD-ROM).
- 1125 Dohm, J.M., Maruyama, S., Baker, V.R., Anderson, R.C., Ferris, J.C., Hare, T.M., 2002b.
1126 Evolution and traits of Tharsis superplume, Mars. *Superplume International Workshop*,
1127 *Abstracts with Programs*, Tokyo, 406-410.
- 1128 Dohm, J.M., Kerry, K., Keller, J.M., Baker, V.R., Maruyama, S., and Anderson, R.C., Ferris,
1129 J.C., Hare, T.M., 2005. Mars geological province designations for the interpretation of GRS
1130 data. *Lunar Planet. Sci. Conf. XXXVI*, #1567 (abstract) (CD-ROM)
- 1131 Dohm, J.M., Maruyama, S., Baker, V.R., Anderson, R.C., 2007a. Traits and evolution of the
1132 Tharsis superplume, Mars. In Yuen, D.A., Maruyama, S., Karato, S.-I., and Windley, B.F.,
1133 eds., *Superplumes: Beyond plate tectonics*: Springer, p. 523-537.
- 1134 Dohm, J.M., Barlow, N.G., Anderson, R.C., et al., 2007b. Possible ancient giant basin and
1135 related water enrichment in the Arabia Terra province, Mars. *Icarus* 190, 74-92, doi:
1136 10.1016/j.icarus.2007.03.006.
- 1137 Dohm, J.M., Anderson, R.C., Barlow, N.G., et al., 2008. Recent geological and hydrological
1138 activity on Mars: The Tharsis/Elysium Corridor. *Planet. Space Sci.* 56, 985–1013.
- 1139 Dohm, J.M., Williams, J.-P., Anderson, R.C., et al., 2009a. New evidence for a magmatic
1140 influence on the origin of Valles Marineris, Mars. *Journal of Volc. Geoth. Res.* 185, 12–27,
1141 doi:10.1016/j.jvolgeores.2008.11.029.
- 1142 Dohm, J.M., Baker, V.R., Boynton, W.V., et al., 2009b. GRS evidence and the possibility of
1143 ancient oceans on Mars. *Planet. Space Sci.* 57, 664-684.
- 1144 Dohm, J.M., Ferris, J.C., Baker, V.R., Komatsu, G., Buczkowski, D.L., El Maarry, M.R., Hare,
1145 T.M., Mahaney, W.C., Kim, K.J., Davila, A.F., Fairén, A.G., 2011a. Did a large Argyre lake
1146 source the Uzboi Vallis drainage system?: Post-Viking-era geologic mapping investigation.
1147 *Lunar Planet. Sci. Conf. XXXIII*, Abstract #2255 (CD-ROM).

- 1148 Dohm, J.M., Miyamoto, H., Ori, G.G., et al., 2011b. An inventory of potentially habitable
1149 environments on Mars: geological and biological perspectives. In Garry, W.B., and Bleacher,
1150 J.E., eds., *Analogs for Planetary Exploration: Geological Society of America Special Paper*
1151 483, 317–347, doi:10.1130/2011.2483(21).
- 1152 Dohm, J.M., Miyamoto, H., Maruyama, S., et al., 2013. Mars Evolution. In *Mars: Evolution,*
1153 *Geology, and Exploration*. A.G. Fairén (ed.). Book entitled: "Mars: Evolution, Geology and
1154 Exploration", Nova Science Publishers, Inc., pgs. 1-33.
- 1155 Dohm, J.M., Maruyama, S., Miyamoto, H., Viviano-Beck, C.E., Anderson, R.C., 2014a.
1156 Accretionary complexes: recorders on Earth and possibly Mars. 2014 GSA Annual Meeting
1157 in Vancouver British Columbia, Paper No. 25-9.
- 1158 Dohm, J.M., Maruyama, S., Miyamoto, H., Viviano-Beck, C.E., Anderson, R.C., 2014b.
1159 Accretionary complexes: recorders on Earth and possibly Mars. 2014 AGU Fall Meeting in
1160 San Francisco, Paper No. P33E-07.
- 1161 El Maarry, M.R., Dohm, J.M., 2013. Regional morphologies of the smooth deposits in the
1162 mountainous regions of Argyre, Mars: Results from high resolution mapping. *Lunar Planet.*
1163 *Sci. Conf. XXXXIV, #2806 (abstract) (CD-ROM).*
- 1164 El Maarry, M.R., Dohm, J.M., Michael, G., Thomas, N., Maruyama, S., 2013. Morphology and
1165 evolution of the ejecta of Hale crater in Argyre basin, Mars: results from high resolution
1166 mapping. *Icarus* 226, 905-922.
- 1167 Fairén, A.G., Dohm, J.M., 2004. Age and origin of the lowlands of Mars. *Icarus* 168, 277–284,
1168 doi:10.1016/j.icarus.2003.11.025.
- 1169 Fairén, A.G., Ruiz, J., Anguita, F., 2002. An origin for the linear magnetic anomalies on Mars
1170 through accretion of terranes: implications for dynamo timing. *Icarus* 160, 220–223,
1171 doi:10.1006/icar.2002.6942.
- 1172 Fairén, A.G., Dohm, J.M., Baker, V.R., de Pablo, M.A., Ruiz, J., Ferris, J.C., Anderson, R.C.,
1173 2003. Episodic flood inundations of the northern plains of Mars. *Icarus* 165, 53–67,
1174 doi:10.1016/S0019-1035(03)00144-1.
- 1175 Fairén, A.G., Stokes, C.R., Davies, N.S., Schulze-Makuch, D., Rodríguez, J.A.P., Davila,
1176 Alfonso F., Uceda, Esther R., Dohm, J.M., Baker, V.R., Clifford, S.M., McKay, Christopher
1177 P., Squyres, S.W., 2014. A cold hydrological system in Gale Crater, Mars. *Planetary and*
1178 *Space Science* 93, 101-118.
- 1179 Fastook, J.L., Head, J.W., Marchant, D., Forget, F., 2008. Tropical mountain glaciers on Mars:
1180 Altitude-dependence of ice accumulation, accumulation conditions, formation times, glacier
1181 dynamics, and implications for planetary spin-axis/orbital history. *Icarus* 198, 305–317.

- 1182 Feldman, W.C., Boynton, W.V., Tokar, R.L., et al., 2002. Global distribution of neutrons from
1183 Mars: Results from Mars Odyssey. *Science* 297, 75-78.
- 1184 Ferris, J.C., Dohm, J.M., Baker, V.R., and Maddock, T. (2002) Dark slope streaks on Mars: Are
1185 aqueous processes involved? *Geophysical Research Letters* 29, doi:10.1029/2002GL014936.
- 1186 Fink, W., Dohm, J.M., Tarbell, M.A., Hare, T.M., Baker, V.R., 2005. Next-generation robotic
1187 planetary reconnaissance missions: a paradigm shift. *Planet. Spa. Sci.* 53, 1419-1426.
- 1188 Fink, W., Dohm, J.M., Tarbell, M.A., Hare, T.M, Baker, V.R, Schulze-Makuch, D., Furfaro, R.,
1189 Fairén, A.G., Ferre, T.P.A., Miyamoto, H., Komatsu, G., Mahaney, W.C., 2007a. Tier-
1190 scalable reconnaissance missions for the autonomous exploration of planetary bodies. *IEEE*
1191 *Aerospace Conference Proceedings*, paper #1199; DOI: 10.1109/AERO.2007.352715
- 1192 Fink, W., George, T., Tarbell, M.A., 2007b. Tier-scalable reconnaissance: the challenge of
1193 sensor optimization, sensor deployment, sensor fusion, and sensor interoperability. *Proc.*
1194 *SPIE*, Vol. 6556, 655611 (2007); DOI:10.1117/12.721486.
- 1195 Fink W., Tarbell, M.A., Jobling, F.M., 2008. Tier-Scalable Reconnaissance - A Paradigm Shift
1196 in Autonomous Remote Planetary Exploration of Mars and Beyond. Chapter 1 in “Planet
1197 Mars Research Focus”, Ed. L. A. Costas. Nova Science Publishers, Hauppauge, NY. ISBN:
1198 1-60021-826-1. Frey, H.V., Roark, J.H., Shockey, K.M., Frey, E.L., Sakimoto, S.E.H., 2002.
1199 Ancient lowlands on Mars. *Geophys. Res. Lett.*, 29, 10.1029/2001GL013832.
- 1200 Garvin, J.B., Sakimoto, S.E.H., Frawley, J.J., and Schnetzler, C., 2002. Global geometric
1201 properties of Martian impact craters. *Lunar Planet. Sci. Conf. XXXIII*, abstract 1255.
- 1202 Glamoclija, M., Marinangeli, L., Komatsu, G., 2011. Harmakhis Vallis Source Region, Mars:
1203 Insights into the recent geothermal history based on geological mapping. *Planet. Space Sci.*
1204 59, 1179–1194, 10.1016/j.pss.2010.09.017.
- 1205 Harrison, T.M., 2009. The Hadean Crust: Evidence from >4 Ga Zircons. *Annual Review of Earth*
1206 *and Planetary Sciences* 37, 479-505.
- 1207 Harrison, K.P., Grimm, R.E., 2009. Regionally compartmented groundwater flow on Mars. *J.*
1208 *Geophys. Res.* 114, doi:10.1029/2008JE003300.
- 1209 Hartmann, W.K., 2005. Martian cratering 8: isochron refinement and the chronology of Mars.
1210 *Icarus* 174, 294-320.
- 1211 Hartmann, W.K., Neukum, G., 2001. Cratering Chronology and the Evolution of Mars. *Space*
1212 *Sci. Rev.* 96,165-194.

- 1213 Head, J.W., Pratt, S., 2001. Extensive Hesperian-aged south polar ice sheet on Mars: Evidence
1214 for massive melting and retreat, and lateral flow and ponding of meltwater. *J. Geophys. Res.*
1215 106, 12,275-12,299.
- 1216 Head, J.W., Mustard, J.F., Kreslavsky, M.A., Milliken, R.E., Marchant, D.R., 2003. Recent ice
1217 ages on Mars. *Nature* 426, 797-802.
- 1218 Hiesinger, H., Head J.W., 2002. Topography and morphology of the Argyre basin, Mars:
1219 Implications for its geologic and hydrologic history. *Planet. and Space Sci.* 50, 939-981.
- 1220 Hodges, C.A., 1980. Geological map of the Argyre quadrangle of Mars. U.S. Geol. Sur. Misc.
1221 Inv. Series Map I-1181, scale 1:500,000.
- 1222 Howenstine, J.B, Kiefer, W.S., 2005. Morphometry of large Martian impact craters. *Lunar*
1223 *Planet. Sci. Conf. XXXVI*, abstract 1742.
- 1224 Hynek, B.M., Beach, M., Hoke, R.T., 2010. Updated global map of Martian valley networks and
1225 implications for climate and hydrologic processes. *J. Geophys. Res.* 115, doi:
1226 10.1029/2009JE003548.
- 1227 Irwin, R.P., III, Tanaka, K.L., Robbins, S.J., 2013. Distribution of Early, Middle, and Late
1228 Noachian cratered surfaces in the Martian highlands: Implications for resurfacing events and
1229 processes, *J. Geophys. Res. Planets*, 118, 278–291, doi:10.1002/jgre.20053
- 1230 Ivanov, B.A., 2001. Mars/Moon cratering rate ratio estimates. *Spa. Sci. Rev.* 96, 87-104.
- 1231 Jones, A.P., McEwen, A.S., Tornabene, L.L., Baker, V.R., Melosh, H.J., Berman, D.C., 2011. A
1232 geomorphic analysis of Hale crater, Mars: The effects of impact into ice-rich crust. *Icarus*
1233 211, 259–272.
- 1234 Kargel, J.S., 2004. *Mars: A warmer wetter planet*. Praxis-Springer, 557 p.
- 1235 Kargel, J.S., Strom, R.G., 1990. Ancient glaciation on Mars. *Lunar Planet. Sci.* 597– 598.
- 1236 Kargel, J.S., Strom, R.G., 1992. Ancient glaciation on Mars. *Geology* 20, 3-7.
- 1237 Kargel, J.S., Baker, V.R., Beget, J.E., Lockwood, J.F., Pewe, T.L., Shaw, J.S., Strom, R.G.,
1238 1995. Evidence of ancient continental glaciation in the Martian northern plains. *J. Geophys.*
1239 *Res.*100, 5351–5368.
- 1240 Kargel, J.S., Leonard, G.J., Bishop, M.P., Kaab, A., Raup, B. (Eds), 2014. *Global Land Ice*
1241 *Measurements from Space* (Springer-Praxis), Heidelberg—e-book and hard-cover print
1242 publication, LXXIX, 876 p., 409 illus., 336 illus. in color. With extra online material.
- 1243 Kasting, J. F., Whitmire, D. P., Reynolds, R. T., 1993. Habitable Zones around Main Sequence
1244 Stars. *Icarus* 101, 108-128.

- 1245 Komatsu, G., Ori, G.G., Cardinale, M., et al., 2011. Roles of methane and carbon dioxide in
1246 geological processes on Mars. *Planet. Spa. Sci.* 59, 169–181, doi:10.1016/j.pss.2010.07.002.
- 1247 Komatsu, G., Okubo, C.H., Wray, J.J., Gallagher, R., Orosei, R., Cardinale, M., Chan, M.A., and
1248 Ormö, J., 2012. Small mounds in Chryse Planitia, Mars: Testing a mud volcano hypothesis.
1249 *Lunar Planet. Sci. Conf. XXXXIII*, abstract #1103.
- 1250 Konopliv A.S., Asmar S. W., Carranza E., et al., 2001. Recent gravity models as a result of the
1251 Lunar prospector mission. *Icarus* 150: 1-18.
- 1252 Konopliv, A.S., Asmar, S.W., Folkner, W.M., Karatekin, Ö., Nunes, D.C., Smrekar, S.E., Yoder,
1253 C.F., Zuber, M.T., 2011. Mars high resolution gravity fields from MRO, Mars seasonal
1254 gravity, and other dynamical parameters. *Icarus* 211, 401-428.
- 1255 Lane, M.D., Goodrich, C.A, 2010. High-magnesian olivine in the Argyre rim: derived from a
1256 primitive magma? LPSC XLI, abs. 2094, (CD-ROM), Lunar Planet. Inst., Houston, TX.
- 1257 Laskar, J., Correia, A.C.M., Gastineau, M., Joutel, F., Levard, B., Robutel, P., 2004. Long term
1258 evolution and chaotic diffusion of the insolation quantities of Mars. *Icarus* 170, 343-364.
- 1259 Lefort, A., Russell, P.W., McEwen, A.S., Dundas, C.M., Kirk, R.L., 2009. Observations of
1260 periglacial landforms in Utopia Planitia with the High Resolution Imaging Science
1261 Experiment (HiRISE). *J. Geophys. Res.* 114, E04005, doi:10.1029/2008JE003264.
- 1262 Lefort, A., et al., 2010. Scalloped terrain in the Peneus and Amphitrites Paterae region of Mars
1263 as observed by HiRISE. *Icarus* 205, 1, 259-268, doi:10.1026/j.icarus.2009.06.005.
- 1264 Leonard, G.J., Tanaka, K.L., 2001. Geologic map of the Hellas region of Mars, US Geol. Survey
1265 Map I-2694.
- 1266 Levy, J., Head, J., Marchant, D., 2009. Thermal contraction crack polygons on Mars:
1267 classification, distribution and climatic implications from HiRISE observations. *J. Geophys.*
1268 *Res.* 114, E01007, doi:10.1029/2008JE003273.
- 1269 Levy, J.S., Head, J.W., Marchant, D.R., 2011. Gullies, polygons and mantles in Martian
1270 permafrost environments: cold desert landforms and sedimentary processes during recent
1271 Martian geological history. in Martini, I.P., French, H.M., Perez Alberti, A., (eds.) *Ice*
1272 *marginal and periglacial processes and sediments*, Geological Society of London, 354, 167-
1273 182 doi:10.1144/SP35410 0305-8719.
- 1274 Liestol, O., 1975. Pingos, springs, and permafrost in Spitsbergen, Nor. *Polar Årbook*, 7-29.
- 1275 Lias, J.H., Dohm, J.M., Tanaka, K.L., 1997. Geologic history of Lowell impact. *Lunar Planetary*
1276 *Science Conference, XXVIII*, #1650 (abstract) [CD-ROM].

- 1277 Lillis, R.J., et al., 2008. An improved crustal magnetic field map of Mars from electron reflectometry: Highland volcano magnetic history and the end of the Martian dynamo. *Icarus* 194,
1278 575-596. doi: 10.1016/j.icarus.2007.09.032.
1279
- 1280 Madeleine, J.B., Forget, F., Head, J.W., Levrard, B., Montmessin, F., Millour, E., 2009.
1281 Amazonian northern mid-latitude glaciation on Mars: a proposed climate scenario. *Icarus*
1282 203, 390-405, doi:10.1016/j.icarus.2009.04.037.
- 1283 Mahaney, W.C., Dohm, J.M., Baker, V.R., et al., 2001. Morphogenesis of Antarctic paleosols:
1284 Martian analog. *Icarus* 154, 113-130.
- 1285 Mahaney, W.C., Dohm, J.M., Kapran, B., et al., 2009. Secondary Fe and Al in Antarctic
1286 paleosols: Correlation to Mars with prospect for the presence of life. *Icarus* 203, 320–330,
1287 doi:10.1016/j.icarus.2009.05.007.
- 1288 Mahaney, W.C., Hart, K.M., Dohm, J.M., Hancock, R.G.V., Costa, P., O'Reilly, S.S., Kelleher,
1289 B.P., Schwartz, S., Lanson, B., 2011. Aluminum extracts in Antarctic paleosols: proxy data
1290 for organic compounds and bacteria and implications for Martian paleosols Sedimentary.
1291 *Geology* 237, 84-94.
- 1292 Malin, M.C., Bell, J.F., III, Cantor, B.A., and 11 others, 2007. Context Camera investigation on
1293 board the Mars Reconnaissance Orbiter. *J. Geophys. Res.* 112, doi:10.1029/2006JE002808.
- 1294 Mangold, N., 2011. Ice sublimation as a geomorphic process: a planetary perspective.
1295 *Geomorph.* 126, 1-17, doi:10.1016/2010.11.009.
- 1296 Maruyama, S., 1997. Pacific-type orogeny revisited: Miyashiro-type orogeny proposed. *Island*
1297 *Arc* 6, 91–120, doi:10.1111/j.1440-1738.1997.tb00042.x.
- 1298 Maruyama, S., Isozaki, Y., Kimura, G., Terabayashi, M., 1997. Paleogeographic maps of the
1299 Japanese Islands: plate tectonic synthesis from 750 Ma to the present. *The Island Arc* 6, 121–
1300 142.
- 1301 Maruyama S., Dohm, J.M., Baker, V.R., 2001a. Mars plate tectonics (1): an Earth prospective.
1302 American Geophysical Union, Fall Meeting 2001, 82(47), Suppl., Abstract P32C-0565.
- 1303 Maruyama, S., Dohm, J.M., Baker, V.R., 2001b. Tharsis superplume (1): Why superplume?
1304 *Geol. Soc. America Abstracts with Programs*, 33(7), A310.
- 1305 Maruyama, S., Baker, V.R., Dohm, J.M., 2008. Life and Land of Mars, 4.6 Billion Years.
1306 Koudansha, Tokyo, 256 p. (In Japanese)
- 1307 Maruyama, S., Ikoma, M., Genda, H., Hirose, K., Yokoyama, T., Santosh, M., 2013. The naked
1308 planet Earth: most essential pre-requisite for the origin and evolution of life. *Geosci. Front.* 4,
1309 141-165.

- 1310 Maruyama, S., Sawaki, Y., Ebisuzaki, T., Ikoma, M., Omori, S., Komabayashi, T., 2014.
1311 Initiation of leaking Earth: An ultimate trigger of the Cambrian explosion. *Gondwana Res.*
1312 25, 910-944.
- 1313 Matsumoto K., Goossens S., Ishihara Y., et al., 2010. An improved lunar gravity field model
1314 from SELENE and historical tracking data: Revealing the farside gravity features. *J.*
1315 *Geophys. Res.* 115 (E6): E06007.
- 1316 McCauley, J.F., 1978. Geologic map of the Coprates quadrangle of Mars. US Geol. Survey Map
1317 Misc. Invest. Ser. Map I-897, scale 1:5,000,000.
- 1318 McEwen, A.S., Eliason, E.M., Bergstrom, J.W., 2007. Mars Reconnaissance Orbiter's High
1319 Resolution Imaging Science Experiment (HiRISE). *J. Geophys. Res.* 112, DOI:
1320 10.1029/2005JE002605.
- 1321 McEwen, A.S., Dundas, C., Mattson, S., et al., 2013. Recurring slope lineae (RSL) in equatorial
1322 Mars. European Planetary Science Congress 2013, Abstract #846.
- 1323 McGill, G.E., 1978. Geologic map of the Thaumasia quadrangle of Mars: US Geol. Survey Misc.
1324 Invest. Ser. Map I-1077, scale 1:5,000,000.
- 1325 McGill, G.E., 1989. Buried topography of Utopia, Mars: persistence of a giant impact
1326 depression. *J. Geophys. Res.* 94, 2753-2759.
- 1327 Mest, S.C., Crown, D.A., 2001. Geology of the Reull Vallis region, Mars, *Icarus*, 153, 89-110.
- 1328 Milliken, R.E., Mustard, J.F., Goldsby, D.L., 2003. Viscous flow features on the surface of Mars:
1329 Observations from high-resolution Mars Orbiter Camera (MOC) images. *J. Geophys. Res.*
1330 108, E6, 5057, doi:10.1029/2002JE002005.
- 1331 Miyamoto, H., Dohm, J.M., Beyer, R.A., Baker, V.R., 2004. Fluid dynamical implications of
1332 anastomosing slope streaks on Mars. *J. Geophys. Res.* 109, E06008,
1333 doi:10.1029/2003JE002234.
- 1334 Moore, J.M., Wilhelms, D.E., 2007. Geologic map of part of western Hellas Planitia, Mars. US
1335 Geol. Survey Map SIM-2953, 2007.
- 1336 Morgenstern, A., Hauber, E., Reiss, D., van Gasselt, S., Grosse, G., Schirrmeyer, L., 2007.
1337 Deposition and degradation of a volatile-rich layer in Utopia Planitia, and implications for
1338 climate history on Mars. *J. Geophys. Res.* 112, E06010. doi:10.1029/ 2006JE002869.
- 1339 Müller, F., 1959. Beobachten über pingos (Observationsonpingos). *Medd. Grønland*. 153 (3), 127.
1340 Reprinted as Technical Translation 1073 by National Research Council of Canada, Ottawa,
1341 Canada, 1963.

- 1342 Muller, P.M., Sjogren, W.L., 1968. Mascons: Lunar mass concentrations. *Science* 161, 680-684.
- 1343 Murchie, S., Arvidson, R., Bedini, P., Beisser, K., Bibring, J.-P., Bishop, J., Boldt, J., Cavender,
1344 P., Choo, T., Clancy, R.T., Darlington, E.H., Des Ma-rais, D., Espiritu, R., Fort, D., Green,
1345 R., Guinness, E., Hayes, J., Hash, C., Heffernan, K., Hemmler, J., Heyler, G., Humm, D.,
1346 Hutcheson, J., Izenberg, N., Lee, R., Lees, J., Lohr, D., Malaret, E., Martin, T., McGovern,
1347 J.A., McGuire, P., Morris, R., Mustard, J., Pelkey, S., Rhodes, E., Robinson, M., Roush, T.,
1348 Schaefer, E., Seagrave, G., Seelos, F., Silverglate, P., Slavney, S., Smith, M., Shyong, W.-J.,
1349 Strohbehn, K., Taylor, H., Thompson, P., Tossman, B., Wirzburger, M., Wolff, M., 2007.
1350 CRISM (Compact Reconnaissance Imaging Spectrometer for Mars) on MRO (Mars
1351 Reconnaissance Orbiter). *J. Geophys. Res.* 112, 1-57.
- 1352 Murchie S.L., Seelos, F.P. Buczkowski, D.L. Mustard, J.F. Ehlmann, B.L. Milliken, R.E. Noe
1353 Dobrea, E.Z. Bishop, J.L. McKeown, N.K. Wiseman, S.M. Arvidson, R.E. Wray, J.J.
1354 Swayze, G., Clark R.N., 2009a. A synthesis of Martian aqueous mineralogy after one Mars
1355 year of observations from the Mars Reconnaissance Orbiter. *J. Geophys. Res.* 114, E00D06,
1356 doi:10.1029/2009JE003342.
- 1357 Murchie, S.L., Seelos, F.P., Hash, C.D., et al., 2009b. The Compact Reconnaissance Imaging
1358 Spectrometer for Mars investigation and data set from the Mars Reconnaissance Orbiter's
1359 primary science phase. *J. Geophys. Res.* 114, E00D07, doi:10.1029/2009JE003344.
- 1360 Mustard, J.F., Cooper, C.D., Rifkin, M.R., 2001. Evidence for recent climate change on Mars
1361 from the identification of youthful near-surface ground ice. *Nature* 412, 411-414.
1362 doi:10.1038/35086515.
- 1363 Mustard, J., Murchie, S., Pelkey, S.M., Ehlmann, B.L., Milliken, R.E., Grant, J.A., Bibring, J.-P.,
1364 Poulet, F., Bishop, J., Noe Dobrea, E., Roach, L., Seelos, F., Arvidson, R.E., Wiseman, S.,
1365 Green, R., Hash, C., Humm, D., Malaret, E., McGovern, J.A., Seelos, K., Clancy, T., Clark,
1366 R., Des Marais, D., Izenberg, N., Knudson, A., Langevin, Y., Martin, T., McGuire, P.,
1367 Morris, R., Robinson, M., Roush, T., Smith, M., Swayze, G., Taylor, H., Titus, T., Wolff M.,
1368 2008. Hydrated silicate minerals on Mars observed by the CRISM instrument on MRO.
1369 *Nature* 454, 305-309.
- 1370 Nahm, A. L., and R. A. Schultz, 2011. Magnitude of global contraction of Mars from analysis of
1371 surface faults: implications for Martian thermal history. *Icarus* 211, 389–400.
- 1372 Neukum, G., Ivanov, B.A., Hartmann, W.K., 2001. Cratering records in the inner solar system in
1373 relation to the lunar reference system. In *Chronology and Evolution of Mars* (R. Kallenbach,
1374 J. Geiss, and W. K. Hartmann, eds.), Kluwer Academic Publishers, 55-86.
- 1375 Neumann, G.A., Zuber, M.T., Smith, D.E., Lemoine, F.G., 1996. The lunar crust: global
1376 structure and signature of major basins. *J. Geophys. Res.* 101, 16841 –16,863.

- 1377 Neumann, G.A., Smith, D.E., Zuber, M.T., 2003. Two Mars years of clouds detected by the Mars
1378 Orbiter Laser Altimeter. *J. Geophys. Res. Planets* 108, 5023. doi:10.1029/2002JE001849.
- 1379 Ody, A., Poulet, F., Langevin, Y., Bibring, J.-P., Bellucci, G., Altieri, F., Gondet, B., Vincendon,
1380 M., Carter, J., Manaud, N., 2012. Global maps of anhydrous minerals at the surface of Mars
1381 from OMEGA/MEx. *J. Geophys. Res.* 117, E00J14, doi:10.1029/2012JE004117.
- 1382 Oehler, D.Z., Allen, C.C., 2010. Evidence for pervasive mud volcanism in Acidalia Planitia,
1383 Mars. *Icarus* 208, 636–657, doi:10.1016/j.icarus.2010.03.031.
- 1384 Öhman, T., Aittola, M., Kostama, V.-P., Raitala, J., Korteniemi, J., 2008. Polygonal impact
1385 craters in Argyre region, Mars: implications for geology and cratering mechanics.
1386 *Meteoritics & Planetary Science* 43, 1605-1628.
- 1387 Parker, T.J., 1985. Geomorphology and geology of the southwestern Margaritifer Sinus -
1388 northern Argyre region of Mars. Master's thesis, Geology Department, California State
1389 University, Los Angeles, 165pp.
- 1390 Parker, T.J., 1989. Channels and valley networks associated with Argyre Planitia, Mars. *Lunar*
1391 *Planet. Sci.* XX, 826-827.
- 1392 Parker, T.J., 1994. Martian paleolakes and oceans. Ph.D. dissertation, Geological Sciences,
1393 University of Southern California, 200pp.
- 1394 Parker, T.J., 1996. Highlights from 1:500K geologic mapping of central and southern Argyre
1395 Planitia. *Lunar Planet Sci.* XXVII, 1003-1004.
- 1396 Parker, T.J., Gorsline, D.S., 1991. Where is the source for Uzboi Vallis, Mars? *Lunar Planet Sci.*
1397 XXII, 1033-1034.
- 1398 Parker, T.J., Gorsline, D.S., 1992. Preliminary geologic mapping of the MTM-55036 and -55043
1399 quadrangles, southern Argyre Planitia, Mars (abs.). *Lunar Planet Sci.* 23, 1031-1032.
- 1400 Parker, T.J. Gorsline, D.S., 1993. Extent and timing of fluvial and lacustrine events in Argyre
1401 Planitia, Mars. *Am. Geophys. Union Spring Meeting*, 1pp.
- 1402 Parker, T.J., Clifford, S.M., Banerdt, W.B., 2000. Argyre Planitia and the Mars global hydrologic
1403 cycle. *Lunar Planet Sci.* [CD-ROM], 31th, abstract 2033.
- 1404 Platz, T., Michael, G.G., 2011. Eruption history of the Elysium Volcanic Province, Mars. *Earth*
1405 *and Planetary Science Letters* 312, 140–151, doi:10.1016/j.epsl.2011.10.001.
- 1406 Platz, T., Michael, G.G., Tanaka, K.L., et al., 2013. Crater-based dating of geological units on
1407 Mars: Methods and application for the new global geological map. *Icarus* 225, 806–827,
1408 doi:10.1016/j.icarus.2013.04.021.

- 1409 Poulet, F., Bibring, J.P., Mustard, J.F., et al., 2005. Phyllosilicates on Mars and implications for
1410 early Martian climate. *Nature* 438, 623–627.
- 1411 Poulet, F., Gomez, C., Bibring J.-P., Langevin, Y., Gondet, B., Pinet, P., Belluci, G., Mustard J.,
1412 2007. Martian surface mineralogy from Observatoire pour la Minéralogie, l'Eau, les Glaces et
1413 l'Activité on board the Mars Express spacecraft (OMEGA/MEx): Global mineral maps. *J.*
1414 *Geophys. Res.* 112, E08S02, doi:10.1029/2006JE002840.
- 1415 Quaide, W.L., Gault, D.E., Schmidt, R.A., 1965. Gravitative effects on lunar impact structures.
1416 *Annals of the New York Academy of Sciences* 123, 641-655.
- 1417 Raack, J., Reiss, D., Heisinger, H., 2012. Gullies and their relationship to the dust-ice mantle in
1418 the northwestern Argyre Basin, Mars. *Icarus* 219, 129-141, doi:10.1016/j.icarus.2012.
1419 02.0125.
- 1420 Robbins, S.J., Hynek, B.M., 2012. A new global database of Mars impact craters ≥ 1 km: 1.
1421 Database creation, properties, and parameters. *J. Geophys. Res.* 117, doi:
1422 10.1029/2011JE003966.
- 1423 Robbins, S.J., Hynek, B.M., Lillis, R.J., Bottke, W.F., 2013. Large impact crater histories of
1424 Mars: The effect of different model crater age techniques. *Icarus* 225, 173–184. doi:
1425 10.1016/j.icarus.2013.03.019.
- 1426 Roberts, J.H., Arkani-Hamed, J., 2012. Impact-induced mantle dynamics on Mars. *Icarus* 218,
1427 278-289.
- 1428 Roberts, J.H., Lillis, R.J., Manga, M., 2009. Giant impacts on early Mars and the cessation of the
1429 Martian dynamo. *J. Geophys. Res.* 114, E04009, doi: 10.1029/2008JE003287.
- 1430 Rodriguez, J.A.P., Kargel, J.S., Tanaka, K.L., Crown, D.A., Berman, D.C., Fairén, A.G., Baker,
1431 V.R., Furfaro, R., Candelaria, P., Sasaki, S., 2011. Secondary chaotic terrain formation in
1432 higher outflow channels of southern circum-Chryse, Mars. *Icarus* 213,150-194.
- 1433 Rodriguez, J.A.P., Kargel J.S., et al., 2014. Evidence for Middle Amazonian catastrophic
1434 flooding and glaciation on Mars. *Icarus* 242, Pages 202–210.
- 1435 Rossi, A.P., Gasselt, S.V., Pondrelli, M., Dohm, J.M., Hauber, E., Dumke, A., Zegers, T.,
1436 Neukum, G., 2011. Evolution of periglacial landforms in Thaumasia Highland, Mars. *M.R.*
1437 *Balme, A.S. Bargery, C.J. Gallagher, and S. Gupta (eds.) In Geomorphology on Mars and*
1438 *other planets, Geological Society, London, Special Publications 356, 69-85.*
- 1439 Rotto, S.L., Tanaka, K.L., 1995. Geologic/geomorphologic map of the Chryse Planitia region of
1440 Mars. *US Geol. Survey Map I-2441 (1:5,000,000).*

- 1441 Ruiz, J., 2014. The early heat loss evolution of Mars and their implications for internal and
1442 environmental history. *Sci. Rep.* 4, doi:10.1038/srep04338.
- 1443 Saunders, R.S., 1979. Geologic map of the Margaritifer Sinus quadrangle of Mars. US Geol.
1444 Survey Map Misc. Invest. Ser. Map I-1144, scale 1:5,000,000.
- 1445 Schubert, G., Turcotte, D.L., 2002. *Geodynamics*, Cambridge University Press.
- 1446 Schubert, G., Solomon, S.C., Turcotte, D.L., Drake, M.J., Sleep, N.H., 1992. Origin and thermal
1447 evolution of Mars. In *Mars*, University of Arizona Press, Tucson, pp. 147-183.
- 1448 Schultz, R.A., Tanaka, K.L. (1994) Lithospheric-scale buckling and thrust structures on Mars:
1449 The Coprates rise and south Tharsis ridge belt. *J. Geophys. Res.* 99, 8371-8385.
- 1450 Schulze-Makuch, D., Head, J.N., Houtkooper, J.M., et al. 2012. The biological oxidant and life
1451 detection (BOLD) mission: a proposal for a mission to Mars. *Planet. Space Sci.* 67, 57-69.
- 1452 Scott, D.H., Carr, M.H., 1978. Geologic map of Mars. US Geol. Survey Map I-1083.
- 1453 Scott, D.H., Tanaka, K.L., Greeley, R., Guest, J.E., 1986-87. Geologic maps of the western and
1454 eastern equatorial and polar regions of Mars. US Geol. Survey Map Misc. Inv. Ser. Map I-
1455 1802-A, B, C.
- 1456 Segura, T.L., Toon, O.B., Colaprete, A., Zahnle, K., 2002. Environmental Effects of Large
1457 Impacts on Mars. *Science* 298, 1977-1980.
- 1458 Seibert, N.M., Kargel, J.S., 2001. Small-Scale Martian Polygonal Terrain: Implications for
1459 Liquid Surface Water. *Geophys. Res. Lett.* 28, 899– 903.
- 1460 Shoemaker, E.M., 1963. Impact mechanics at Meteor crater, Arizona. In Middlehurst, B.M., and
1461 Kuiper, G.P., eds., *The Moon, Meteorites, and Comets*: Chicago, University of Chicago
1462 Press, p. 301-336.
- 1463 Shreve, R.L., 1985. Esker characteristics in terms of glacier physics, Katahdin esker system,
1464 Maine. *Geol. Soc. Am. Bull.* 96, 639-646.
- 1465 Skinner, J.A., Tanaka, K.L., 2007. Evidence for and implications of sedimentary diapirism and
1466 mud volcanism in the southern Utopia highland-lowland boundary plain, Mars. *Icarus* 186,
1467 41–59.
- 1468 Skinner, J.A., Mazzini, A., 2009. Martian mud volcanism: terrestrial analogs and implications for
1469 formational scenarios. *Marine and Petroleum Geology* 26, 1866–1878.
- 1470 Skinner, J.A., Jr., Tanaka, K.L., Platz, T., 2012. Widespread loess-like deposit in the Martian
1471 northern lowlands identifies Middle Amazonian climate change. *Geology* 40, 1127-1130,
1472 doi:10.1130/G33513.1.

- 1473 Sleep, N. H., 1994. Martian plate tectonics. *J. Geophys. Res.* 99, 5639-5655.
- 1474 Smith D.E., et al., 1999. The global topography of Mars and implications for surface evolution.
1475 *Science* 284, 1495-1503.
- 1476 Soare, R.J., Conway, S.J., Dohm, J.M., 2012a. Evidence of landscape modification in and around
1477 the Argyre impact basin, Mars, by “wet” periglacial processes. 2012 GSA Annual Meeting
1478 and Exposition, Charlotte, North Carolina, 44, 7, 64.
- 1479 Soare, R.J., Conway, S.J., Dohm, J.M., Sejourne, A., 2012b. Climate-change and the origin of
1480 ice-rich permafrost in mid Utopia Planitia, Mars. Mars recent climate change workshop,
1481 Ames Research Center, Moffett Field, California.
- 1482 Soare, R.J., Conway, S.J., Dohm, J.M., El-Maarry, M.R., 2014a. Possible ice-wedge polygons
1483 and recent landscape modification by “wet” periglacial processes in and around the Argyre
1484 impact basin, Mars. *Icarus* 233, 214-228.
- 1485 Soare, R.J., Conway, S.J., Dohm, J.M., El-Maarry, M.R., 2014b. Possible open-system
1486 (hydraulic) pingos in and around the Argyre impact regions of Mars. *Earth and Planet. Lett.*
1487 398, 25-36.
- 1488 Soare, R.J., Conway, S.J., Gallagher, C., Balme, M.R., Dohm, J.M., 2015. Pre- and post- glacial
1489 periglaciation in Argyre Planitia, Mars. *Lunar Planet. Sci. Conf. XXXXVI*, Houston, Texas.
1490 Abstract #1218.
- 1491 Solomon, S., Head, J.W., 1980. Lunar mascon basins: lava filling, tectonics, and evolution of the
1492 lithosphere. *Rev. Geophys. Space Phys.* 18, 107-141.
- 1493 Spagnuolo, M.G., Dohm, J.M., 2004. Triggering the end of plate tectonics by forced climate
1494 changes. Workshop on Martian Hemispheres, Lunar Planetary Institute, #4001(abstract)
1495 [CD-ROM].
- 1496 Tanaka, K.L., 1986. The stratigraphy of Mars. *Proc. Lunar Planet. Sci. Conf. 17th*, Part 1, J.
1497 *Geophys. Res.*, 91, suppl., E139-158, 1986.
- 1498 Tanaka, K.L., Isbell, N.K., Scott, D.H., Greeley, R., Guest, J.E., 1988. The resurfacing history of
1499 Mars: A synthesis of digitized, Viking-based geology. *Proc. Lunar Planet. Sci. Conf. 18*, 665-
1500 678.
- 1501 Tanaka, K.L., Skinner, J.A., Hare, T.M., 2005. Geologic map of the northern plains of Mars.
1502 USGS Misc. Scientific Investigations. Map 2888, scale 1:15,000,000.
- 1503 Tanaka, K.L., Skinner, J.A., Dohm, J.M., Rossman, R.P. III, Kolb, E.J., Fortezzo, C.M., Platz,
1504 T., Michael, G.G., Hare, T.M., 2014. Geologic map of Mars. US Geol. Survey Map
1505 Scientific Investigations Map 3292.

- 1506 Thomas, G., Masson, H., 1984. Geology and tectonics of the Argyre area on Mars: comparisons
1507 with other basins in the solar system. *Earth, Moon, and Planets* 31, 25-42.
- 1508 Touma, J., Wisdom, J., 1993. The chaotic obliquity of Mars. *Science* 259, 1294-1296.
- 1509 Werner, S.C., Tanaka, K.L., 2011. Redefinition of the crater-density and absolute-age boundaries
1510 for the chronostratigraphic system of Mars. *Icarus* 215, 603-607.
- 1511 Wichman, R.W., Schultz, P.H., 1989. Sequence and mechanisms of deformation around the
1512 Hellas and Isidis impact basins on Mars. *J. Geophys. Res.* 94, 17,333-17,357.
- 1513 Wieczorek, M.A., Phillips, R.J., 1999. Lunar multiring basins and the cratering process. *Icarus*
1514 139, 246-259.
- 1515 Wilhelms, D.E., 1987. The geologic history of the Moon. US Geol. Survey Prof. Pap. 1348.
- 1516 Williams, D.A., Greeley, R., 1994. Assessment of antipodal-impact terrains on Mars. *Icarus* 110,
1517 196-202.
- 1518 Williams, J.-P., Dohm, J. M., Lopes, R. M., and Buczkowski, D.L., 2014. A large vent structure
1519 within Argyre Basin, Mars. LPSC XXXXV, abs. 2807, (CD-ROM), Lunar Planet. Inst.,
1520 Houston, TX.
- 1521 Wilmes, M., Reiss, D., Hiesinger, H., Zanetti, M., 2012. Surface age of the ice-dust mantle
1522 deposit in Malea Planum, Mars. *Planet. and Space Sci.* 60, 199-206, doi:10.1016/j.pss.2011.
1523 08.006.
- 1524 Yin, A., 2012a. An episodic slab-rollback model for the origin of the Tharsis rise on Mars:
1525 implications for initiation of local plate subduction and final unification of kinematically
1526 linked global plate-tectonic network on Earth. *Lithosphere* 4, 553-593, doi: 10.1130/L195.1.
- 1527 Yin, A., 2012b. Structural analysis of the Valles Marineris fault zone: possible evidence for
1528 large-scale strike-slip faulting on Mars. *Lithosphere*, doi: 10.1130/L192.
- 1529 Zanetti, M., Hiesinger, H., Reiss, D., Hauber, E., Neukum, G., 2010. Distribution and evolution
1530 of scalloped terrain in the southern hemisphere, Mars. *Icarus* 206, 691-706,
1531 doi:10.1016/j.icarus.2009.09.010.
- 1532

1533 **Table 1.** Unit symbols, unit names, and unit areas (see corresponding geologic map shown in **Fig. 3**). Interpreted
 1534 sedimentary deposits include aeolian, lacustrine, glacial, periglacial, fluvial, alluvial, and colluvial deposits.
 1535 Magmatic includes both intrusive (exposed through differential erosion and impact excavation) and volcanic. The
 1536 primary basin materials (members NAb1, NAb2, NAb3, NAb4b, HAb4a) occur at distinct elevation ranges (see
 1537 **Figs. 3, 5, 6** and Sections 4.2 and 4.3,1). See **Table 2** for description and interpretation and **Table 3** for relative age
 1538 information through comprehensive crater statistics. Not shown below are the older impact crater materials (unit
 1539 C1), younger impact crater materials (unit C2), smooth impact crater materials (unit Cfs), and rough crater floor
 1540 materials (unit Cfr). Note that the Argyre rim materials are diverse in stratigraphy, topography, and morphology, as
 1541 thus separated into Argyre rim (unit NAr; mainly rim materials), Argyre rim and basin (Unit NArb; majority being
 1542 rim materials with interspersed basin (including valley) deposits), Argyre basin and rim (unit NAbr; majority being
 1543 basin infill deposits with intervening rim materials in the form of knobs and mesas), Argyre rim smooth plains (rim
 1544 materials with large distinct patches of relatively smooth plains) materials.

Unit	Unit Names	Area (km ²)	Brief Interpretation (see Table 2 for greater details)
Nh1	Highlands member 1	327,794	Sedimentary; impact; magmatic
Nh2	Highlands member 2	1,096,085	Sedimentary; impact; magmatic
HNh3	Highlands member 3	168,887	Sedimentary; impact; magmatic
HNh4	Highlands member 4	262,637	Sedimentary; impact; magmatic
Nhb	Highland basin	67,049	Local basins infilled by sedimentary deposits
HNTTh	Thaumasia highlands	28,531	Sedimentary; highly modified basement complex; magmatic; impact
AHTp	Thaumasia plateau	16,282	Magmatic (e.g., ignimbrites); sedimentary
NAr	Argyre rim	58,067	Mantle and lower crustal materials; basement complex; sedimentary; hydrothermal
NArb	Argyre rim and basin	109,274	Mantle and lower crustal materials; basement complex; sedimentary; hydrothermal
NAbr	Argyre basin and rim	577,012	Similar to unit Arb but more basin materials (sedimentary); hydrothermal
NArsp	Argyre rim smooth plains	38,939	Similar to Arb but plains-forming materials mostly sedimentary
NAb1	Argyre basin, member 1	100,203	Sedimentary deposits
NAb2	Argyre basin, member 2	209,887	Sedimentary deposits
NAb3	Argyre basin, member 3	208,086	Sedimentary deposits
HAb4a	Argyre basin, member 4a	341,499	Sedimentary deposits
NAb4b	Argyre basin, member 4b	18,541	Sedimentary deposits; basin marginal unit, which underlies unit Ab4a, is related to unit NAb3

1545

1546 **Table 2.** Description and interpretation of map units. For cumulative crater densities and estimated unit ages of the
 1547 geologic units in the Argyre and surrounding region of Mars, see **Table 3**.

Unit Name	Unit Label	Description	Interpretation
Argyre basin sequence stratigraphy (units HAb4a, NAb4b, NAb3, NAb2, NAb1)			
Argyre basin member 4a	HAb4a	Younger Argyre plains-forming basin floor deposits marked by sinuous ridges, knobs, broken terrain, topographic depressions of varying geometric shapes, buried/subdued impact craters, and dune fields. The younger floor materials are approximately or gradationally in contact with either unit HAb4b or unit NAb3 materials.	The upper most part of the Argyre basin infill floor materials representative of environmental change induced by Stage 4 (Late Hesperian; for Tharsis-Stage information see Section 2 and Fig. 4) Tharsis magmatic-driven activity with lesser activities including Elysium. This includes ice melt, spring-fed activity, flooding, gelifluction, and lake and glacier formation along its margin, with subsequent resurfacing, including aeolian, fluvial, volatile-release, glacial, alluvial, impact cratering including secondaries, and/or colluvial, some processes of which are active today; the lower parts (those underlying unit HAb4a materials with associated impact craters exposed at the surface or not totally buried by unit HAb4a) of the infill deposits (extending at depth to the ancient Argyre basin floor) were emplaced by earlier perturbations in climate/environmental conditions from Tharsis and less prominent activities such as Elysium volcanism. The relative timing of these activities are indicated by stratigraphy and impact crater densities (Table 3). The rock materials source from diverse provenances, including the Argyre rim and ejecta deposits (upper mantle materials and older primordial crustal materials excavated to and near the Martian surface by the impact event and associated overturn and inversion of stratigraphy; materials also include hydrothermal deposits) and beyond, even including materials transported from as far north as Tharsis and the Thaumasia highlands and from as far south as the south pole. Therefore, the rock materials are considered to be diverse in both geochemistry and the mineralogic record, representative of diverse environmental conditions. The sinuous ridges located in the southeast part of the basin floor are eskers, associated with the latter stage of lake formation (margins of the lake were freezing) and marginal glaciers were connected to the lake. The subglacial rivers followed topography.
Argyre basin member 4b	NAb4b	Older Argyre plains-forming basin floor deposits marked by flows, erosional scarps, systems of sinuous valleys, and highly degraded and subdued impact craters, which partly form the contact separating these deposits from the younger plains-forming basin floor deposits. These materials are buried and/or embayed by unit HAb4a materials and gradational with generally higher-standing unit NAb3 materials.	Argyre basin floor materials representing older basin infill materials emplaced largely by early Tharsis magmatic-driven activity (e.g., Stages 1-2), which includes unit NAb3 materials with subsequent resurfacing, including aeolian, fluvial, volatile-release, glacial, alluvial, impact cratering, which includes secondaries, and/or colluvial. The rock materials source from diverse provenances, including the Argyre rim and ejecta deposits (upper mantle materials and older primordial crustal materials excavated to and near the Martian surface by the impact event and associated overturn and inversion of stratigraphy; materials also include hydrothermal deposits) and beyond, even including materials transported from as far north as Tharsis and the Thaumasia highlands and from as far south as the south pole. Therefore, the rock materials are considered to be diverse in both geochemistry and the mineralogic record, representative of diverse environmental conditions (e.g., assortment of varying pressure, temperature, and volatile conditions).
Argyre basin member 3	NAb3	Deposits that are gradationally in contact with the younger and older plains-forming basin floor deposits, which are marked by flows, networking channel systems such as highlighted in the southeast part of the basin at the juncture of the floor and rim-associated slope (e.g., troughs delineated on the geologic map near the terminus of Nia Vallis; Fig. 3) and Moanda impact crater in the northeast part (Figs. 3), aprons along the margins of promontories and other flow-feature types, degraded and partly buried impact craters, knobs and other quasi-circular promontories with marginal aprons, erosional scarps, and irregular depressions. In addition, deposits which occur on the lower-most valley segment extending from the margin of the basin floor inset within the Argyre-impact-induced radial valleys, with distinct breaks in slope (including terrace-like topography in places) at the contact between these deposits and the older deposits of unit NAb2 at higher elevations along the valley floor, particularly distinct along the floors of the three valleys that debouch into the southern and southeast parts of the Argyre basin, Surlus Vallis and Dzigai and Nia Valles, respectively (Figs. 1, 3, and 6).	Hillslope-forming materials in contact with the basin floor materials related to changes in environmental conditions/climate, as well as gravity-driven processes of ice-enriched rock materials through time. Major surface modification related to Tharsis-driven activity (e.g., Stages 1-3), indicated by stratigraphy and impact crater densities (Table 3), which includes hydrologic activity (ice melt, flooding, gelifluction, and lake formation, as well as incisement of the radial valleys related to a changing hydraulic head linked to the changing hydrologic system of groundwater, surface lakes, and glaciers), with subsequent surface modification including Tharsis- (Stages 4-5) and obliquity-driven, aeolian, fluvial, volatile-release, glacial, alluvial, impact cratering, which includes secondaries, and/or colluvial, some processes of which are active today. Wind and water (liquid and ice) activity has modified the landscape. The rock materials source from diverse provenances, including the Argyre rim and ejecta deposits (upper mantle materials and older primordial crustal materials excavated to and near the Martian surface by the Argyre impact event and associated overturn and inversion of stratigraphy; materials also include hydrothermal deposits) and beyond, even including materials transported from as far north as Tharsis and the Thaumasia highlands and from as far south as the south pole. Therefore, the rock materials are considered to be diverse in both geochemistry and the mineralogic record, representative of diverse environmental conditions (e.g., assortment of varying pressure, temperature, and volatile conditions). Argyre-impact-induced basement structures are conduits for the internal heat release of Mars and associated groundwater migration resulting in local geologic and hydrologic activity, including linear gullies with systems of faults and fractures and open-system pingos (Soare et al., 2014b).

Argyre basin member 2	NAb2	Deposits are gradationally in contact with rock materials of units NAb3 and Nab1 and Argyre rim materials such as unit NArb materials. The unit is marked by flows, aprons along the margins of promontories and other flow feature types, degraded and partly buried impact craters, knobs and other quasi-circular promontories with marginal aprons (more prevalent than the younger unit NAb3), erosional scarps, and irregular depressions. In addition, the deposits include valley fill extending through the rim materials; they are topographically between unit NAb3 and unit Nab1, separated by gradational contacts of which often are breaks in slope such as terraces, exemplified in the three valleys that debouch into the southern and southeast parts of the Argyre basin, Surlus Vallis and Dzigai and Nia Valles, respectively (Figs. 1, 3, and 6).	Hillslope-forming materials associated with changes in environmental conditions/climate, as well as gravity-driven processes such as colluvial activity of ice-enriched rock materials through time. Major surface modification related to Tharsis-driven activity (e.g., Stages 1-3), indicated by stratigraphy and impact crater densities (Table 3), which includes hydrologic activity (ice melt, flooding, gelifluction, and lake formation, as well as incisement of the radial valleys related to a changing hydraulic head linked to the changing hydrologic system of groundwater, surface lakes, and glaciers), with subsequent surface modification including obliquity-driven, aeolian, fluvial, volatile-release, glacial, alluvial, impact cratering which includes secondary impacts, and/or colluvial. Wind and water (liquid and ice) activity has modified the landscape. The crater retention age of unit NAb2 is less than unit Nab3 due to higher energy conditions and activity at higher reaches, including those associated with the incisement of the valleys radial about the basin such as Surlus Vallis and Dzigai and Nia Valles. The rock materials source from diverse provenances, including the Argyre rim and ejecta deposits (upper mantle materials and older primordial crustal materials excavated to and near the Martian surface by the Argyre impact event and associated overturn and inversion of stratigraphy; materials also include hydrothermal deposits) and beyond, even including materials transported from as far north as Tharsis and the Thaumasia highlands and from as far south as the south pole. Therefore, the rock materials are considered to be diverse in both geochemistry and the mineralogic record, representative of diverse environmental conditions (e.g., assortment of varying pressure, temperature, and volatile conditions).
Argyre basin member 1	NAb1	Deposits are gradationally in contact with unit NAb2. The unit is marked by flows, aprons along the margins of promontories and other flow feature types, degraded and partly buried impact craters, knobs and other quasi-circular promontories with marginal aprons (more prevalent than the younger member NAb3), erosional scarps, and irregular depressions. In addition, the deposits include valley fill extending through the rim materials and onto the surrounding highlands; they are the elevationally highest occurring fill deposits in the valleys that debouch into the Argyre basin. Prime examples of the stratigraphy are observed in Surlus and Dzigai Valles, which are the two southern most valley systems that debouch into the Argyre basin (Figs. 1, 3, and 6).	High-standing basin-fill deposits which were emplaced directly following the Argyre impact event, including ice melt at regional and possibly global scale and related hydrologic conditions, which includes the Mediterranean-size lake that sourced Uzboi Valles. The Argyre-induced lake formed several million years subsequent to the termination of the dynamo and a reported ancient phase of plate tectonism (Baker et al., 2007), as well as a once interacting atmosphere, ocean, and landmass (e.g., southern cratered highlands as a hypothesized supercontinent (Spagnuolo and Dohm, 2004)), referred to as Habitable-Trinity conditions (Dohm and Maruyama, 2014b). Through time, the deposits have largely diminished resulting from degradational processes related to subsequent climatic/environmental perturbations; though, in addition to materials related to Argyre-induced activity including lake formation which have been largely degrading through time, this unit also includes rock materials emplaced during subsequent activity such as related to the growth of the Tharsis Superplume (e.g., the upper reaches of the Argyre-impact-controlled valleys). Deposits include channel and floodplain materials related to the initial formation of Uzboi Vallis. The rock materials source from diverse provenances, including the Argyre rim and ejecta deposits (upper mantle materials and older primordial crustal materials excavated to and near the Martian surface by the Argyre impact event and associated overturn and inversion of stratigraphy; materials also include hydrothermal deposits) and beyond, even including materials transported from as far north as the Thaumasia highlands and from as far south as the south pole.
Argyre rim materials (units NAr, NArb, NAb, NArsp)			
Argyre rim materials	NAr	High-relief, heavily cratered massifs tens of kilometers across and intervening broad linear troughs and valleys. Massifs of varying geometric shapes display basins at distinct breaks in slope with the higher parts of the massifs, knife-like ridges, amphitheatre-like valley heads, pyramidal peaks, and u-shape valleys. The massifs display aprons along their flanks. Similar to some of the other Argyre rim and basin materials, but this particular unit is mostly composed of rim-related massifs, whereas the other units include a combination of massifs and valley and basin infill deposits. The impact retention ages reflect extremely ancient Argyre impact rim materials and ejecta deposits with a significant crater population being destroyed by processes such as glaciation along steep slopes of the rim massifs.	Argyre rim materials and ejecta deposits (upper mantle materials and older primordial crustal materials excavated to and near the Martian surface by the impact event and associated overturn and inversion of stratigraphy; materials include hydrothermal deposits) and dissected by basin-related fault structures and erosional valleys, and degraded through time by wind-, water-, and gravity-driven processes. Glacial activity is prominent in the geologic and hydrologic records of the Argyre provinces, as highlighted by the tarns, aretes, cirques, horns, and U-shape valleys that mark the prominent impact-crater massifs. The chiseled landscape records diverse geologic and hydrologic activity, including ice melt and associated hydrologic conditions following the giant Argyre impact event, including lake formation and subsequent perturbations to the climate and environmental conditions driven by Tharsis pulses and to a lesser extent Elysium and other volcanic provinces, subsequent impact events such as Lowell and Galle, and changes in obliquity and eccentricity.
Argyre rim and basin materials	NArb	High-relief, heavily cratered massifs tens of kilometers across and intervening basins, broad linear troughs, and valleys. Massifs of varying geometric shapes display basins at distinct breaks in slope with the higher parts of the massifs, knife-like ridges, amphitheatre-like valley heads, pyramidal peaks, and u-	Argyre rim materials and ejecta deposits (upper mantle materials and older primordial crustal materials excavated to and near the Martian surface by the impact event and associated overturn and inversion of stratigraphy) and dissected by basin-related fault structures and erosional valleys, and degraded through time by wind-, water-, and gravity-driven processes. Glacial activity is prominent in the geologic and hydrologic records of the Argyre provinces, as highlighted by the tarns, aretes, cirques, horns, and -shape valleys. The chiseled landscape records diverse geologic and hydrologic activity,

		shape valleys. The massifs display aprons along their flanks. Intervening basins display both relatively smooth plains-forming materials and massifs which occur isolated or in groups.	including ice melt and associated hydrologic conditions following the giant Argyre impact event, including lake formation and subsequent perturbations to the climate and environmental conditions driven by Tharsis pulses and to a lesser extent Elysium and other volcanic provinces, subsequent impact events such as Lowell, and changes in obliquity. These materials are similar to unit NAr but more degraded and thus basins, which partly mark inversion of topography due to the destruction of the rim materials through time, and massifs, with more isolated (i.e., individual) promontories when compared to unit NAr.
Argyre basin and rim materials	NAbr	High-relief, heavily cratered and degraded massifs tens of kilometers across with intervening basins including valleys and broad linear troughs. Massifs of varying geometric shapes display basins at distinct breaks in slope with the higher parts of the massifs, knife-like ridges, amphitheatre-like valley heads, pyramidal peaks, and u-shape valleys. The massifs display aprons along their flanks. Intervening basins display both relatively smooth plains-forming materials and massifs which occur isolated or in groups. Similar to NArb but basins are more prevalent compared to the massifs, and the basins are not as distinct, large, and isolated as those associated with unit NArsp materials.	Argyre rim materials and ejecta deposits (upper mantle materials and older primordial crustal materials excavated to and near the Martian surface by the impact event and associated overturn and inversion of stratigraphy) and dissected by basin-related fault structures and erosional valleys, and degraded through time by wind-, water-, and gravity-driven processes; rock materials include those emplaced directly following the Argyre impact event, such as those associated with the formation of the Uzboi-sourcing lake, as well as those emplaced during subsequent activity, including major stages of activity of the Tharsis Superplume (Fig. 4). Local basins which formed during and/or subsequent to the Argyre impact event. The basins have served as catchments for fluvial, lacustrine, glacial, periglacial, alluvial, and colluvial deposits. The knobs are markers of the major degradation of the rim materials which has resulted in an inversion of topography in places. Major degradation through processes including glacial have highly degraded the rim materials resulting in massifs and basins. This map unit generally marks a more significant degradational state when compared to unit NArb, and thus a greater amount of basin materials vs rim massifs. The CRISM data corroborates the Argyre-rim materials in part being uplifted ancient upper mantle materials, and that the terrains, which are distinctly hydrologically modified, contain magnesian lithologies such as olivine-dominated rocks (Buczowski et al., 2008a,b, 2010) (Fig. 10).
Argyre rim smooth plains materials	NArsp	Smooth plains-forming materials in basins among the Argyre rim materials, marked by knobs, valley networks, flows which include aprons along the flanks of knobs, and dune fields. These basins are generally more distinct and isolated than those of unit NAbr.	Distinct local basins which formed during and/or subsequent to the Argyre impact event. The basins have served as catchments for fluvial, lacustrine, glacial, periglacial, alluvial, hydrothermal, and colluvial deposits. The knobs are markers of the major degradation of the rim materials.
Highlands materials (units AHTp, NTh, HNh4, HNh3, Nhb, Nh2, Nh1)			
Thaumasia plateau SE	AHTp	Corresponds to unit HNpl of Dohm et al. (2001a). Uneven surface dissected by numerous networking large troughs along the southeastern margin of the Thaumasia plateau; many troughs abruptly terminate on up-slope end at large graben and depressions. Marked in places by ridges.	Easily eroded (i.e., friable) volcanic materials with morphologic expression appearing similar to dissected ignimbrites which occur along the margin of the Andes (Fig. 9 of Dohm et al. (2001a)). The troughs may have formed in part due to Tharsis-driven magmatism, such as related to the Thaumasia plateau, and associated groundwater conditions along the distinct break in slope (at the southeast part of the Thaumasia plateau where there appears to be a discontinuity between the Thaumasia highlands and Coprates rise mountain ranges).
Thaumasia highlands	HNTh	Corresponds to unit HNpl of Dohm et al. (2001a). Highly modified impact crater of the eastern part of the Thaumasia highlands mountain range, which is embayed and partly buried by unit HNh4 materials along its southern margin, at the juncture between the mountain range and the plains.	Highly degraded ancient impact crater that impacted into the Thaumasia highlands mountain range; highly dissected and locally deformed. Materials include Thaumasia highlands mountain-building materials, therefore, the geochemical composition and environmental conditions of the rock materials are interpreted to be diverse and far-reaching both in time and space, which includes rocks ranging from basalt to felsic compositions, and rocks with varying grades of metamorphism such as those associated with orogenic complexes of Earth (Maruyama, 1997; Maruyama et al., 1997, 2013, 2014; Dohm and Maruyama, 2014a; Dohm et al., 2014a,b).
Highlands member 4	HNh4	Moderately smooth plains-forming materials; wrinkle ridges, ridge crests, troughs, and lineaments in places.	Undifferentiated impact, volcanic, aeolian, fluvial, alluvial, and colluvial materials; locally degraded and contractionally deformed. Materials include Argyre ejecta materials and materials shed from the Thaumasia plateau and the Thaumasia highlands mountain range. Thus the geochemical composition and environmental records of the rock materials are interpreted to be diverse and far-reaching both in time and space, which includes rocks ranging from basalt to felsic compositions, and rocks with varying grades of metamorphism such as those associated with orogenic complexes of Earth (Maruyama, 1997; Maruyama et al., 1997). Thus unit includes phyllosilicate through analysis of CRISM data (Buczowski et al. (2008a,b)). This is consistent with the interpretation of resurfacing and weathering which includes aqueous processes as per above.
Highlands member 3	HNh3	Moderately smooth plains-forming materials; wrinkle ridges and lineaments in places.	Undifferentiated impact, volcanic, aeolian, fluvial, alluvial, and colluvial materials; locally degraded and contractionally deformed. Materials include Argyre ejecta materials and materials shed from the Thaumasia plateau and the Coprates rise mountain range. Similar to unit HNh4, the geochemical composition and environmental records of the rock materials are interpreted to be diverse and far-reaching both in time and space, which includes rocks ranging from basalt to felsic compositions, and rocks with varying grades of metamorphism such as those associated with orogenic complexes of Earth (Maruyama, 1997; Maruyama et al., 1997).
Highlands basin	Nhb	Relatively smooth plains-forming materials in basins located in the cratered highlands along	Basins, many of which are controlled by Argyre-impact-derived basement structures. Many of the basins record changing environmental and hydrologic conditions, including

materials		the margin of and away from the Argyre rim materials. Several of the basins are elongated with linear margins and/or tectonic structures, including AWMP paleolake basin (Figs. 1, 7, and 8) on the west-central margin of the Argyre basin and rim materials. The basins are similar to those of unit NArsp, but many occur away from the rim materials, and many appear to have more numerous valley networks along their margins.	those that were influenced by changing conditions with the Argyre basin. For example, AWMP was occupied by a lake at least at the zero datum, though there is evidence that the lake and associated hydraulic head could have reached at least 1 km above the Martian datum. The basins also record glacial, periglacial, fluvial, aeolian, alluvial, colluvial, and/or hydrothermal activity, as well as groundwater activity along the basement structures possibly indicated by channels which occur along the structures (Fig. 15-16). Though, the channels could be structurally-controlled surface runoff. Many of the basins occur away from the rim materials and in many cases appear to have margins dissected by more numerous valley networks when compared to the basins of the unit NArsp. The distinct younger crater-retention age of unit Nhb when compared to unit NArsp (see Table 3) possibly reflects greater resurfacing of the former, in part due to possible enhanced geologic and hydrologic activity in the transition zone that connects the Thaumasia highlands and plateau with the Argyre rim and basin (Figs 1-3.). The basins contain sedimentary, lacustrine, evaporite, and hydrothermal deposits, as well as lower crustal materials and/or upper mantle materials largely related to the Argyre impact event and eolian deposits sourcing from nearby (rim materials) and distant provenances (e.g., Tharsis).
Highlands member 2	Nh2	Rolling topography marked by scarps, structurally-controlled basins, faults, troughs, channels, and ridges. Highly dissected in places such as along the margin of the unit Nhb materials which infill the AWMP paleolake basin (Figs. 1, 3, 7).	Undifferentiated impact, volcanic, fluvial, lacustrine, alluvial, colluvial, and basin infill materials including sedimentary deposits, moderately to heavily degraded. This includes modified Argyre rim and ejecta deposits (upper mantle materials and older primordial crustal materials transferred at and near the Martian surface by the impact event and associated overturn and inversion of stratigraphy). Materials also include those transported from as far north as Tharsis and the Thaumasia highlands, such as recorded in the outcrops in the transitional zone between the Thaumasia highlands and the Argyre basin and rim materials emplaced by fluvial, colluvial, alluvial, and glacial activities (Fig. 3), and from as far south as the south pole, as recorded in the outcrops which occur to the south of the Argyre basin and rim materials primarily by glacial and fluvial activities. The geochemical composition and environmental records of the rock materials are interpreted to be diverse and far-reaching both in time and space, which includes rocks ranging from basalt to felsic compositions, and rocks with varying grades of metamorphism such as those associated with orogenic complexes of Earth (Maruyama, 1997; Maruyama et al., 1997). For example, an Argyre-impact, structurally-controlled basin with drainages along its margins (Fig. 16) are shown to include phyllosilicate (Buczowski et al., 2008). This is consistent with the interpretation of resurfacing and weathering which includes aqueous processes as per above.
Highlands member 1	Nh1	High plateau-forming outcrops extending hundreds of kilometers, many controlled by basement structures related to the Argyre impact event. Densely cratered and valley networks and scarps mark the landscape.	Extremely ancient crustal materials, which includes igneous, sedimentary, and metamorphic rocks, buried by Argyre impact ejecta deposits mixed through time due to impact cratering and water (liquid and ice), wind, and gravity-driven processes. The elongated and high-standing plateaus are in part due to the Argyre impact and other tectonism, including pre-Argyre basement structures. Elongated mesas have faults along their margins, and thus are structurally controlled.
Impact crater materials post-dating the Argyre impact event (units C1, C2, Cfs, Cfr)			
Young crater materials	C2	Relatively pristine impact crater materials of the ~ 230-km-diameter Galle impact crater overly surrounding rock materials of various units, including younger smooth-plains-forming basin floor deposits.	Stratigraphically-young, relatively large impact crater. The event contributed to major change in the topography/terrain of the east-central margin of the Argyre basin and rim materials. Compared to the ~ 200-km-diameter Lowell impact crater, which impacted into a relatively large basin located to the west of the Argyre province influenced by ancient tectonism and impact cratering, as well as triggered major ice melt and associated flooding and valley network formation (Lias et al., 1997; Dohm and Tanaka, 1999), Galle does not appear to have triggered major flood events. This might be explained by the impact occurring in the rim materials along the margin of the basin where there are massifs composed of upper mantle and ancient crustal materials with intervening water-enriched valleys and local basins (i.e., less volume of water). In addition there may have been ice melt in the basin, but due to the relatively low gradient, distinct valley networks did not develop. There are troughs, however, mapped along parts of the southern margin of the Galle ejecta blanket that could be the result of impact-generated flooding.
Old crater materials	C1	Degraded impact crater rims and ejecta deposits.	Most impact >50-kilometer-diameter craters are highly degraded due to the subsequent impact events and diverse geologic and hydrologic activities in the Argyre province through time. In the case of Hale crater, CRISM-based identification of low- and high-calcium pyroxenes and prehnite and chlorite on the floor, the central peak, and the rim of Hale crater (Fig. 11) are consistent with Argyre-impact-modified terrain, including the excavation of relatively olivine-rich, deep mantle and/or primordial crustal materials transferred at or near the Martian surface by the impact event and associated overturn and inversion of stratigraphy. In addition, the mineralogy is also consistent with hydrothermal activity possibly associated both with the initial Argyre impact event followed by the Hale impact event into a potentially water-enriched target materials associated with hydrologic conditions associated of the Uzboi-Vallis spillway.
Smooth	Cfs	Smooth plains-forming materials in the highly	Impact basin infill deposits with remnants of rim materials and central peaks.

crater floor materials		degraded impact basins. Some basins display knobs.	
Rough crater floor materials	Cfr	Occurrence only in few impact crater basins, including Galle impact crater. Irregular topography, including knobs, depressions, and scarps.	Degradation of central peak materials, but also disruption of the terrain due to hydrologic conditions such as Galle-impact-driven following the impact cratering event.

1548

1549 **Table 3.** Cumulative crater densities and unit ages of geologic units in the Argyre and surrounding region of Mars.
 1550 Note that (1) average crater density $N(D)$ equals number of craters larger than diameter D per million square
 1551 kilometers, (2) relative ages based on time-stratigraphic scale from Tanaka (1986), (3) “ALL” refers to both highly
 1552 degraded and “Superposed” (pristine impact craters with distinct rims and ejecta blankets that are not visibly
 1553 resurfaced). See **Tables 1 and 2** for unit names, description, and interpretation. Estimated absolute ages are based
 1554 on the Hartmann (2005) (referred to as Hartmann in column 2) and Neukum et al. (2001) (referred to as Neukum in
 1555 column 2) chronology systems. These ages were assigned a range of chronostratigraphic epochs based on the
 1556 boundaries defined in Neukum et al. (2001), Hartmann (2005), and Werner and Tanaka (2011), also compared with
 1557 that shown in Tanaka et al. (2014). Epochs include Early Noachian (EN), Middle Noachian, (MN), Late Noachian
 1558 (LN), Early Hesperian (EH), Late Hesperian (LH), Early Amazonian (EA), Middle Amazonian (MA), and Late
 1559 Amazonian.
 1560

Unit Symbol	Model	Area (km ²)	Total Craters	$N(3)$ Age, Ga	$N(5)$ Age, Ga	$N(16)$ Age, Ga	Isochron Age, Ga/Epoch	Estimated Range of Epochs
Highlands materials								
Nh1 All	Hartmann	327,794	290	3.63±0.01	3.72±0.02	3.89±0.02	3.82±0.03	LN-MN
Nh1 All	Neukum	327,794	290	3.88±0.01	3.82±0.01	3.95±0.02	3.94±0.02	MN-EN
Nh1 Superposed	Hartmann	327,794	71	2.25±0.27	2.94 ^{+0.26} _{-0.44}	3.39 ^{+0.14} _{-0.70}	3.17 ^{+0.20} _{-0.60}	EA-LH
Nh1 Superposed	Neukum	327,794	71	3.61±0.03	3.63±0.04	3.54 ^{+0.09} _{-0.23}	3.61 ^{+0.04} _{-0.06}	LH-EH
Nh2 All	Hartmann	1,096,085	846	3.60±0.01	3.71±0.01	3.86±0.01	3.78±0.01	LN- MN
Nh2 All	Neukum	1,096,085	846	3.85±0.01	3.90±0.01	3.82±0.01	3.90±0.01	LN- MN
Nh2 Superposed	Hartmann	1,096,085	189	1.78±0.13	2.70 ^{+0.22} _{-0.25}	2.89 ^{+0.37} _{-0.72}	2.64 ^{+0.33} _{-0.37}	EA
Nh2 Superposed	Neukum	1,096,085	189	3.54±0.02	3.61±0.03	3.36 ^{+0.11} _{-0.33}	3.56±0.04	EA-LH
HNh3 All	Hartmann	168,887	108	3.55±0.03	3.62±0.04	3.75±0.05	3.66±0.07	EH-LN
HNh3 All	Neukum	168,887	108	3.82±0.02	3.84±0.02	3.82±0.05	3.83±0.04	LN-MN
HNh3 Superposed	Hartmann	168,887	39	2.41±0.38	3.22 ^{+0.15} _{-0.44}	2.87 ^{+0.56} _{-1.88}	3.11 ^{+0.25} _{-0.79}	EA
HNh3 Superposed	Neukum	168,887	39	3.62±0.04	3.67±0.05	3.36 ^{+0.20} _{-1.93}	3.62 ^{+0.05} _{-0.08}	EA -EH
HNh4 All	Hartmann	262,637	129	3.46±0.04	3.58±0.04	3.72 ^{+0.04} _{-0.06}	3.63±0.05	EH-LN
HNh4 All	Neukum	262,637	129	3.78±0.02	3.81±0.02	3.78±0.05	3.80±0.03	LN
HNh4 Superposed	Hartmann	262,637	81	3.10 ^{+0.14} _{-0.25}	3.39 ^{+0.07} _{-0.11}	3.22 ^{+0.25} _{-1.39}	3.35 ^{+0.10} _{-0.22}	EA-LH
HNh4 Superposed	Neukum	262,637	81	3.69±0.03	3.72±0.03	3.46 ^{+0.13} _{-0.83}	3.68±0.04	LH -LN
Nhb All	Hartmann	67,049	44	3.58±0.05	3.67±0.05	3.80 ^{+0.06} _{-0.09}	3.71 ^{+0.06} _{-0.09}	LN

Nhb All	Neukum	67,049	44	3.84±0.03	3.87±0.04	3.86 ^{+0.05} _{-0.09}	3.86 ^{+0.04} _{-0.06}	MN
Nhb Superposed	Hartmann	67,049	12	2.25 ^{+0.62} _{-0.65}	3.18 ^{+0.23} _{-0.92}	3.58 ^{+0.12} _{-1.09}	3.44 ^{+0.14} _{-1.01}	EA- LN
Nhb Superposed	Neukum	67,049	12	3.60 ^{+0.06} _{-0.10}	3.66 ^{+0.06} _{-0.10}	3.67 ^{+0.10} _{-0.43}	3.66 ^{+0.08} _{-0.16}	LH- EH
HNTTh All	Hartmann	28,531	19	3.57 ^{+0.05} _{-0.08}	3.59 ^{+0.07} _{-0.13}	3.73 ^{+0.10} _{-0.38}	3.60 ^{+0.07} _{-0.14}	LN
HNTTh All	Neukum	28,531	19	3.83 ^{+0.03} _{-0.05}	3.82 ^{+0.05} _{-0.07}	3.80 ^{+0.09} _{-0.28}	3.82 ^{+0.05} _{-0.07}	LN
HNTTh Superposed	Hartmann	28,531	13	3.44 ^{+0.09} _{-0.23}	3.56 ^{+0.08} _{-0.18}		3.57 ^{+0.09} _{-0.28}	EH -LN
HNTTh Superposed	Neukum	28,531	13	3.77 ^{+0.04} _{-0.06}	3.80 ^{+0.05} _{-0.08}		3.78 ^{+0.06} _{-0.11}	LN
AHTp All	Hartmann	16,282	3	2.88 ^{+0.54} _{-1.65}	2.29 ^{+1.07} _{-1.88}		2.29 ^{+1.06} _{-1.83}	EA
AHTp All	Neukum	16,282	3	3.66 ^{+0.09} _{-0.29}	3.56 ^{+0.14} _{-2.31}		3.57 ^{+0.13} _{-1.98}	LH -EH
AHTp Superposed	Hartmann	16,282	3	2.88 ^{+0.54} _{-1.65}	2.29 ^{+1.07} _{-1.88}		2.29 ^{+1.06} _{-1.83}	EA
AHTp Superposed	Neukum	16,282	3	3.66 ^{+0.09} _{-0.29}	3.56 ^{+0.14} _{-2.31}		3.57 ^{+0.13} _{-1.98}	LH -EH
Argyre materials								
<i>Rim materials</i>								
NAr All	Hartmann	58,067	31	3.50 ^{+0.05} _{-0.08}	3.63 ^{+0.05} _{-0.07}	3.78 ^{+0.06} _{-0.11}	3.71 ^{+0.06} _{-0.10}	EH-LN
NAr All	Neukum	58,067	31	3.79±0.04	3.84±0.04	3.84 ^{+0.06} _{-0.10}	3.84 ^{+0.05} _{-0.07}	LN-MN
NAr Superposed	Hartmann	58,067	1					
NAr Superposed	Neukum	58,067	1					
NArb All	Hartmann	109,274	70	3.56±0.04	3.66±0.04	3.88±0.04	3.75 ^{+0.05} _{-0.07}	EH- MN
NArb All	Neukum	109,274	70	3.83±0.02	3.87±0.03	3.94±0.04	3.88±0.05	LN -MN
NArb Superposed	Hartmann	109,274	8	1.06±0.37	1.05±0.50		0.92±0.47	MA-EA
NArb Superposed	Neukum	109,274	8	3.27 ^{+0.18} _{-0.88}	3.07 ^{+0.35} _{-1.40}		2.78 ^{+0.57} _{-1.36}	EA- LN
NAbr All	Hartmann	577,012	432	3.60±0.01	3.68±0.01	3.89±0.02	3.78±0.02	LN -MN
NAbr All	Neukum	577,012	432	3.85±0.01	3.88±0.01	3.95±0.02	3.90±0.02	MN- EN
NAbr Superposed	Hartmann	577,012	50	0.91±0.13	1.23±0.24	3.35 ^{+0.13} _{-0.50}	1.54±0.35	MA- LH
NAbr Superposed	Neukum	577,012	50	3.13 ^{+0.15} _{-0.32}	3.28 ^{+0.12} _{-0.30}	3.51 ^{+0.08} _{-0.16}	3.30 ^{+0.12} _{-0.31}	EA-LH

NArsp All	Hartmann	38,939	39	3.67±0.04	3.75±0.04	3.98±0.05	3.93±0.06	MN-EN
NArsp All	Neukum	38,939	39	3.90±0.03	3.94±0.04	4.04±0.05	4.02±0.05	MN-EN
NArsp Superposed	Hartmann	38,939	7	1.88±0.71	1.86 ^{+1.07} _{-1.11}		1.90 ^{+1.06} _{-1.11}	EA
NArsp Superposed	Neukum	38,939	7	3.56 ^{+0.08} _{-0.19}	3.50 ^{+0.13} _{-1.21}		3.51 ^{+0.12} _{-0.87}	LH
<i>Basin materials</i>								
NAb1 All	Hartmann	100,203	42	3.39 ^{+0.07} _{-0.12}	3.59 ^{+0.04} _{-0.06}	3.91±0.04	3.95 ^{+0.05} _{-0.08}	LH-MN
NAb1 All	Neukum	100,203	42	3.75±0.03	3.82±0.04	3.96±0.04	4.01 ^{+0.05} _{-0.09}	LN-EN
NAb1 Superposed	Hartmann	100,203	6	0.66±0.27	1.03±0.51		0.91±0.55	MA
NAb1 Superposed	Neukum	100,203	6	2.38 ^{+0.77} _{-0.97}	3.03 ^{+0.39} _{-1.48}		2.57 ^{+0.77} _{-1.47}	LN
NAb2 All	Hartmann	209,887	105	3.47±0.05	3.57±0.04	3.72±0.06	3.63±0.06	EH-LN
NAb2 All	Neukum	209,887	105	3.78±0.02	3.81±0.02	3.78±0.05	3.80±0.04	LN
NAb2 Superposed	Hartmann	209,887	15	0.80±0.21	1.03±0.36	1.78 ^{+1.25} _{-1.33}	1.12±0.57	MA-EA
NAb2 Superposed	Neukum	209,887	15	2.85 ^{+0.40} _{-0.72}	3.04 ^{+0.33} _{-0.99}	2.55 ^{+0.85} _{-1.91}	2.83 ^{+0.51} _{-1.21}	EA
NAb3 All	Hartmann	208,086	127	3.54±0.03	3.65±0.03	3.79±0.05	3.72±0.05	EH-LN
NAb3 All	Neukum	208,086	127	3.81±0.02	3.86±0.02	3.85±0.04	3.87±0.04	LN-MN
NAb3 Superposed	Hartmann	208,086	18	0.98±0.23	1.45±0.42	2.63 ^{+0.74} _{-1.63}	1.76±0.78	MA-EA
NAb3 Superposed	Neukum	208,086	18	3.22 ^{+0.17} _{-0.53}	3.39 ^{+0.11} _{-0.36}	3.29 ^{+0.24} _{-1.85}	3.34 ^{+0.16} _{-0.87}	EA-LH
HAb4a All	Hartmann	341,499	125	3.31 ^{+0.06} _{-0.09}	3.45 ^{+0.05} _{-0.06}	3.55 ^{+0.07} _{-0.13}	3.46 ^{+0.06} _{-0.10}	LH-EH
HAb4a All	Neukum	341,499	125	3.73±0.02	3.74 ^{+0.02} _{-0.03}	3.65 ^{+0.06} _{-0.09}	3.72±0.03	EH-LN
HAb4a Superposed	Hartmann	341,499	21	0.70±0.15	1.11±0.29	1.67±1.02	1.29±0.56	MA-EA
HAb4a Superposed	Neukum	341,499	21	2.51 ^{+0.49} _{-0.55}	3.17 ^{+0.21} _{-0.67}	2.40 ^{+0.90} _{-1.46}	2.91 ^{+0.43} _{-1.07}	EA
NAb4b All	Hartmann	18,541	11	3.53 ^{+0.07} _{-0.15}	3.62 ^{+0.08} _{-0.16}	3.88 ^{+0.07} _{-0.15}	3.71 ^{+0.07} _{-0.14}	EH- MN
NAb4b All	Neukum	18,541	11	3.81 ^{+0.04} _{-0.06}	3.84 ^{+0.06} _{-0.09}	3.94 ^{+0.07} _{-0.14}	3.86 ^{+0.06} _{-0.10}	LN-MN
NAb4b Superposed	Hartmann	18,541	1					
NAb4b Superposed	Neukum	18,541	1					

1561
1562
1563
1564
1565

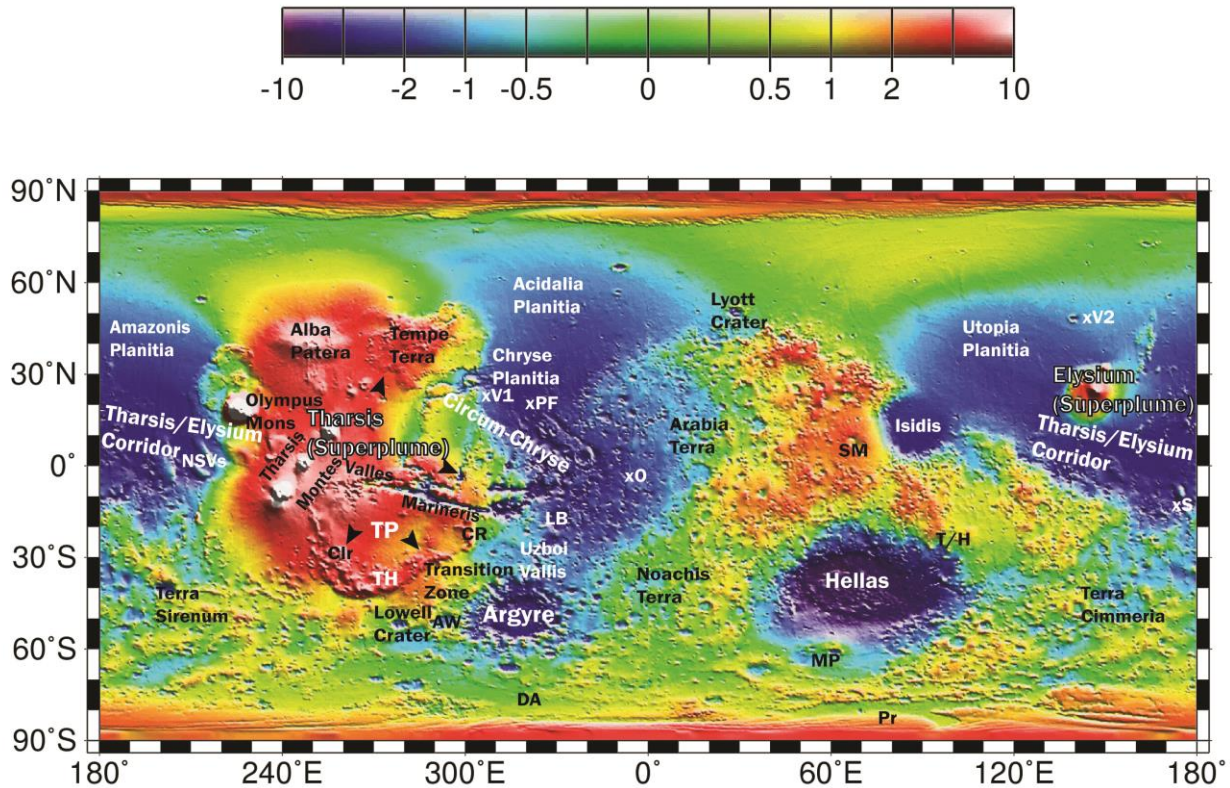
Table 4. Locations and diameters of impact craters that were subtracted from unit polygons and either deleted (if embayed or buried by the geologic-unit materials) or added to older adjacent polygons, if the impact craters were insufficient in size to map at scale (impact craters < 50 km were not mapped) and that form part of the basement of an adjacent unit.

Crater Latitude	Crater Longitude	Crater Diameter	Original Unit	New Unit
-40.305	-28.184	9.75	NAb1	NAbr
-36.638	-44.771	14.79	NAb1	NAbr
-39.801	-30.932	18.02	NAb1	NAbr
-37.044	-44.678	25.36	NAb1	NAbr
-53.828	-60.247	26.26	NAb1	NAbr
-54.075	-60.848	33.1	NAb1	NAbr
-51.854	-56.198	32.57	NAb2	NAb1
-36.417	-34.001	13.33	NAb2	NAbr
-49.567	-57.932	15.36	NAb2	NAbr
-47.44	-56.569	19.99	NAb2	NAbr
-39.722	-50.336	20.18	NAb2	NAbr
-38.712	-36.819	21.86	NAb2	NAbr
-40.061	-50.62	30	NAb2	NAbr
-47.25	-51.091	30.31	NAb2	NAr
-55.86	-28.366	17.63	NAb2	NAbr
-45.429	-51.322	21.64	NAb2	NAbr
-55.077	-28.822	29.97	NAb2	NAbr
-58.758	-37.004	31.71	NAb2	NAbr
-54.424	-30.015	40.3	NAb2	NAbr
-60.278	-31.703	34.99	NAb2	C1
-59.801	-32.414	88.48	NAb2	C1
-57.532	-47.336	15.77	NAb2	DELETED
-57.321	-47.132	22.4	NAb2	DELETED
-57.711	-47.689	23.27	NAb2	DELETED
-37.414	-45.548	65.84	NAb2	Nh2
-37.663	-44.297	24.88	NAb3	NAb1
-41.183	-44.762	10.88	NAb3	NAb2
-36.456	-40.301	12.41	NAb3	NAb2
-41.452	-45.804	26.73	NAb3	NAb2
-43.959	-35.512	37.55	NAb3	NAb4b
-38.684	-40.428	7.07	NAb3	NAbr
-59.475	-34.64	13.25	NAb3	NAbr
-38.493	-40.22	17.02	NAb3	NAbr
-38.617	-40.194	18.65	NAb3	NAbr

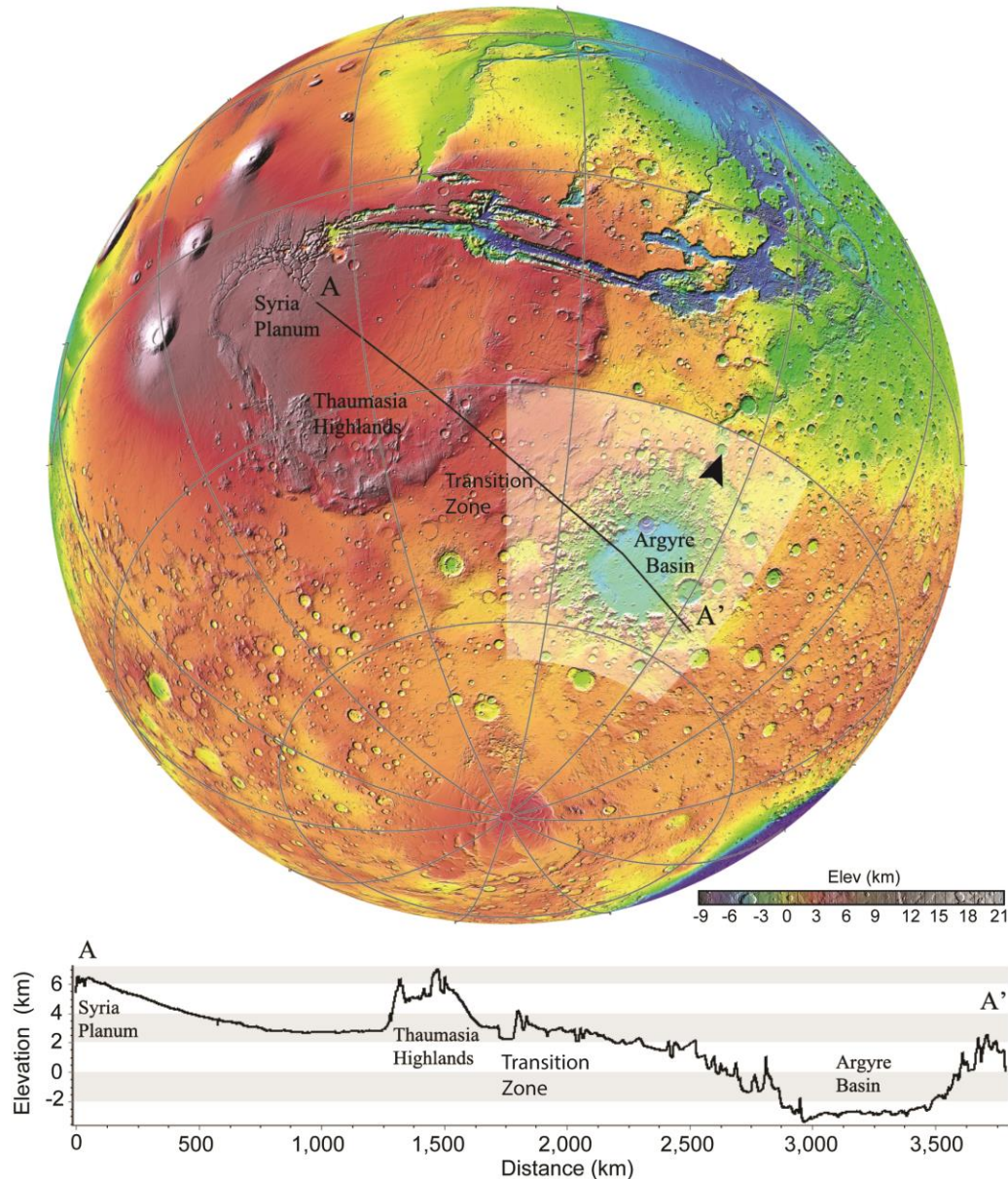
-44.446	-50.275	19.05	NAb3	NAbr
-42.065	-42.51	19.53	NAb3	NAbr
-42.374	-40.675	22.18	NAb3	NAbr
-40.849	-45.449	22.76	NAb3	NAbr
-37.562	-40.259	24.17	NAb3	NAbr
-35.936	-39.94	39.08	NAb3	NAbr
-56.377	-48.634	33.93	NAb3	NAbr
-44.244	-47.438	44.76	NAb3	NAbr
-45.635	-53.679	55.35	NAb3	NAbr
-48.295	-51.868	12.25	HAb4a	NAb3
-45.997	-45.204	17.43	HAb4a	NAb3
-45.164	-48.919	21.76	HAb4a	NAb3
-44.109	-43.14	25.08	HAb4a	NAb3
-49.686	-51.647	41.16	HAb4a	NAb3
-50.331	-52.102	50.74	HAb4a	NAb3
-44.555	-44.613	61.66	HAb4a	NAb3
-44.921	-44.396	137.65	HAb4a	NAb3
-44.662	-41.999	13.39	HAb4a	NAb4b
-44.655	-42.172	31.36	HAb4a	NAb4b
-56.185	-38.817	16.12	HAb4a	NAbr
-58.668	-43.38	40.02	NAbr	NAbr
-37.595	-48.313	16.77	NAbr	C1
-38.721	-51.999	9.75	NAbr	NH1
-46.861	-59.793	46.16	NAbr	NH1
-35.02	-38.202	29.98	NAbr	NH2
-51.892	-25.252	5.65	NAb1	NAbr
-52.208	-25.259	18.01	Nab1	NAbr
-43.181	-27.659	18.88	NArsp	NAbr
-43.062	-21.139	31.6	NArsp	NAbr
-41.351	-21.413	37.88	NArsp	NAbr
-42.975	-24.089	92.95	NArsp	NAbr
-57.411	-41.322	16.92	NArsp	NAbr
-44.129	-32.156	79.2	Cfs	NAbr
-37.056	-60.805	30.2	Nh2	Nh1
-64.622	-24.344	30.95	Nh2	Nh1
-63.796	-20.772	50.89	Nh2	Nh1
-64.161	-24.627	52.77	Nh2	Nh1
-63.402	-22.169	65.09	Nh2	Nh1
-38.218	-61.205	105.4	HNh4	Nh1

-57.335	-60.314	34.04	Nhb	Nh1
-57.532	-61.383	36.48	Nhb	Nh1
-37.224	-47.579	27.2	Nhb	Nh2
-51.377	-64.965	30.86	Nhb	Nh2
-51.692	-65.646	34.66	Nhb	Nh2
-49.95	-67.362	36.85	Nhb	Nh2
-35.987	-47.608	47.77	Nhb	Nh2
-50.833	-68.723	101.32	Nhb	Nh2

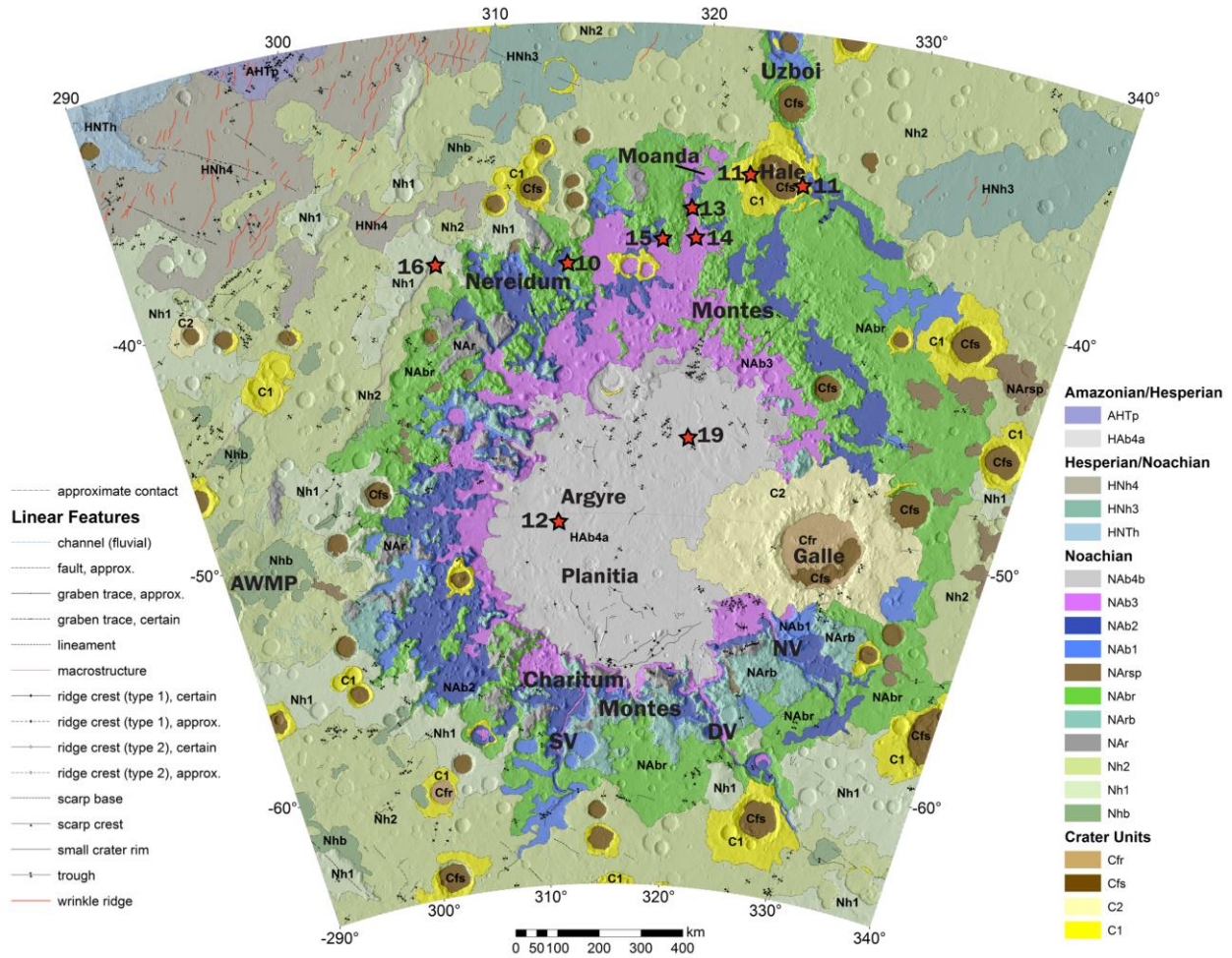
1566



1567
 1568 **Fig. 1.** Mars Orbiter Laser Altimeter Map showing the planet shape with the zonal spherical harmonic degree 1
 1569 removed (Smith et al. 1999) and nomenclature and general locations of features of interest, including Argyre basin,
 1570 Tharsis and Elysium, both interpreted here as superplumes, Uzboi Vallis, the Argyre western-margin-paleolake
 1571 basin (AW), Thaumasia plateau (TP), Thaumasia highlands mountain range (TH), Coprates rise mountain range
 1572 (CR), Claritas Rise (Clr), Prometheus crater (Pr), Dorsa Argentea (DA), Ladon basin (LB), the northwestern slope
 1573 valleys (NSVs), the ancient Europe-size drainage basin which may have contributed floodwaters to the circum-
 1574 Chryse outflow channel system (black arrowheads pointing to the northern, eastern, southern, and western margins),
 1575 Malea Planum volcanic province (MP), Tyrrhenus/Hadriacus volcanic province (T/H), Syrtis Major volcanic
 1576 province (SM), Pathfinder landing site (xPF), Viking 1 landing site (xV1), Viking 2 landing site (xV2), Spirit landing
 1577 site (xS), and Opportunity landing site (xO). Note that this geologic investigation points to the dark blue patches in
 1578 the Argyre province (see **Fig. 2** for outline of province), representative of relatively low topography, being
 1579 inundated by water directly following the Argyre impact event (please also compare with **Fig. 9**). Also note the
 1580 southeastern margin of the Thaumasia plateau paralleling the multi-ring structure of the Argyre impact, and as such,
 1581 one of the many pieces of evidence of the influence that Tharsis and Argyre had on one another (also see **Fig. 2**).
 1582
 1583

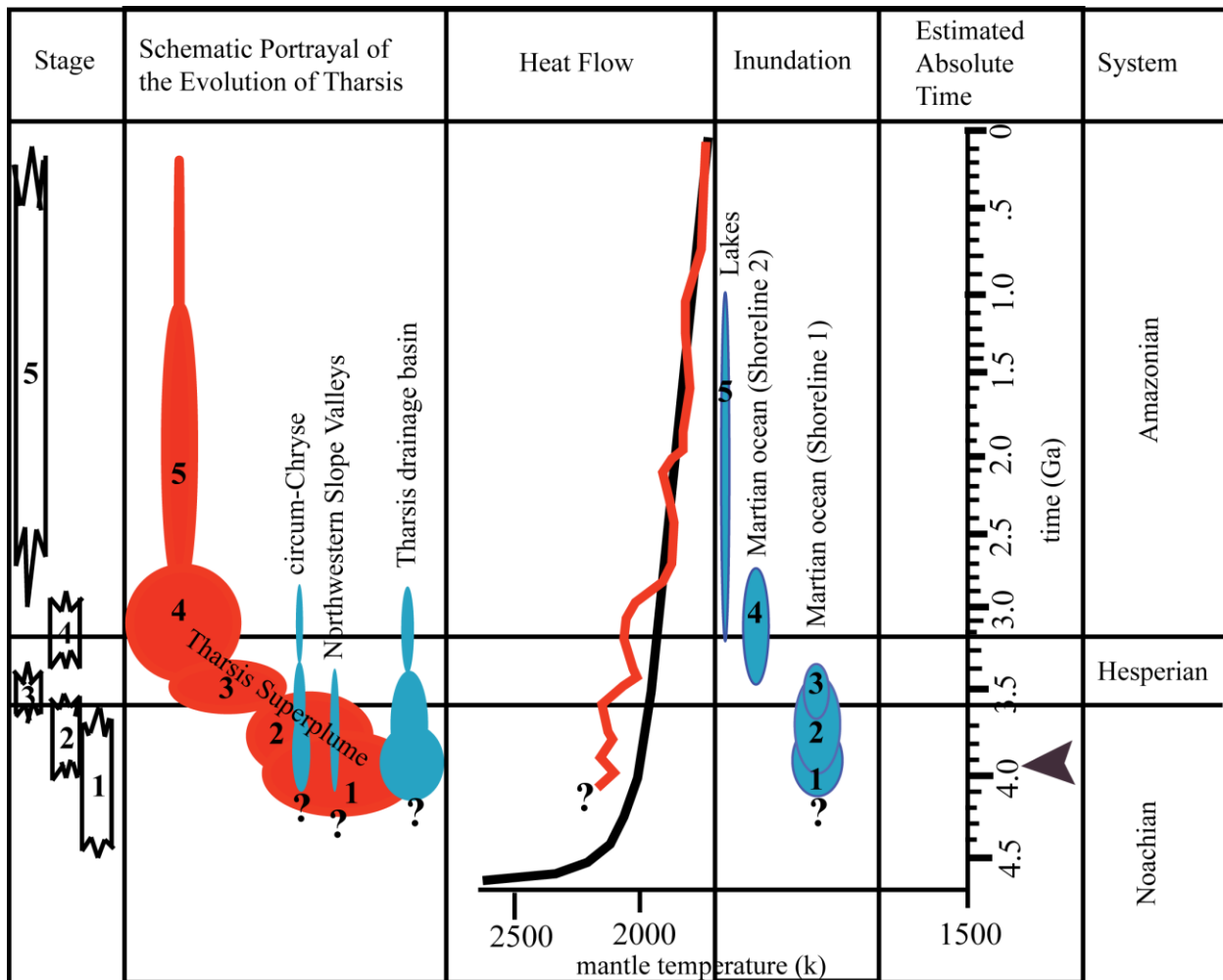


1584
 1585 **Fig. 2.** MOLA map (top) with transect line of corresponding topographic profile (bottom) through Syria Planum
 1586 (i.e., a shield complex and one of the major components of Tharsis), Thaumasia Highlands (i.e., mountain range
 1587 with a length nearing 2,400 km, or approximating that of the Himalayas), Transition Zone, and the Argyre Basin.
 1588 The Argyre province is also highlighted at top (transparent box). Also shown is the possible headwaters of Uzboi
 1589 Vallis (arrow). Note the rugged topography in the Argyre province resulting from the giant impact event including
 1590 mountainous rim materials and structurally-controlled basins, including the deep primary basin. Both Tharsis and
 1591 Argyre had a major influence on one another. For example, Tharsis magmatic-driven hydrological cycling included
 1592 floods and associated inundations in the northern plains and associated precipitation in and surrounding the Argyre
 1593 basin to form lakes and grow glaciers, as well as groundwater activity along Argyre impact-induced basement
 1594 structures, which includes the possible migration at great distances (e.g., thousands of kilometers from Tharsis
 1595 through the ancient Thaumasia highlands mountain range and eventually into the deep Argyre basin). Other diverse
 1596 climatic and hydrologic phenomena may include fog in the Argyre basin and local precipitation due to the regional
 1597 topographic variation. Yin (2012a) proposed an oblique impact event to help explain the distinct topography to the
 1598 northwest of the Argyre basin, and the development of Tharsis, while other hypotheses for the origin of Tharsis
 1599 include focused subduction of hydrated crustal materials through an ancient phase of plate tectonism (Baker et al.,
 1600 2007).



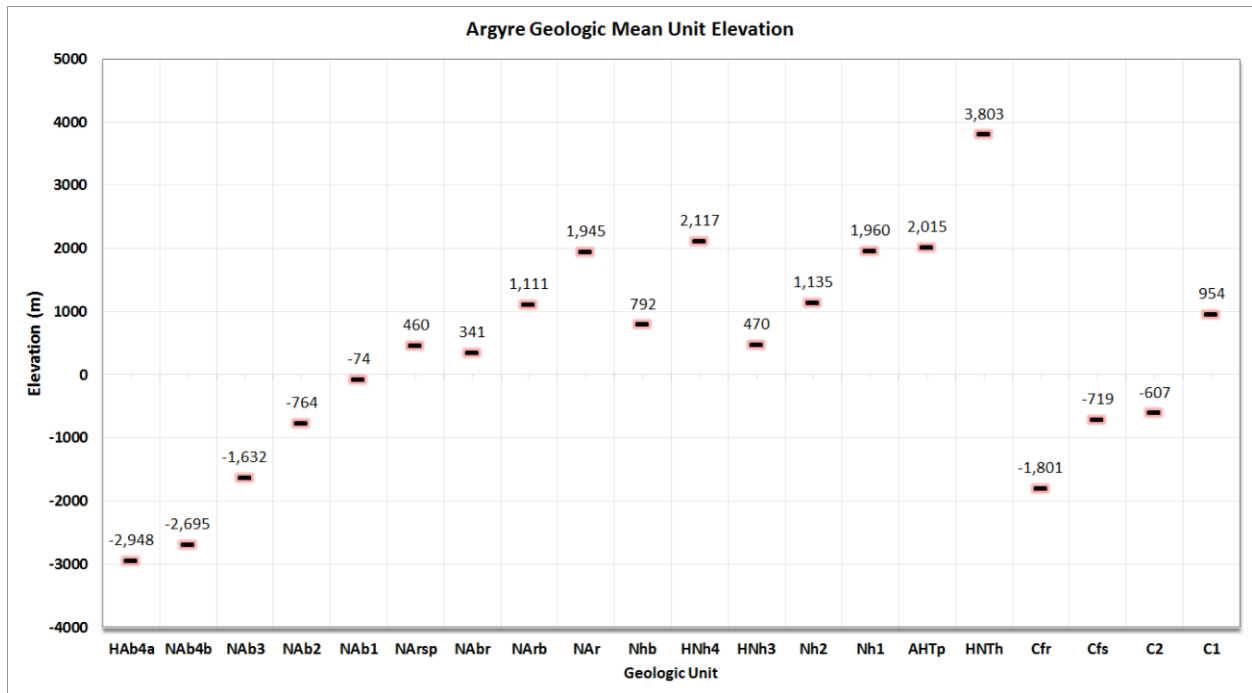
1601
 1602
 1603
 1604
 1605
 1606
 1607
 1608

Fig. 3. Geologic map of the Argyre and surrounding region of Mars showing stratigraphy and structure (Dohm et al., USGS map in preparation). Map units are detailed in **Tables 1-3**. Also highlighted are the major valley systems, Uzboi Vallis (Uzboi), Sursium Vallis (SV), Dzigai Vallis (DV), and Nia Vallis (NV), the Argyre western-margin-paleolake basin (AWMP), and locations of Figs. 10, 11, 12, 13, 14, 15, 16, and 19.



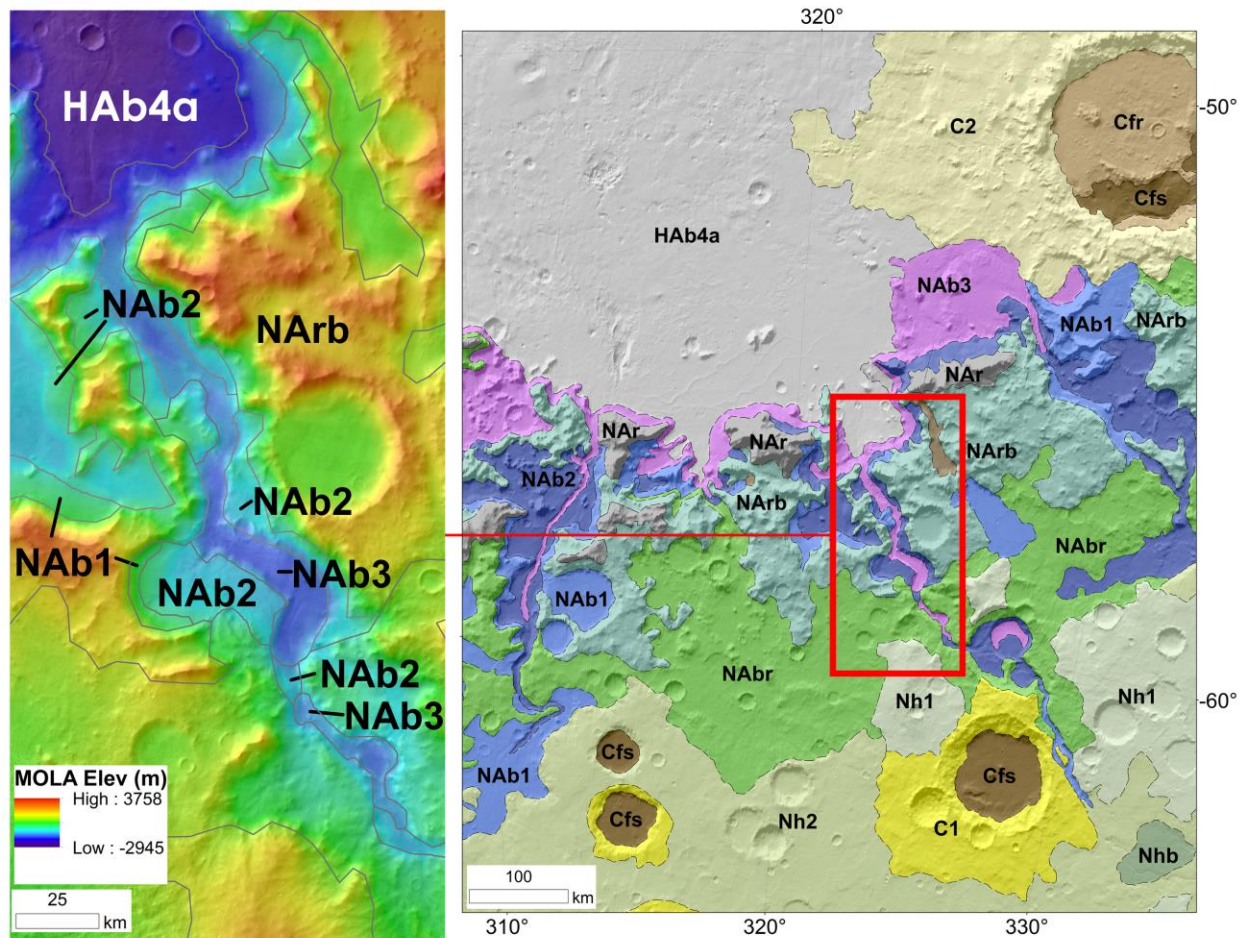
1609
1610
1611
1612
1613
1614
1615
1616
1617
1618
1619
1620
1621
1622
1623
1624

Fig. 4. Modified from Dohm et al. (2007a), chart comparing the major stages of the Tharsis Superplume, which includes circum-Chryse, NSVs, and Tharsis drainage basin/aquifer system, with: (1) heat flow; note the maximum effective heat flow from the core to lithosphere in the Early and Middle Noachian (black line) and non-steady-state decline in subjective heat flow extending from part of the Early Noachian to present (red line) compared to proposed steady-state decline in mantle temperature with time (black line; Schubert et al., 1992) based on published geologic information (e.g., Dohm and Tanaka, 1999; Dohm et al., 2001a,b, 2007a, 2013; Anderson et al., 2001; Fairén et al., 2003; Baker et al., 2007), (2) hypothesized Tharsis-triggered inundations in the northern plains ranging from oceans to lakes (Shorelines 1 and 2 as per Fairén et al. (2003)), (3) inferred absolute time (Hartmann, 2005), and (4) System information of Scott et al. (1986-87). Sizes of solid areas are roughly proportional to degree of exposed activity. The estimated timing of the Argyre impact is also shown (black arrowhead), based on Robbins and Hynek (2012) and Robbins et al. (2013). The onset of Tharsis and other features are queried. Based on uncertainties in the unit age ranges and error in crater statistics, we conservatively show overlap among the stages with sawtooth lower and upper bounds of each column. Subjective heat flow greater than 4.0 Ga is queried, with consideration of a dynamo and plate tectonism reportedly active at that time (Baker et al., 2007; Dohm et al., 2013).



1625
 1626
 1627
 1628
 1629
 1630
 1631

Fig. 5. Mean elevations for Argyre map units detailed in **Tables 1-3**. Note the distinct step-like mean elevation ranges of the basin units (NAb1, NAb2, NAb3, NAb4b, HAB4a) representative of distinct stratigraphy within the basin.

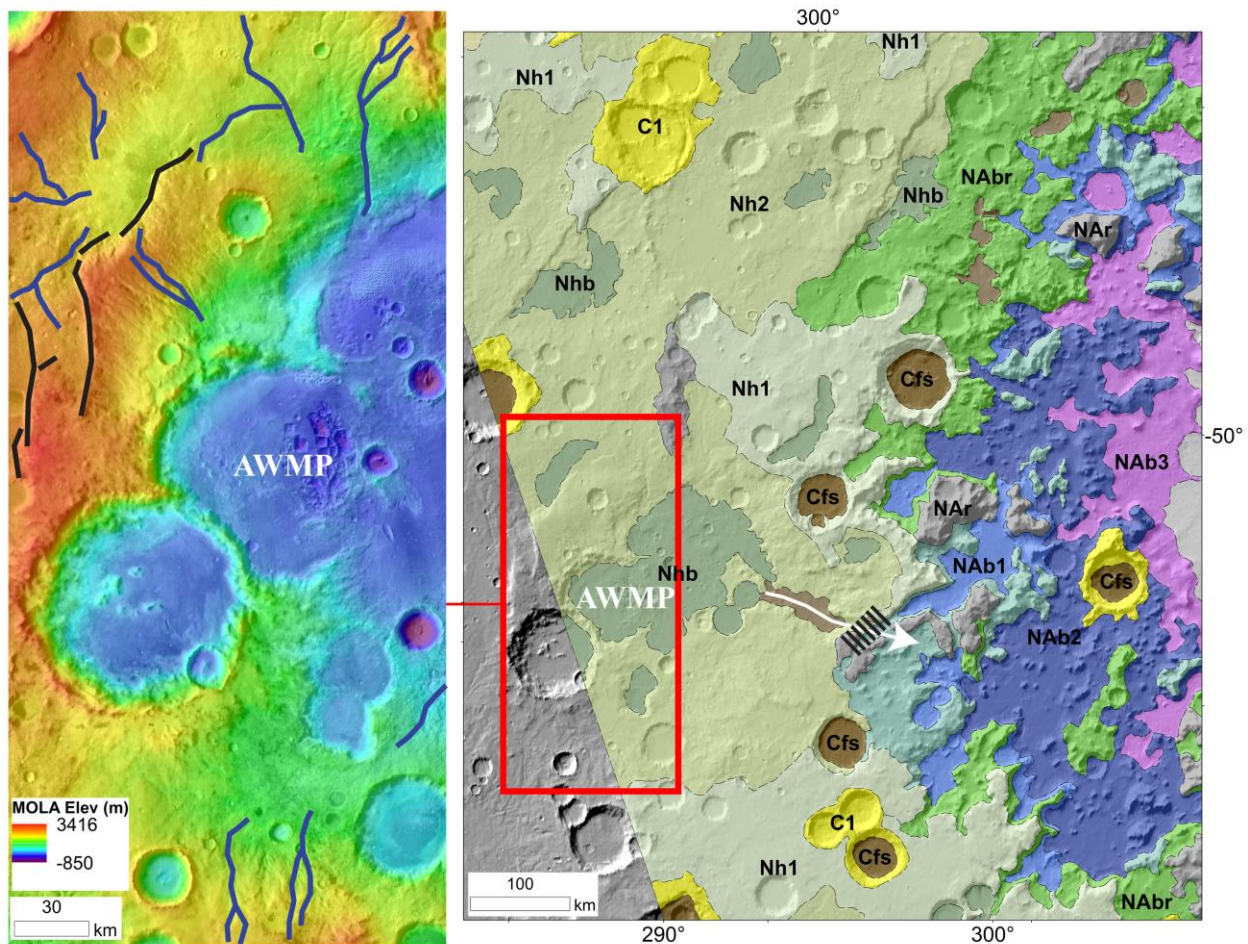


1632
 1633
 1634
 1635
 1636
 1637
 1638
 1639
 1640
 1641
 1642
 1643
 1644
 1645
 1646
 1647

Fig. 6. Merged Daytime THEMIS with MOLA topography using Geographic Information Systems with approximate geologic contacts delineating distinct stratigraphic relations highlighted in and surrounding Dzigai Vallis (left), as portrayed in the geologic map of **Fig. 3** (right; part of the geologic map shown at the right; note the structure symbols are not shown), one of three distinct valleys that debouch into the Argyre basin (the other two being western Surius Vallis and eastern Nia Vallis). Note the spatial correlations among the map units, scarps, and distinct elevation ranges generally highlighted by the topographic-based color scheme with (from young to old generally with increasing mean elevations shown in **Fig. 5**): dark blue to violet demarking the lowest and youngest basin materials—unit HAb4a (gray on geologic map), dark blue to light blue—unit Nab3 (violet on map), light blue—unit NAb2 (dark blue on map), and light green delineating the oldest and highest standing—unit Nab1 (light blue on map). These stratigraphic sequences, which generally occur at elevational ranges, are consistently observed around the basin, interpreted to mark changing hydraulic head and associated major changes in basin conditions such as related to Tharsis magmatic-driven pulses.

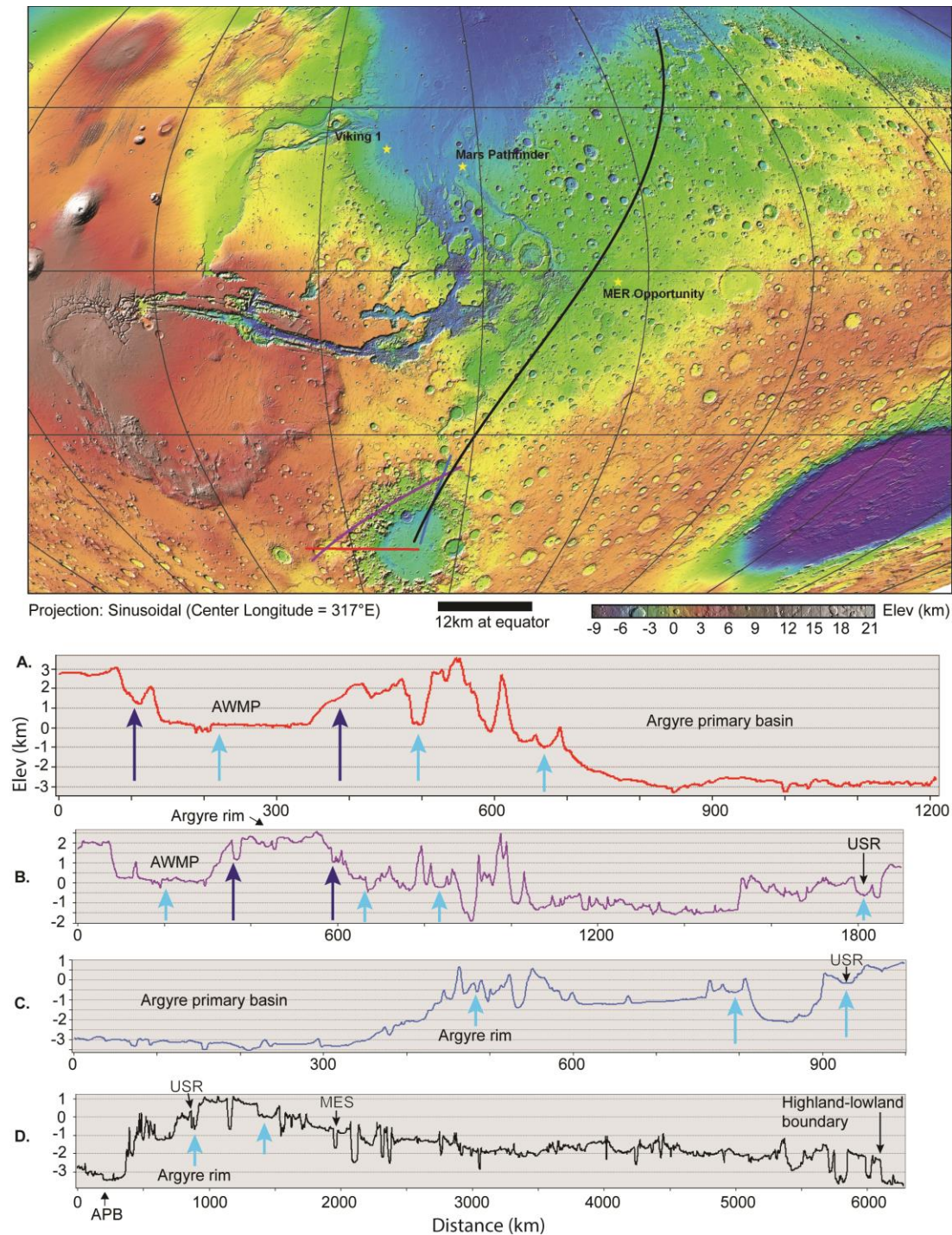
1648 **Fig. 7.** Based on Dohm et al. (2011a), MOLA color shaded relief map coupled with a THEMIS IR daytime mosaic
 1649 highlighting the western part of the Argyre western margin paleolake (AWMP, left) and its location with respect to
 1650 the Argyre basin as shown on part of the geologic map of **Fig. 3** (right). Argyre-induced tectonic structures (left,
 1651 black lines), drainage systems that debouched into the basin (left, representative drainages highlighted by blue
 1652 lines), and a possible spillway (right, white arrow which also marks a graben-like structure that may have influenced
 1653 water flow or later deformed the possible spillway). Note that the drainage systems terminate within a contour
 1654 interval generally ranging from 0 to 1.5 km (within the green-highlighted topography, which could mark a
 1655 topographic bench and once associated high-standing lake); the latter elevation occurs at a possible spillway divide
 1656 (right, dashed black line) at present-day topography (see **Fig. 8**).

1657



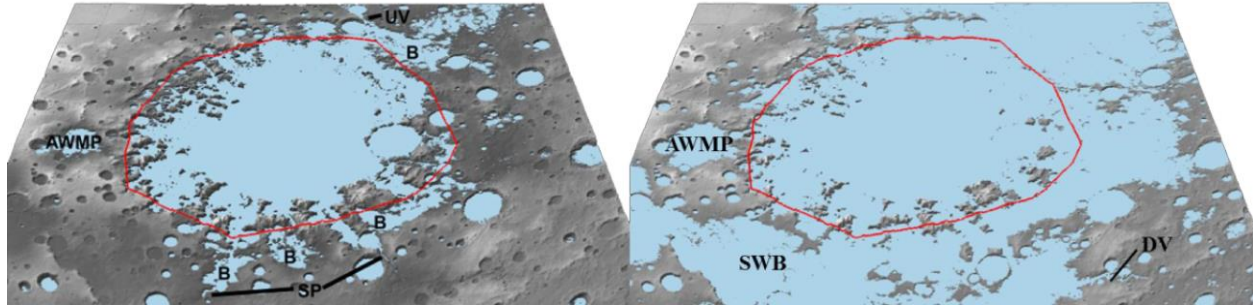
1658

1659



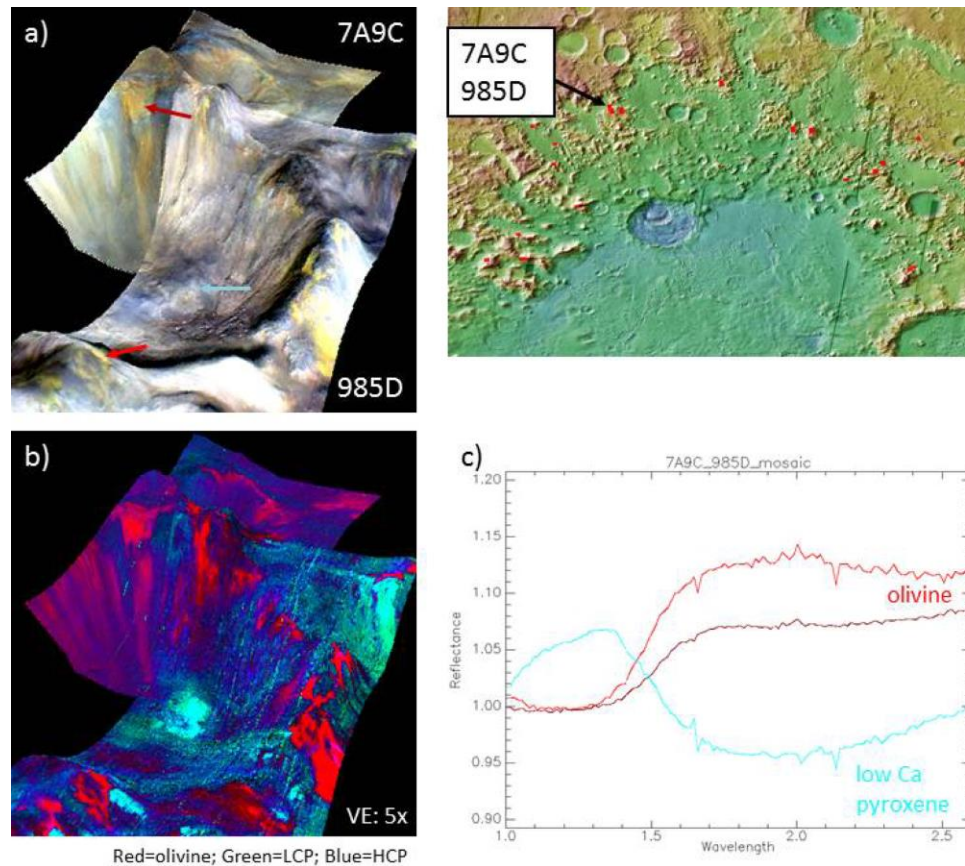
1660

1661 **Fig. 8.** Topographic profiles (A. red, B. violet, C. blue, and D. black) and associated transects annotated on a MOLA
 1662 map (top) through the Argyre west margin paleolake (AWMP), Uzboi spillway (USR), Argyre primary basin (APB),
 1663 and Argyre rim materials. Note the potential equipotential surface of the highest standing Argyre lake, AWMP, and
 1664 USR, and the mean elevation of the highest occurring and oldest member/sequence of the basin infilling materials
 1665 (unit NAb1) at a similar elevation shown in **Fig. 5** (hovering around an elevation of zero (light blue arrows)), as well
 1666 as an even higher potential equipotential surface indicated by benches, terraces, possible spillway of AWMP into the
 1667 primary Argyre impact basin, and higher reaches of unit NAb1 (nearing 1.5 km (dark blue arrows)). Hydrologic
 1668 activity would have involved the margins at higher reaches, and the Uzboi drainage system would have cut into the
 1669 impact crater rim materials.



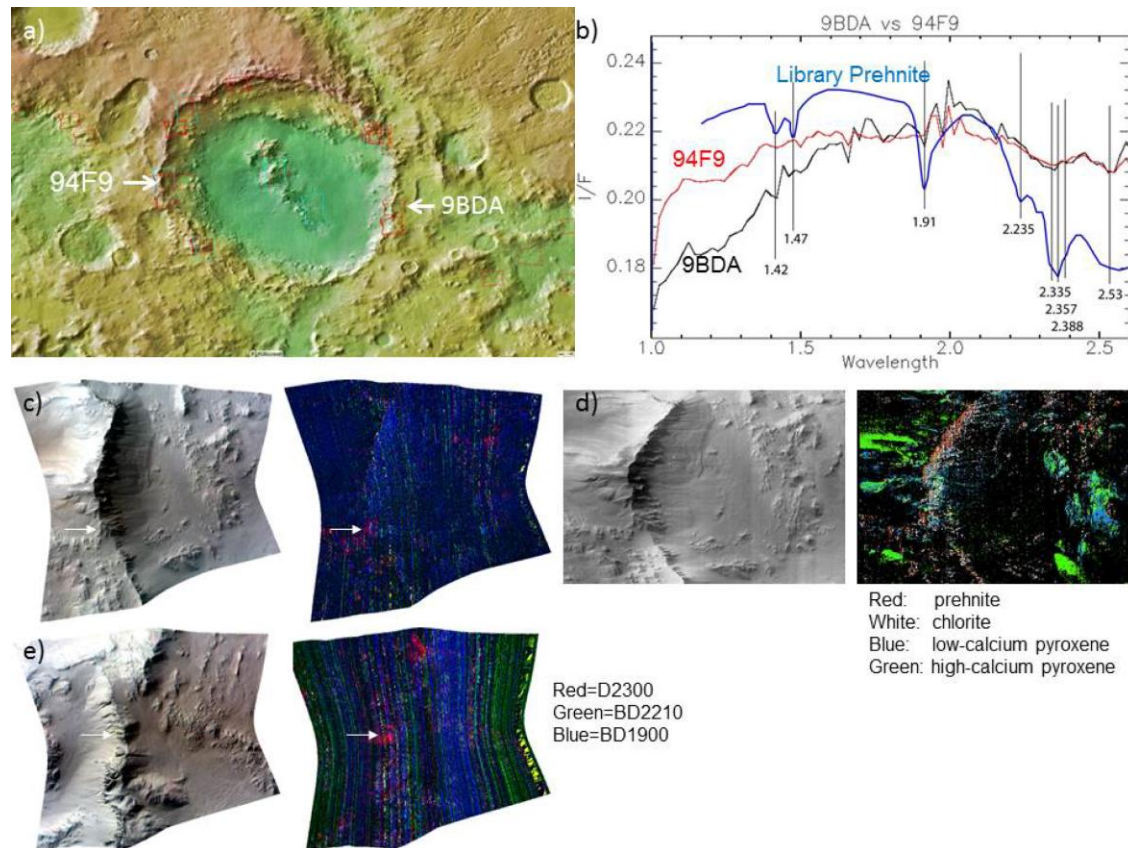
1670
1671
1672
1673
1674
1675
1676
1677
1678
1679
1680
1681
1682
1683
1684

Fig. 9. (left) Based on Dohm et al. (2011a), schematic paleolake map of the Argyre basin using a maximum topographic elevation of 0 km based on MOLA topography (regions in blue). An estimated extent of the hypothesized Argyre lake based on geomorphologic and topographic analyses, as well as detailed geologic mapping is also shown (red line). In addition to the estimated extent, dendritic channel systems (SP), local basins (B) which occur among the crater rim materials, and the Uzboi Vallis system (UV) correspond to the blue-highlighted region. Also shown is a small extent (near base level) of AWMP. The volumes of the hypothesized AWMP and Argyre lakes are estimated to be 1.6×10^4 and 1.9×10^6 km³, respectively, using MOLA. There is significant evidence of water-ice modification (e.g., glaciation) as shown by e.g., Hiesinger and Head (2002). Ever changing conditions in the Argyre basin includes a possible interplay among lakes, ice sheets, and glaciers through time, including waning water bodies. Also compare with **Figs. 3, 5-8.** (right) Similar to left, but at 1 km with an estimated volume of 3.1 million km³, nearing that of the Mediterranean Sea. Note that the potential water extent maps to a greater extent of the AWMP lake, the drainage basin located to the southwest of the Argyre basin (SWB), which displays drainage networks along its margins, and a distinct dendritic valley located to the southeast of the primary Argyre basin (DV).

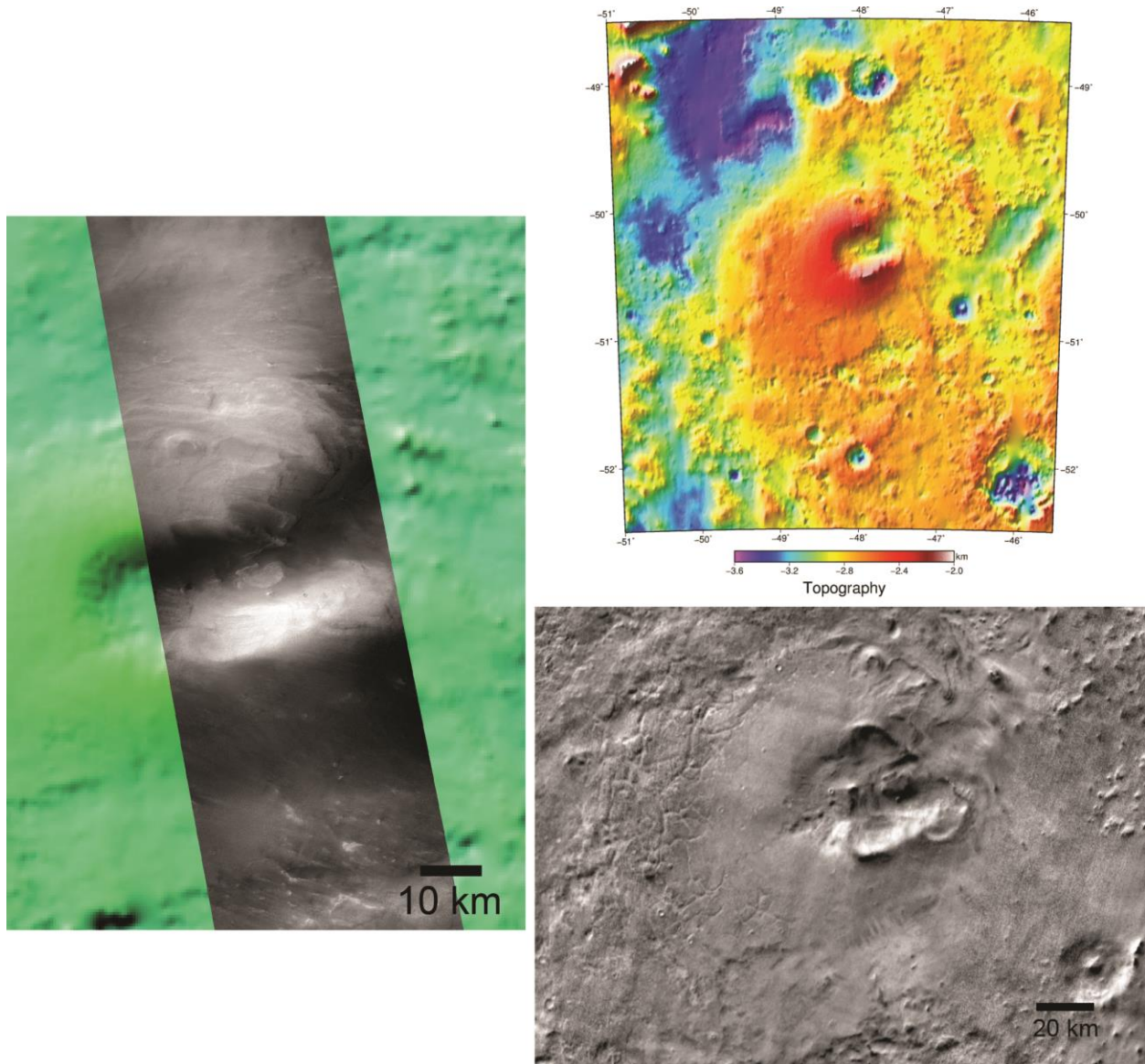


1685
 1686 **Fig. 10.** CRISM-based information combined with the MOLA data and geologic map of this
 1687 investigation and for spectroscopic/stratigraphic investigation (spectroscopic information
 1688 corresponds with unit NAb—Argyre basin and rim materials; see location on geologic map of
 1689 **Fig. 3**). Example of olivine and low-calcium pyroxene outcrops in the Neridium Montes; these
 1690 are mountainous highly degraded Argyre rim materials mapped as unit NAb materials. a)
 1691 Mosaic of CRISM FRT observations 7A9C and 985D, with location shown on a MOLA map
 1692 (top right), draped over MOLA topography (vertical exaggeration x5). b) Mosaic of summary
 1693 parameters of FRT 7A9C and 985D. Red indicates olivine, green indicates low-calcium
 1694 pyroxene and blue indicates high-calcium pyroxene. c) Sample ratioed spectra from FRT 7A9C
 1695 and 985D. Location of where each spectrum was acquired is indicated by arrows in part a. Dark
 1696 red arrow indicates location of dark red olivine spectrum, bright red arrow indicates location of
 1697 bright red olivine spectrum, teal arrow indicates location of teal low-calcium pyroxene spectrum.
 1698 The CRISM data corroborates the Argyre-rim materials in part being uplifted ancient upper
 1699 mantle materials, and that the terrains, which are distinctly hydrologically modified, contain
 1700 magnesian lithologies such as olivine-dominated rocks (Buczowski et al., 2008a,b, 2010).
 1701

1702

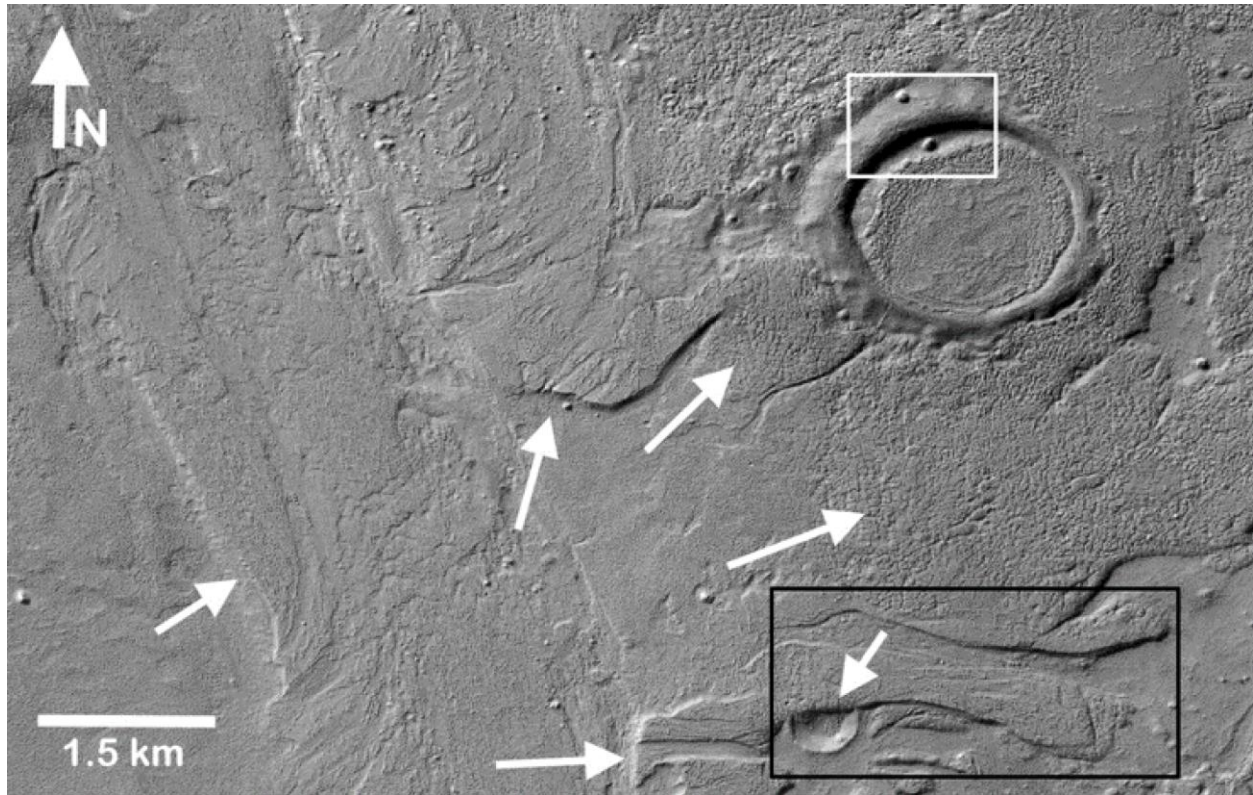


1703
 1704 **Fig. 11.** CRISM-based information combined with the MOLA data and geologic map of this
 1705 investigation for spectroscopic/stratigraphic investigation (spectroscopic information
 1706 corresponds with unit C1—old crater materials; see location on geologic map of **Fig. 3**).
 1707 Location of CRISM images FRT94F9 and FRT 9BDA observations covering parts of the rim and
 1708 floor materials of Hale crater shown on a MOLA map ((a) white arrows). b) Sample spectra from
 1709 CRISM FRT 9BDA (black line) and 94F9 (red line). Blue spectrum is of a library prehnite
 1710 (USGS spectral library splib06a). Black vertical lines mark out wavelengths of interest. c) Geo-
 1711 referenced CRISM image FRT 94F9 (left) and summary parameter image (right). Arrows point
 1712 to location where spectrum in part (b) was sampled. d) Tetracorder analysis of FRT 94F9
 1713 indicates that chlorite and prehnite are common on the Hale crater rim, while both low- and high-
 1714 calcium pyroxenes are present both on the crater floor and outside the crater. e) Geo-referenced
 1715 CRISM image FRT 9BDA (left) and summary parameter image (right). Arrows point to location
 1716 where spectrum in part (b) was sampled. These minerals are consistent with Argyre-impact-
 1717 modified terrain, including the excavation of relatively olivine-rich, deep mantle and/or
 1718 primordial crustal materials transferred at or near the Martian surface by the impact event and
 1719 associated overturn and inversion of stratigraphy, as well as hydrothermal activity possibly
 1720 persisting for millions of years following the Argyre impact event. The Hale-crater-forming
 1721 impact event occurred near the spillway of Uzboi Vallis, and thus possible water enrichment of
 1722 the Hale target materials may have contributed to hydrothermal activity related to the Hale
 1723 impact event subsequent to the relatively long-lived Argyre-driven hydrothermal activity
 1724 (estimated to have persisted for 10 Ma (Abramov and Kring, 2005) following the ~ 3.93 Ga
 1725 Argyre impact event (based from Robbins et al., 2013).
 1726



1727
 1728 **Fig. 12.** Based on Williams et al. (2014), possible vent structure at the floor of Argyre basin (see location on
 1729 geologic map of Fig. 3). The landform could be a sedimentary (e.g., mud volcano), volcanic (e.g., cinder cone or
 1730 maar), or impact-related feature, either formed before (i.e., now exhumed through differential erosion), during
 1731 emplacement of unit HAb4a, or following emplacement of unit HAb4a; high-standing ‘rim’ is ~1 km higher than
 1732 interior and surrounding terrain. (top) MOLA DEM and (bottom) THEMIS daytime IR (middle) CTX superposed on
 1733 MOLA. Late Hesperian (or younger) venting of volatiles during the emplacement of unit HAb4a sediments, which
 1734 includes flooding, ponding to form a lake, and rapid sedimentation during the final sequence of the basin infill
 1735 deposits, could have resulted in mud volcanism along the floor of the basin.

1736
 1737
 1738



1739

1740

1741

1742

1743

1744

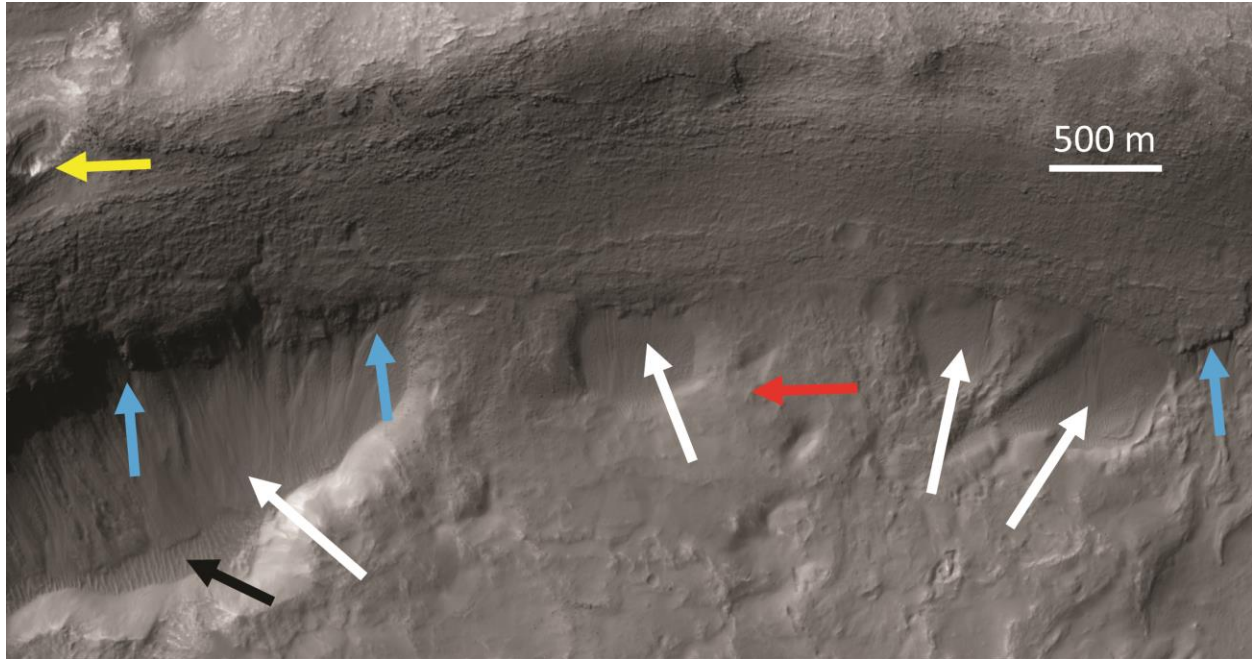
1745

1746

1747

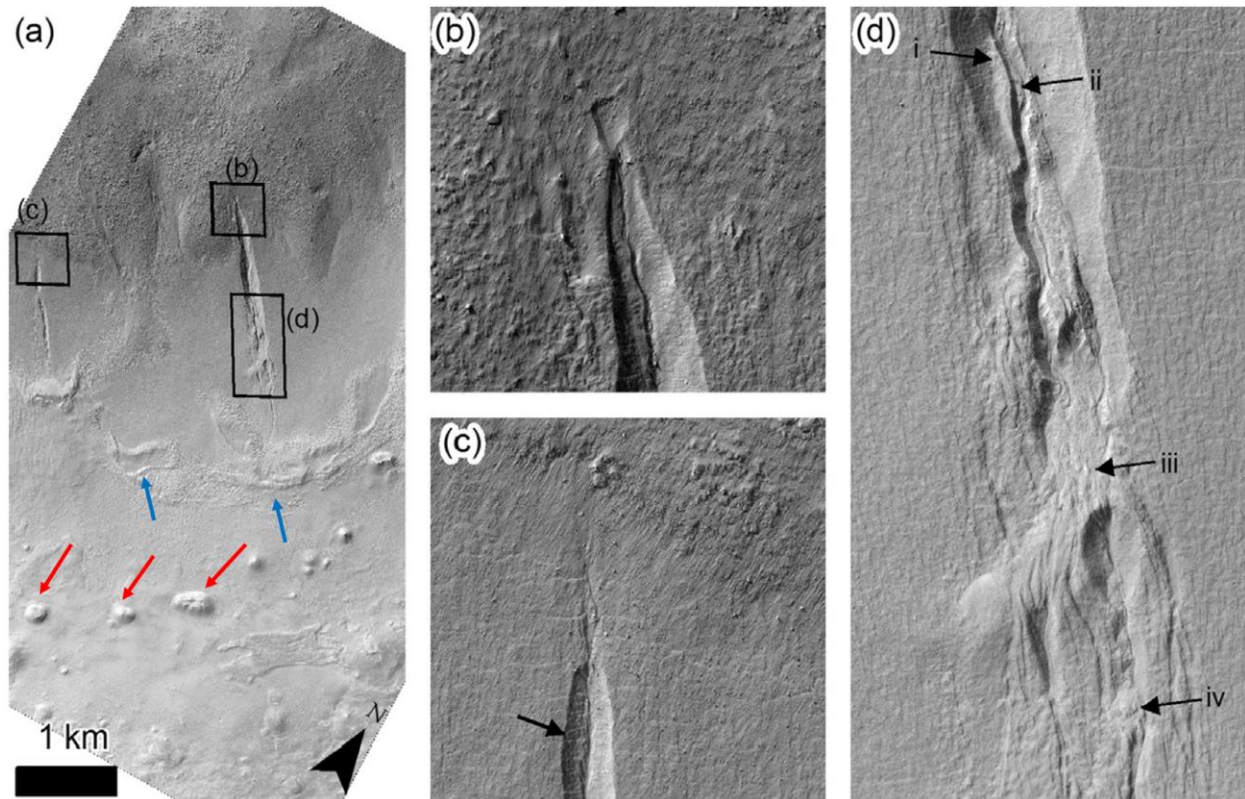
1748

Fig. 13. Based on El Maarry et al. (2013), CTX image of the Moanda crater-valley system (MCVS) deposits (see location on geologic map of **Fig. 3**) showing several stages of environmental change and associated surface modification (white arrows point to multiple resurfacing events by varying processes, including possible glacial, alluvial, periglacial, fluvial, among others). Several small valleys dissect the MCVS deposits, which may have covered the whole region after their emplacement, as is evident from the deposits filling a 1.5-km-wide impact crater at the upper right of the view. Note the circular hills (white box) and flow materials partly covering the impact crater (black box) which may yet contain significant amounts of volatiles beneath a dry mantle (El Maarry et al., 2013). Part of image ID: P17_007745_1410_XN_39S040W.



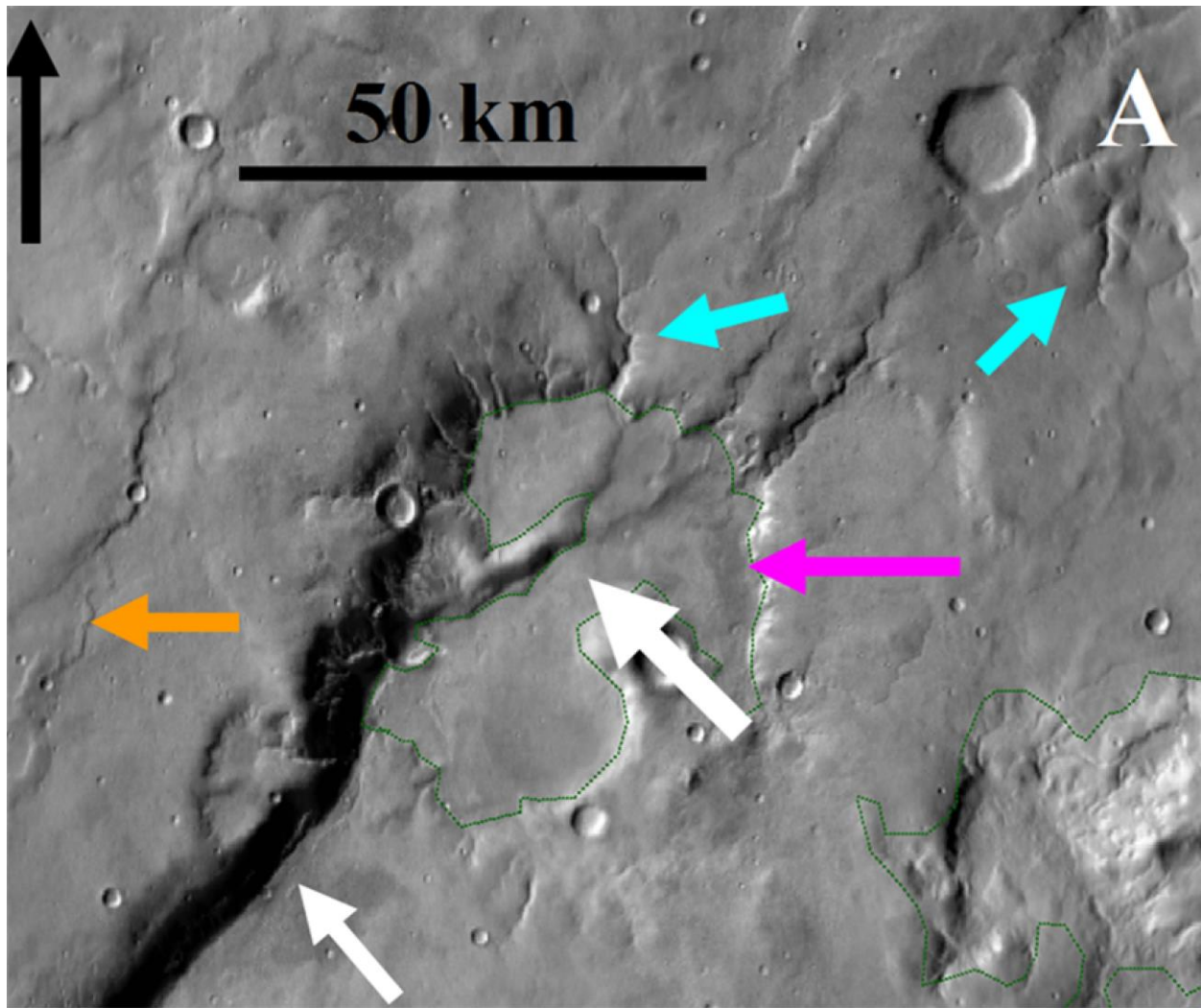
1749
 1750
 1751
 1752
 1753
 1754
 1755
 1756

Fig. 14. The northern part of HiRISE image PSP_006888_1410 (see location on geologic map of **Fig. 3**) clearly shows gullies that source at a geologic contact (blue arrows), which separates the overlying layered deposits (yellow arrows) from more massive-appearing deposits (red arrows). The gullies occur within distinct topographic depressions (terrestrial thermokarst- or karst-like; white arrows) with associated debris aprons partly infilling the depressions, as well as partly burying dune deposits (black arrow). Groundwater and stratigraphic control appear influential on gully formation.



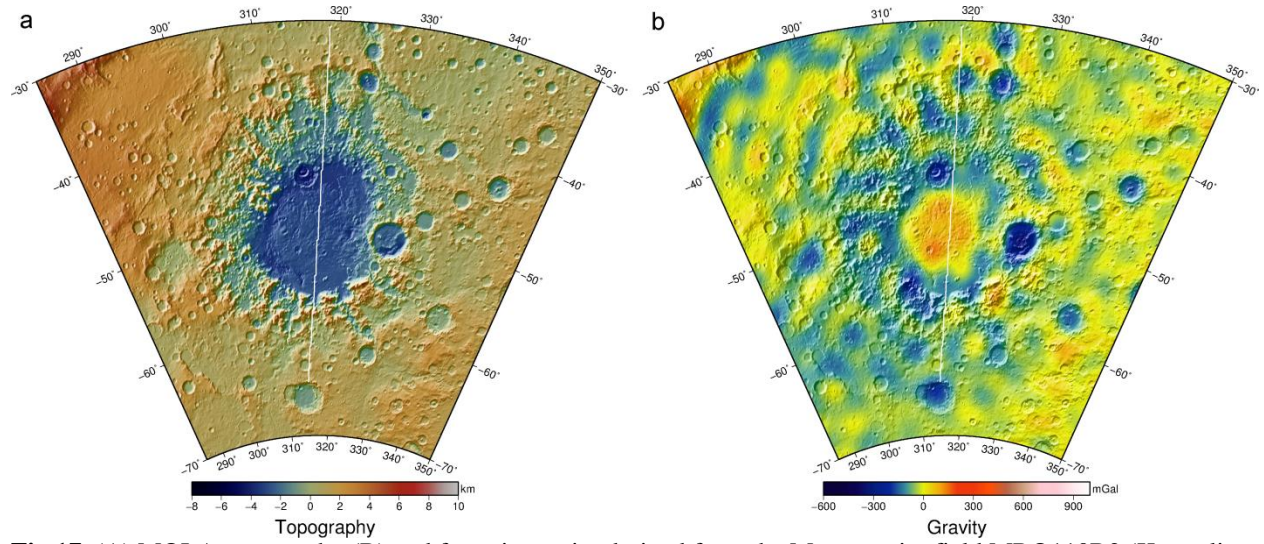
1757
 1758
 1759
 1760
 1761
 1762
 1763
 1764
 1765
 1766
 1767
 1768
 1769
 1770
 1771
 1772
 1773
 1774

Fig. 15. Based on Soare et al. (2014b), gullies and graben-like cavities upslope of candidate open system pingos (OSP, red arrows), with arcuate ridges in between, interpreted to be moraines (blue arrows) (see location on geologic map of **Fig. 3**). HiRISE image ESP_020720_1410. (a) Overview of the site, showing the locations of insets b–d and the downslope position of the putative OSPs relative to the gullies and arcuate ridges. (b) Top of the alcove of the eastern gully, showing an abrupt start of the channel embedded in the graben-like elongated depression. A possible landslide scar is located at the northern tip of the cavity. (c) Top of the alcove of the western gully, with rill-like features running into the graben-like cavity; the features seem to originate upslope from the non-polygonised terrain. Note the polygonal network within the cavity and in the surrounding terrain; black arrow points to location with low-centered polygons. (d) Mid-part of the eastern gully, with multiple terraces (i,ii) and multiple self-blocking digitate deposits (iii,iv), as indicated by black arrows. Note the distinct lineaments, which we interpret to be fractures and faults, as well as a polygonal network within the cavity and in the surrounding terrain. Image credits: NASA/JPL/University of Arizona.



1775
 1776
 1777
 1778
 1779
 1780
 1781
 1782
 1783
 1784

Fig 16. (left) THEMIS IR daytime images showing an Argyre impact-induced prominent fault (narrow white arrow) that plays out to the north-northeast (broad white arrow), deforming a drainage basin (violet arrow) (see location on geologic map of **Fig. 3**); this indicates post-Argyre-impact isostatic adjustment of basement structures. Also shown are drainages (blue arrows) and a wrinkle ridge (orange arrow), some of which appear to be controlled by underlying faults generated by the Argyre impact event. The structural feature is identified as a macrostructure (a structure reaching 100s of kilometers in length) on the geologic map, which locates roughly concentric about and to the northwest of the Argyre basin. Phyllosilicate has been identified in the basin through CRISM-based (Buczowski et al., 2008).



1785
1786
1787
1788

Fig 17. (A) MOLA topography (B) and free-air gravity derived from the Mars gravity field MRO110B2 (Konopliv et al., 2011) of Argyre Province. Lines show ground tracks of profiles in **Fig. 18**.

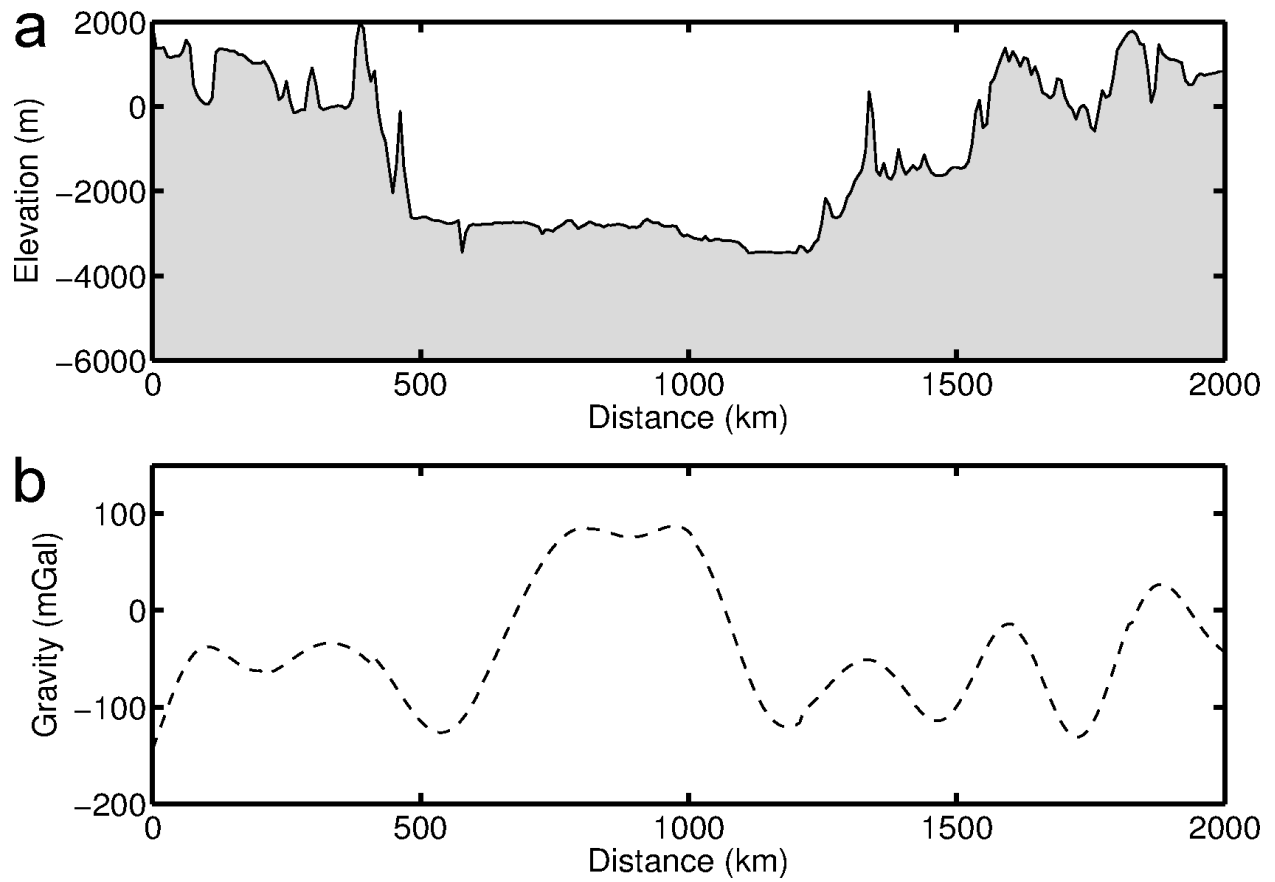
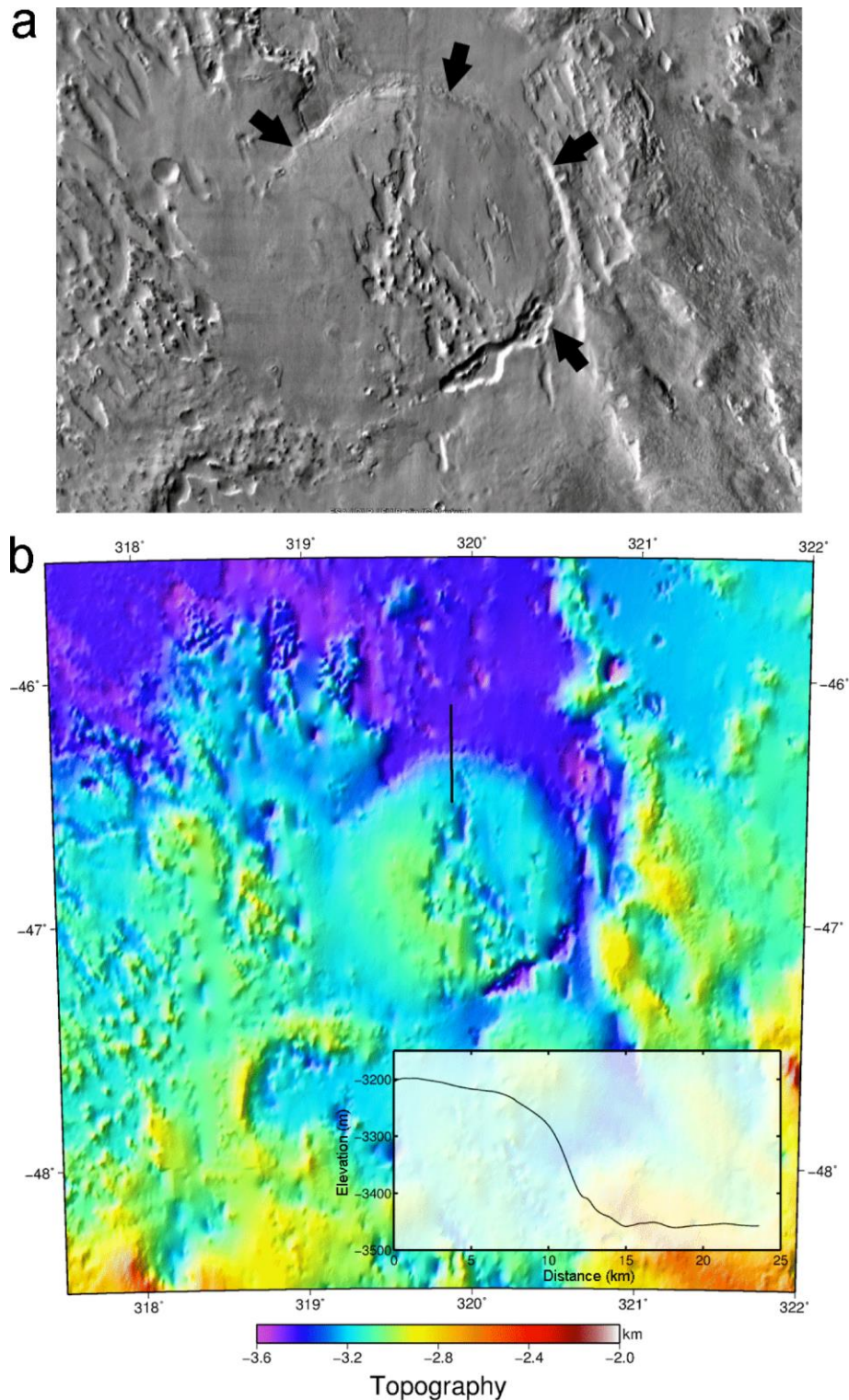


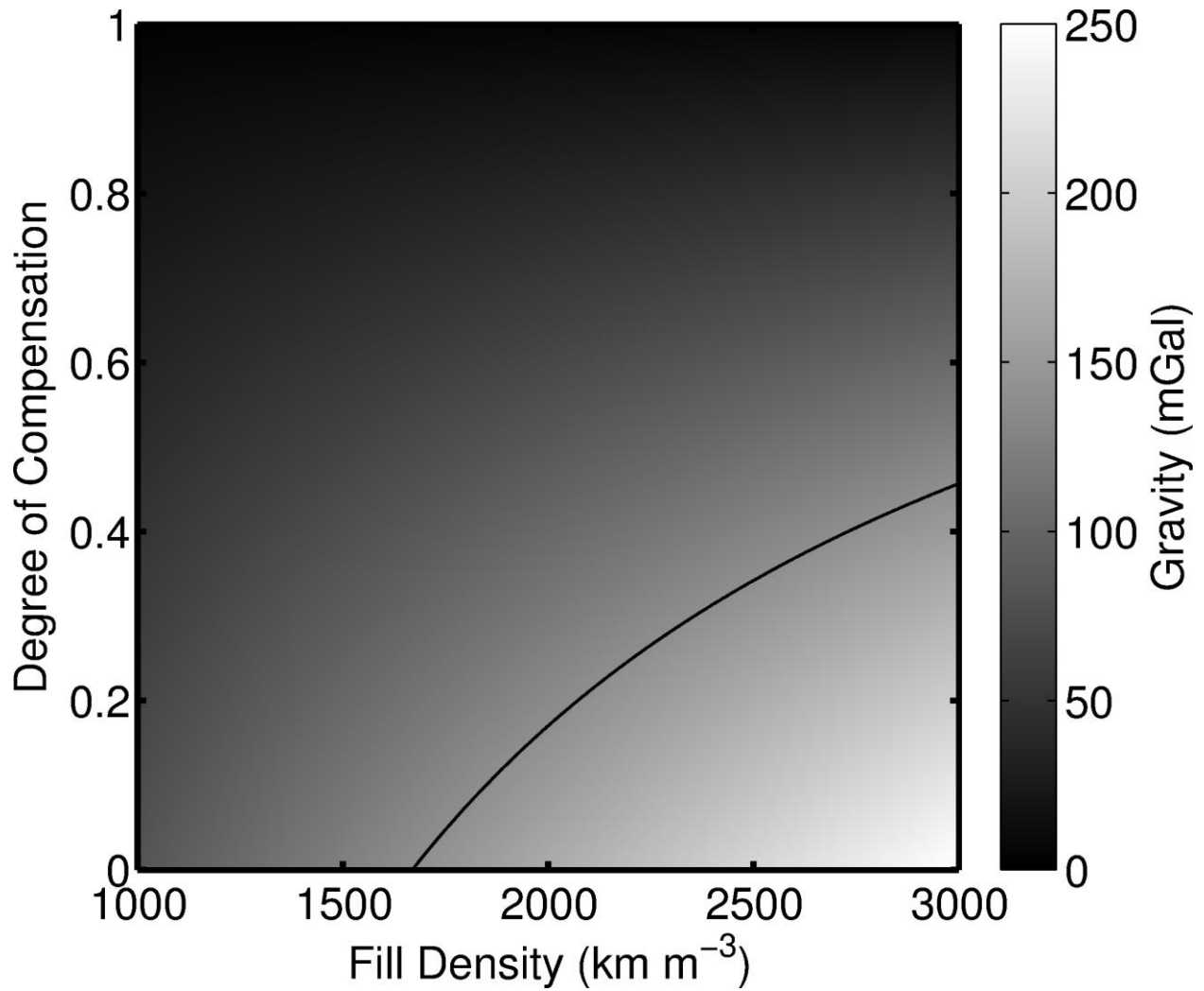
Fig. 18. (a) Topography and (b) free-air gravity anomaly profiles through the center of the Argyre basin.

1789
1790
1791
1792



1793
1794
1795
1796
1797

Fig. 19. (a) THEMIS daytime IR image of the floor of Argyre basin. The quasi-circular feature (black arrows) is interpreted to be a ~60 km diameter buried crater. (b) Topography of the putative buried impact structure. The northern edge appears to have been exhumed creating a nearly 300 m arcuate scarp seen in the inset profile (location shown with black line).



1798
 1799
 1800
 1801
 1802
 1803

Fig. 20. The free-air gravity anomaly for a slab of material 2 km thick as a function of material density and degree of compensation. The 140 mGal contour (black curve), the approximate magnitude of the mascon within the basin interior, is shown for reference.